Chemical bonding analysis of complex solids in real space from the projector augmented-wave method

DISSERTATION

zur Erlangung des akademischen Grades

Doctor rerum naturalium

(Dr. rer. nat.)

vorgelegt

der Fakultät Mathematik und Naturwissenschaften der Technischen Universität Dresden

von

M. Sc. Pavlo Golub

geboren am 28. Februar 1987 in Chernigiv, Ukraine

Eingereicht am 16. May 2017

Die Dissertation wurde in der Zeit von Februar 2014 bis März 2017 auf der Fakultät Mathematik und Naturwissenschaften der Technischen Universität Dresden angefertigt.

Gutachter:	Prof. Dr. rer. Nat. habil. Michael Ruck (TU Dresden) Prof. Dr. Juri Grin (MPI CpfS, Dresden)
Datum der Verteidigung:	11.08.2017

Abstract

Quantum mechanics became a foundation for incessant development of versatile computational methods for analysis of chemical and physical properties of molecules and crystals. A huge progress has been made in the field of density functional theory, since nowadays this theory offers the best compromise between precision of results and efficiency of computation. The chemical bonding analysis can be easily performed with real space methods based on chemical concepts introduced via partitioning of real space into chemically meaningful domains, since the orbital based approach is not well applicable due to the delocalized nature of plane waves. However the practical usage of those methods often requires a significant amount of computational resources. Some methods require the evaluation of so called domain overlap matrices, that is a formidable task for complex and low-symmetry systems. In the present research the author enables the investigation of complex solid compounds with real space chemical bonding indicators by introducing the derivation of the expression for the evaluation of the domain overlap matrix elements from the projected-augmented wave method. The corresponding program module was developed, which is capable to perform the real space chemical bonding analysis with a number of methods, like electron localizability indicators, electron localization function, localization/delocalization indices and domain averaged Fermi hole orbitals. The efficiency and the accuracy of the developed implementation is demonstrated by the comparison with the domain overlap matrix elements evaluation from the full-potential linearized augmented plane wave method on a set of simple compounds with three atoms per primitive cell at most. A set of complex periodic structures is analyzed and the capability of the present implementation to unravel intricate chemical bonding patterns is demonstrated.

Contents

List of Figures

List of Tables

Abbreviations

AdNDP..... adaptive natural density partitioning
AFQMC..... auxiliary-field quantum Monte-Carlo
APW..... augmented plane wave
BCOOP..... balanced crystal orbital overlap population
CC..... coupled clusters
CI..... configuration interaction
COHP..... crystal orbital Hamiltonian population
COOP..... crystal orbital overlap population
DAFH..... domain averaged Fermi hole
DFT..... density functional theory
DMC..... diffusion Monte-Carlo
ELF..... electron localization function
ELI..... electron localizability indicator
FCI..... full configuration interaction
FFT..... fast Fourier transformation
GGA..... generalized gradient approximation
(L)APW..... linearized augmented plane wave
LCAO..... linear combination of atomic orbitals
LDA..... local density approximation
LSDA..... local spin-density approximation
MCSCF..... multi-configuration self-consistent field
MP..... Möller-Plesset
MRCI..... multi-reference configuration interaction
NADO..... natural adaptive orbitals
NAO..... natural atomic orbital
NBO..... natural bond orbital
NHO..... natural hybrid orbital
NLMO..... natural localized molecular orbital
NO..... natural orbital
PAW..... projector augmented-wave
PBE..... Perdew-Burke-Ernzerhof
pCOHP..... projected crystal orbital Hamiltonian population
PNAO..... pre-orthogonal natural atomic orbital
QMC..... quantum Monte-Carlo

QTAIM..... quantum theory of atoms in molecules
VMC..... variational Monte-Carlo

Introduction

The traditional way of understanding of chemical bonding involves the concepts of ionic, covalent and metallic bonding. The differences between them are generally demonstrated with characterization of simple compounds, like small organic molecules or simple metals. However in reality more complicated compounds, like confined metals or electrides, can not be characterized purely in term of one or another type of bonding. Indeed, the difference between those types of bonding is rather quantitative than qualitative, and the physics underlying them is the same. For example, ionic bonding can be considered as an extreme case of polar covalent bonding, and it is hard to say where is the demarcation line between them.

The motivation for this research is determined by the necessity to perform the analysis of chemical bonding patterns in complex solid structures, which are hard to characterize purely in the frameworks of traditional concepts of chemical bond. This is vital for the understanding of the ground reasons underlying the manifestation of those or other physical and chemical properties, and change of them after the modification of the compound under the investigation. This type of analysis requires the development of an efficient and robust tool, which should demonstrate the much greater performance than the developed by this date counterparts, thus enabling the investigation of structures with low symmetries and large unit cells. The present thesis "Chemical bonding analysis of complex solids in real space from the projector augmented-wave method" is devoted to the development of a such tool and to the consecutive it usage for the chemical bonding analysis of complex compounds in solid state, which comprise transitional metal and post-transitional metal heavy elements.

The present thesis can be divided in three parts: chapters 1-3 serve as a general introduction to density functional theory, electronic structure methods in solid state and methods for analyzing of chemical bonding; chapter 4 reports the adaptation of chosen real-space chemical bonding indicators for projector augmented wave method as well as its program implementation; chapters 5-6 are devoted to practical usage of the developed code.

In **chapter 1** the basis ideas together with main the limitations of density functional theory are shown. Since density functional theory is not the only paradigm in the

framework of which the solution of many-body problem is available, a some alternative theories and approaches are briefly discussed as well. **Chapter 2** describes the main methods for electronic structure calculations in solids from plane wave basis set. The main difference between them is to how effectively to account for a multi nodal structure of corresponding all electron wave function in the vicinity of nuclei. In **chapter 3** a general overview of modern methods for chemical bonding analysis is presented.

Chapter 4 is the starting chapter, where authors original findings are presented. The general equations for the domain overlap matrix elements from projector augmented wave method are given. The implementation peculiarities of those equations in real-space chemical bonding analysis are presented as well as a brief overview of the developed program module.

In **chapter 5** the elaborated module is used for the chemical bonding analysis of a set of chosen simple compounds. The results are verified with the already existing module for analogous chemical bonding analysis from the linearized augmented plane wave method. The comparative efficiency of both implementation is discussed.

Chapter 6 demonstrates the possibility of chemical bonding analysis of complex compounds, which were previously almost unavailable for a such kind of analysis due to their complicity, with described in this work module. A set of complex compounds, which manifest intricate bonding patterns and comprise two and more different types of atoms, was chosen for this purpose.

Chapter 1

Electronic structure theory

The solution of time-independent many-body Schrödinger equation

$$\hat{H}\Psi\big(\{\vec{r}_i\},\{\vec{R}_i\}\big) = E\Psi\big(\{\vec{r}_i\},\{\vec{R}_i\}\big) \tag{1.1}$$

is the base for quantum-chemical revealing of any substance-related property. Here $\{\vec{r}_i\}$ and $\{\vec{R}_i\}$ represent a set of electron and nuclei coordinates respectively, comprising both position and spin components. The total energy operator, $\hat{H}$, of a system with N electrons and M nuclei adopts the following form:

$$\hat{H} = -\frac{1}{2}\sum_{i=1}^{N}\nabla_i^2 \; + \sum_{i=1,j>i}^{N}\frac{1}{r_{ij}} \; - \frac{1}{2}\sum_{A=1}^{M}\frac{1}{M_A}\nabla_A^2 \; + \sum_{A=1,B>A}^{M}\frac{Z_A Z_B}{r_{AB}} \; - \sum_{i}^{N}\sum_{A}^{M}\frac{1}{r_{iA}}, \tag{1.2}$$

where the system of atomic units is used. Symbols A and B run over all nuclei, i and j run over all electrons, Z is a charge of corresponding nucleus, r represents the distance between two corresponding particles. Applying to the Born-Oppenheimer approximation — states that since the nuclei are much heavier and move much slower than electrons, their positions can be considered as frozen and electrons can be considered as influenced by some instantaneous external potential — one can restrict oneself to the consideration of only electron-dependent terms in equation (1.2), that is to consider a motion of the electrons relative to the nuclei. The corresponding reduced total energy operator called an electronic Hamiltonian and is written as:

$$\hat{H}_{elec} = \hat{T} + \hat{V} + \hat{V}_N, \tag{1.3}$$

where $\hat{T} = -\frac{1}{2}\sum_{i=1}^{N}\nabla_i^2$ is the operator that represents the kinetic energy of electrons, $\hat{V} = \sum_{i=1,j>i}^{N}\frac{1}{r_{ij}}$ represents potential energy of the electron-electron interaction and $\hat{V}_N = -\sum_{i}^{N}\sum_{A}^{M}\frac{Z_A}{r_{iA}}$ represents the potential energy of the electron interaction with nu-

clei. The expectation value of the last term is referred as external potential v_{eff} and can comprise external electric and magnetic fields as well. Since electrons are fermions and are subjects to Pauli exclusion principle, the corresponding electronic wave function should be antisymmetric by the nature. Further only electronic Hamiltonian with the corresponding electronic wave function and electronic energy will be considered. Subscript 'elec' will be omitted for brevity.

1.1 Density Functional Theory

One way to solve the many body problem is to use the Density Functional Theory (DFT) method, originally formulated by Hohenberg and Kohn[1]. According to the DFT formalism the properties of many-electron system can be determined by using the functional of electron density.

1.1.1 Hohenberg-Kohn theorems

Density functional theory is based on two Hohenberg-Kohn theorems, that will be further described assuming non-degenerate ground states.

The **first** theorem: *the external potential (and, hence, the total energy) of many-electron system is uniquely determined by its electron density.*

Proof: ◁ Suppose there are two unequal total energies E_1 and E_2 that correspond to the same electron density $n_0(\vec{r})$ associated with the non-degenerate ground state of some N-particle quantum-chemical system. Since the first two term in equation (1.3) depend only on number of electrons the corresponding Hamiltonians $\hat{H}_1$, $\hat{H}_2$ will differ only in external potentials $v_{eff,1}(\vec{r})$, $v_{eff,2}(\vec{r})$, and will be characterized by different ground state wave functions ψ_1 and ψ_2. The usage of the variational principle yields:

$$\begin{aligned} E_1 < \langle \psi_2 \mid \hat{H}_1 \mid \psi_2 \rangle &= \langle \psi_2 \mid \hat{H}_2 \mid \psi_2 \rangle + \langle \psi_2 \mid \hat{H}_1 - \hat{H}_2 \mid \psi_2 \rangle \\ &= E_2 + \int n_0(\vec{r}) \Big(v_{eff,1}(\vec{r}) - v_{eff,2}(\vec{r}) \Big) \, d\vec{r}, \end{aligned} \tag{1.4a}$$

$$\begin{aligned} E_2 < \langle \psi_1 \mid \hat{H}_2 \mid \psi_1 \rangle &= \langle \psi_1 \mid \hat{H}_1 \mid \psi_1 \rangle + \langle \psi_1 \mid \hat{H}_2 - \hat{H}_1 \mid \psi_1 \rangle \\ &= E_1 + \int n_0(\vec{r}) \Big(v_{eff,2}(\vec{r}) - v_{eff,1}(\vec{r}) \Big) \, d\vec{r}. \end{aligned} \tag{1.4b}$$

Summing up these two inequalities one gets the contradiction $E_1 + E_2 < E_1 + E_2$. Hence, the ground state density uniquely determines to within an additive constant the external potential and, correspondingly, the total energy of the many-electron system.▶

Therefore the ground state total energy can be expressed as the functional of the

ground state electron density. In the framework of DFT it is ordinary to write the electron energy functional as the sum of two terms

$$E[n(\vec{r})] = \int n(\vec{r}) v_{ext}(\vec{r}) d\vec{r} + F[n(\vec{r})], \tag{1.5}$$

where the functional $F[n(\vec{r})]$ is called Hohenberg-Kohn functional and includes kinetic and potential energy of interacting electron system (i.e. this functional contains all terms that are universal in the sense of their independence from the actual system defined by the positions and charges of nuclei).

The **second** theorem: *the electron density, which minimizes the total energy of many-electron system, is the ground state density.*

Proof: $\lhd$ The proof of the second theorem is firmly based on variational principle which states that the ground-state energy, E_0, is always less or equal to the energy, obtained as the expectation value of the Hamiltonian calculated with the approximate wave function, ψ':

$$E_0 \leq \langle \psi' | \hat{H} | \psi' \rangle. \tag{1.6}$$

Indeed, assume that the exact solution to the Schrödinger equation is known:

$$\hat{H}\psi_n\big(\{\vec{r}_i\}\big) = E_n \psi_n\big(\{\vec{r}_i\}\big), \tag{1.7}$$

where $n = 0, 1, 2, ...\infty$ and E_0 represents ground-state energy, E_1 represents the energy of the first excited state, E_2 - the energy of the second excited state and so on, $E_0 < E_1 < E_2 < ...$ The solutions form complete basis set thus it is possible to choose orthogonal ones ($\langle \psi_n | \psi_m \rangle = \delta_{nm}$) on the basis of which the approximate wave function can be expanded:

$$\psi'\big(\{\vec{r}_i\}\big) = \sum_{n=0}^{\infty} a_n \psi_n\big(\{\vec{r}_i\}\big). \tag{1.8}$$

Taking into account that the wave functions are already normalized, the energy, W, that corresponds to the approximated wave function, is given as

$$\begin{aligned} W = \langle \psi' | \hat{H} | \psi' \rangle = \langle \sum_n a_n \psi_n | \hat{H} | \sum_m a_m \psi_m \rangle = \sum_{n,m} a_n^* a_m \langle \psi_n | \hat{H} | \psi_m \rangle \\ = \sum_n |a_n|^2 E_n. \end{aligned} \tag{1.9}$$

If one subtracts from it the ground state energy

$$W - E_0 = \sum_n |a_n|^2 (E_n - E_0), \tag{1.10}$$

the results will be equal or bigger than 0, since $|a_n|^2$ is always positive or equal to zero and $E_n \geq E_0$, that proofs the variational principle[2].

Since, according to the previous theorem, the ground state density uniquely determines the total energy and ground state wave function, from variational principle follows that another density, $n'(\vec{r})$, with the corresponding wave function, ψ', will necessarily give a higher energy:

$$E[n^{'}(\vec{r})] = \langle \psi^{'} | \hat{H} | \psi^{'} \rangle > \langle \psi | \hat{H} | \psi \rangle = E[n(\vec{r})]. \tag{1.11}$$

Therefore only the ground-state density minimizes the total energy of a many-electron system. ▶

The original formulation of Hohenberg-Kohn theorems was made for the v - representable densities, that is for the densities which are associated with some external potentials. One should keep in mind that not all densities may be v-representable. Such situation may occur, for example, in the case of a Hamiltonian which has a set of degenerate ground-state wave functions[3].

However it was shown by Levy an Lieb[4,5] that the Hohenberg-Kohn theorems can be generalized for electron densities, which are not v-representable and can be obtained from some antisymmetric N-body wave function:

$$n(\vec{r}) = N \int d^3r_2 \int d^3r_3 ... \int d^3r_N \ \psi^*(\vec{r}_1, \vec{r}_2, ..., \vec{r}_N)\psi(\vec{r}_1, \vec{r}_2, ..., \vec{r}_N). \tag{1.12}$$

The latter condition is called N-representability and it is weaker than v - representability. The corresponding formulation got the name Levy-Lieb constrained search formulation. It was shown by Gilbert[6] that any density which fulfills the requirements $n(\vec{r}) \geq 0$, $\int n(\vec{r}) d\vec{r} = N$, and $\int |\nabla n(\vec{r})^{1/2}|^2 d\vec{r} < \infty$ is N-representable.

1.1.2 Kohn-Sham approach

The knowing of the exact form of Hohenberg-Kohn functional (1.5) leads to the exact solution of Schrödinger equation. It is tempting to perform the computations directly from electron density, that will be only three dimensional task, but the desired analytic expression for electron density is still unknown. The main problem, as appeared, is to derive an accurate approximation to kinetic energy functional[7]. While this is not yet done one should deal with orbital based approach, as was formulated by Kohn and Sham[8]. According to it a fictitious non-interacting system is constructed in such a way that its density is the same as that of the interacting electrons. This allows to perform a more accurate DFT calculations, since the exact form of kinetic functional for a system

of non-interacting electrons is known, and the rest can be approximated.

Thus in accordance with the Kohn-Sham approach the kinetic energy is expressed as the sum of two terms $T_S[n(\vec{r})]$ and $T_C[n(\vec{r})]$. The first term corresponds to the kinetic energy of non-interacting fermions and the second represents the difference between the exact kinetic energy and the kinetic energy of the non-interacting system. Since exact wave function for a system of non-interacting fermions in non-degenerate ground state takes the form of Slater determinant[9]

$$\Theta = \frac{1}{\sqrt{N!}} \begin{vmatrix} \varphi_1(\vec{r}_1) & \varphi_2(\vec{r}_1) & \cdots & \varphi_N(\vec{r}_1) \\ \varphi_1(\vec{r}_2) & \varphi_2(\vec{r}_2) & \cdots & \varphi_N(\vec{r}_2) \\ \vdots & \vdots & \ddots & \vdots \\ \varphi_1(\vec{r}_N) & \varphi_2(\vec{r}_N) & \cdots & \varphi_N(\vec{r}_N) \end{vmatrix} \tag{1.13}$$

the kinetic energy T_S could be expressed in the following form

$$T_S[n(\vec{r})] = -\frac{1}{2}\sum_i^N \langle\varphi_i|\nabla^2|\varphi_i\rangle. \tag{1.14}$$

Here $\{\varphi_i\}$ are Kohn-Sham orbitals. It is important to note, that these orbitals can not be associated with any atomic state, the only their physical meaning is that the sum of their squares gives the total electron density of a real system

$$n(\vec{r}) = \sum_i^N |\varphi_i(\vec{r})|^2 \tag{1.15}$$

The part of Hohenberg-Kohn functional which is responsible for potential energy also can be represented as the sum of two terms $J[n(\vec{r})]$ and $E_{XC}[n(\vec{r})]$. The first term is due to Coulomb interaction

$$J[n(\vec{r})] = \frac{1}{2}\sum_{i,j}^N \int\int |\varphi_i(\vec{r}_1)|^2 \frac{1}{r_{12}} |\varphi_j(\vec{r}_2)|^2 d\vec{r}_1 d\vec{r}_2 \tag{1.16}$$

and the second term contains all effects of Coulomb and exchange correlation together with the self-interaction correction.

Finally the Hohenberg-Kohn functional is written in the following form

$$F[n(\vec{r})] = T_S[n(\vec{r})] + J[n(\vec{r})] + E_{XC}[n(\vec{r})], \tag{1.17}$$

where $E_{XC}[n(\vec{r})] = T_C[n(\vec{r})] + E_X[n(\vec{r})]$ is the so-called exchange-correlation energy. It appears that $E_{XC}[n(\vec{r})]$ is the only unknown term and the quality of calculations directly

depends on it approximation.

Generalization of the DFT method to the spin-polarization case leads to using of two spin densities (here the case of collinear magnetism is considered):

$$n(\vec{r}) = n^{\alpha}(\vec{r}) + n^{\beta}(\vec{r}) \tag{1.18}$$

Consequently one would end up with two sets of Kohn-Sham orbitals and two sets of single particle equations (1.17) one for each spin component.

In the case of non-collinear magnetism the total electron density is represented in terms of 2×2 density matrix[10,11]

$$n^{\alpha\beta}(\vec{r}) = \frac{n_{Tr}(\vec{r})\delta_{\alpha\beta} + \vec{m}(\vec{r})\vec{\sigma}^{\alpha\beta}}{2} = \frac{1}{2}\begin{pmatrix} n_{Tr}(\vec{r}) + m_z(\vec{r}) & m_x(\vec{r}) - im_y(\vec{r}) \\ m_x(\vec{r}) + im_y(\vec{r}) & n_{Tr}(\vec{r}) - m_z(\vec{r}) \end{pmatrix}, \tag{1.19}$$

where $n_{Tr}(\vec{r}) = \sum_{\alpha} n^{\alpha}(\vec{r})$, $\delta_{\alpha\beta}$ is the delta function, $\vec{m}(\vec{r})$ is the magnetization density and for non-interacting electron gas it can be written as

$$\vec{m}(\vec{r}) = \mu_B \sum_j \sum_{\alpha\beta} \phi_j^{\alpha *}(\vec{r})\vec{\sigma}^{\alpha\beta}\phi_j^{\beta}(\vec{r}), \tag{1.20}$$

where $\mu_B = e\hbar/2m_e c$ is Bohr magneton, e is the electron charge, m_e is the electron rest mass and c is the speed of light. $\vec{\sigma}^{\alpha\beta}$ are Pauli spin matrices:

$$\sigma_x = \begin{pmatrix} 0 & 1 \\ 1 & 0 \end{pmatrix} \; \sigma_y = \begin{pmatrix} 0 & -i \\ i & 0 \end{pmatrix} \; \sigma_z = \begin{pmatrix} 1 & 0 \\ 0 & -1 \end{pmatrix}. \tag{1.21}$$

1.1.3 Functionals

One of the most common approximation for exchange-correlation term is Local Spin-Density Approximation (LSDA)

$$E_{XC}^{LSDA}[n^{\alpha}(\vec{r}), n^{\beta}(\vec{r})] = \int n(\vec{r})\varepsilon_{XC}[n^{\alpha}(\vec{r}), n^{\beta}(\vec{r})]d\vec{r}, \tag{1.22}$$

where $\varepsilon_{XC}[n^{\alpha}(\vec{r}), n^{\beta}(\vec{r})]$ is exchange-correlation density per particle of a homogeneous electron gas of density $n^{\alpha}(\vec{r}) + n^{\beta}(\vec{r})$.

The exchange part of exchange-correlation density $\varepsilon_{XC}[n^{\alpha}(\vec{r}), n^{\beta}(\vec{r})]$ is represented by the formula which was derived long ago by Bloch and Dirac:

$$\varepsilon_X^{LSDA}[n^{\alpha}(\vec{r}), n^{\beta}(\vec{r})] = -\frac{3}{4}\left(\frac{3}{\pi}\right)^{1/3}\left(n^{\alpha}(\vec{r})^{1/3} + n^{\beta}(\vec{r})^{1/3}\right). \tag{1.23}$$

The exact analytic expression for the correlation part of the exchange-correlation density is not known. A lot of expressions were derived via interpolation of the results from numerical quantum Monte-Carlo simulations of the homogeneous electron gas performed by Ceperley and Alder[12]. One of the most successful schemes for uniform electron gas was suggested by Perdew and Wang in 1992[13]:

$$\varepsilon_C^{PW92}[n^\alpha(\vec{r}), n^\beta(\vec{r})] = -2A(1+\alpha r_S) ln\left[1 + \frac{1}{2A(\beta_1 r_S^{1/2} + \beta_2 r_S + \beta_3 r_S^{3/2} + \beta_4 r_S^2)}\right]. \quad (1.24)$$

Here A, α, β_1, β_2, β_3, β_4 are parameters different for spin-compensated and fully-polarized cases. $r_S = (3/4\pi(n^\alpha(\vec{r}) + n^\beta(\vec{r})))^{1/3}$ is the radius of sphere that is assumed to contain the charge of electron.

The another and generally more precise approximation is the Generalized Gradient Approximation (GGA) in the framework of which the exchange-correlation functional is dependent not only on the charge density but on gradient of the charge density as well, that helps to account for the non-homogeneity of the true electron density:

$$E_{XC}^{GGA}[n^\alpha(\vec{r}), n^\beta(\vec{r})] = \int n(\vec{r}) \varepsilon_{XC}[n_\alpha(\vec{r}), n^\beta(\vec{r}), \nabla n^\alpha(\vec{r}), \nabla n^\beta(\vec{r})] d\vec{r}. \quad (1.25)$$

Here the exchange part typically written in the form

$$\begin{aligned} \varepsilon_X^{GGA}[n^\sigma(\vec{r})] &= \varepsilon_X^{LSDA}[n^\sigma(\vec{r})]\ F(x_\sigma) \\ x_\sigma &= \frac{|\nabla n^\sigma(\vec{r})|}{n^\sigma(\vec{r})^{4/3}}, \quad \sigma = \alpha, \beta, \end{aligned} \quad (1.26)$$

where x_σ is so called reduced density gradient. The function $F(x_\sigma)$ may adopt different forms depending on the specific functional. For example, the PBE (Perdew-Burke-Ernzerhof)[14] functional based on the following form of this function

$$F(x^\sigma) = 1 - a + \frac{a}{1 + b x^{\sigma 2}}, \quad (1.27)$$

where a and b are non-empirical parameters, fitted in the way that the resulting electron density fulfills a number of conditions: it should be self-interaction-free, in should show an asymptotic behavior at $r \to \infty$, and it should reproduce a result for uniform gas if it appears to be constant[15].

The corresponding correlation part is also written as a combination of the LSDA functional and the position-dependent factor $H(t)$:

$$\varepsilon_C^{PBE}[n^\alpha(\vec{r}), n^\beta(\vec{r})] = \varepsilon_C^{LSDA}[n^\alpha(\vec{r}), n^\beta(\vec{r})] + H(t), \quad (1.28)$$

where t relates to x via spin-polarized function $f(\zeta)$

$$\begin{aligned} t &= \left(2(3\pi^2)^{1/3} f(\zeta)\right)^{-1} x, \\ f(\zeta) &= \frac{1}{2}\left((1+\zeta)^{2/3} + (1-\zeta)^{2/3}\right), \\ \zeta &= \frac{n^{\alpha}(\vec{r}) - n^{\beta}(\vec{r})}{n^{\alpha}(\vec{r}) + n^{\beta}(\vec{r})}. \end{aligned} \tag{1.29}$$

The function $H(t)$ has rather complex form

$$\begin{aligned} H(t) =& cf(\zeta) ln\left[1 + dt^2\left(\frac{1+At^2}{1+At^2+A^2t^4}\right)\right], \\ A =& d\left[exp\left(-\frac{\varepsilon_C^{LDA}}{cf(\zeta)}\right) - 1\right]^{-1}, \end{aligned} \tag{1.30}$$

where coefficients c and d are fitted in the same manner as a and b.

Further improvements can be done by inclusion of either the Laplacian of the orbital kinetic energy density, that leads to the so-called meta-GGA functionals, or by mixing a portion of the exact exchange from Hartree-Fock theory with the density exchange functionals, that leads to the so-called hybrid functionals.

1.1.4 Problems and limitations

Despite efficiency and suitability for most classes of compounds DFT is not free from some disadvantages. The most of failures stem from two general problems - delocalization and correlation errors of approximated functionals[16].

The first one depicts the tendency of existing functionals to spread out electronic density. The root of the problem is "self-interaction" - the consequence of considering an electron density rather then individual particle contribution. Even in the case of a single hydrogen atom one electron creates some charge density, which interacts with it. From mathematical point of view that means that Coulomb and exchange-correlation terms in equation (1.17) do not cancel each other. Thus spurious additional electron-electron interaction tends to push electrons further than in real systems. While this error can be removed for one-electron systems, for example, with inclusion of the exact Hartree-Fock exchange as it was made by Perdew and Zugner[17], for many-electron systems the mathematical formalization of this problem is not so clear and leads to the concept of the "many-electron self interaction error"[18–20]. When one deals with chemical reactions such effect can result in the distribution of the electron density among all centers, rather than in its localization on one of the dissociating fragments, that results in

understated reaction barriers[21]. Besides, such delocalization also leads to the underestimation of atomization energies, to the overestimation of binding energies in charge transfer complexes and the molecular polarizability in the presence of an electric field[16,21]. To fight this problem different refitting of exchange functionals were proposed. The most common examples are the bloated family of "Minnesota" functionals[22–24], which is semiempirical fitted to almost thousand data points and performed well in evaluating thermodynamic parameters for a wide range of molecules, organometallic and transition metal complexes[25,26], and several functinals developed on the base of the PBE functional (revPBE[27], RPBE[28], PBEsol[29]), which are designed specifically for treatment of solid-state compounds and surfaces. Nevertheless, neither aforementioned functionals nor any other semilocal functionals give satisfactory results for all kinds of chemical systems, every of them is performed well only for some restricted set of compounds. Finally, aiming to improve the description of the ground state of correlated systems one can apply the DFT+U method[30–32], which does not solve self-interaction problem by itself, but gives more precise results. Here U stands for the Hubbard-like localized term, which acts only on localized d or f electrons, while other electrons are treated only within LDA or GGA approximations.

The second failure refers to the inability of local potentials to describe degenerate and near-degenerate states, which emerge upon breaking of chemical bonds, in transition metal systems and in strongly correlated materials[16]. The reason is the static correlation, or, in other words, the inability to describe such systems in terms of a single Slater determinant. In principle this issue could be resolved by considering of multideterminant wave functions, but DFT is based on a single determinant and an other way to solve this problem should be elaborated. One way is to make the corresponding wave function unrestricted, but that causes the symmetry breaking and inaccurate description of singlet and triplet states[33]. The other way is to treat the dynamic correlation effect on DFT level while non-dynamic correlation with some other method, for example, with multireference configuration interaction (MRCI) method, that is the main idea of DFT/MRCI approach[34,35]. However, such approach is applicable only for moderate-size systems and not free from empirical parameters, which are necessary for elimination of double accounting of correlation effects. The most recent attempt to cover the static correlation is build up on the approximation from strong-interaction limit (a hypothetical model where electrons repel each other infinitely strongly but have at the same time a given finite density distribution[36]), that was tested for the hydrogen molecule dissociation limit,the He and Be isoelectronic series, and recommended well[37,38]. Still, this approach requires further development, especially in terms of computational efficiency.

It is also should be noticed, that DFT inherently suffers from the locality of exchange-correlation functional, that is it dependent on electron density and its derivatives at a

given point. That makes difficult to describe with DFT charge transfer systems, where an electron run over comparatively large distances[39]. To the difficulties of DFT may be addressed it poor description of dispersion forces[40] and problems with treatment of excited states with the same symmetry as the ground state[39].

Nevertheless, despite the above mentioned problems, DFT offers the best balance between computational efficiency and accuracy of results. Being at the same level of complexity as Hartree-Fock even the simplest functionals LDA and PBE give results that are generally closer to experimental data[14,41,42].

1.2 Alternatives to Density Functional Theory

One of the most known alternatives to DFT is the Hartree-Fock method[43,44], which is an orbital-based approach and actually was developed earlier. In the framework of the Hartree-Fock method each electron is considered separately, moving in the mean field, created by all other electrons. The Schrödinger equation is solved for each one-electron wave function, $\phi_i(\vec{r})$, and the total wave function is taking the form of a Slater determinant (Eq. 1.13). The corresponding Hamiltonian, $\hat{F}$, for one-electron equation:

$$\hat{F}\phi_i(\vec{r}) = \epsilon_i\phi_i(\vec{r}), \tag{1.31}$$

is usually dubbed Fock operator and takes the following form:

$$\hat{F} = \hat{h} + \sum_j^n \left(2\hat{J}_j - \hat{K}_j\right). \tag{1.32}$$

Here $\hat{h}$ is operator that acts on single electronic coordinate:

$$\hat{h} = -\frac{1}{2}\nabla_i - \sum_A^M \frac{Z_A}{r_{iA}}. \tag{1.33}$$

$\hat{J}$ and $\hat{K}$ are known as Coulomb and exchange operators respectively, which act on pairs of electrons:

$$\hat{J}_j(\vec{r}_1)\phi_i(\vec{r}_1) = \int d^3\vec{r}_2 \; \phi_j^*(\vec{r}_2)\phi_j(\vec{r}_2)\frac{1}{r_{12}}\phi_i(\vec{r}_1), \tag{1.34a}$$

$$\hat{K}_j(\vec{r}_1)\phi_i(\vec{r}_1) = \int d^3\vec{r}_2 \; \phi_j^*(\vec{r}_2)\phi_i(\vec{r}_2)\frac{1}{r_{12}}\phi_j(\vec{r}_1). \tag{1.34b}$$

The Hartree-Fock method is comparable by the cost with Kohn-Sham DFT, but in generally produces poorer energies, because it is unable to fully account for the correlation of electronic motion, in other words electrons in average are further apart, than

it is predicted by the Hartree-Fock theory[45]. The difference between energy, produced by Hartree-Fock theory and true energy is called correlation energy. The main reason is inability to count such effects in the framework of single-determinant approach. A serie of methods was developed, often referred as correlated methods, which are able to improve the results by considering multi-determinant wave functions.

Moeller-Plesset (MP) or many-body perturbation theory[46] treats the electron correlation as a perturbation for a reference solution. In that case the Hamiltonian can be written in the following form:

$$\hat{H} = \hat{H}_0 + \lambda \hat{H}', \tag{1.35}$$

where $\hat{H}_0$ is the reference Hamiltonian operator, $\hat{H}'$ is the perturbation operator and λ is a parameter, that determines the strength of the perturbation. The energy and and wave function are written as a Taylor expansion in powers of λ. In the MP theory the reference Hamiltonian is taken as a sum over Fock operators and perturbation operator is given by

$$\hat{H}' = \sum_{i<j} \frac{1}{r_{ij}} - \sum_{ij} \Big(\hat{J}_j(\vec{r}_i) - \hat{K}_j(\vec{r}_i) \Big). \tag{1.36}$$

It can be shown, that the zeroth-order MP wave function gives energy equal to the sum of energies of molecular orbitals, the first-order MP wave function recovers results given by Hartree-Fock theory, and the improvements begin only with second-order perturbation[46,47] (MP2). In average MP2 accounts for 80-90% of the correlation energy[47], however the whole procedure is purely mathematical. MP2 method scales as fifth order of the system size. MP3 and MP4 scale as sixth and seventh powers of system size, that makes them prohibitively expensive for use in even moderate size systems.

The more straightforward approach for accounting of correlation energy is to consider a total wave function as a linear combination of determinants, that is the procedure known as configuration interaction (CI)[48]:

$$\psi_{CI}(\{\vec{r}_i\}) = c_0\psi_0(\{\vec{r}_i\}) + c_1\psi_1(\{\vec{r}_i\}) + c_2\psi_2(\{\vec{r}_i\}) + ... \tag{1.37}$$

The first term is normally the Hartree-Fock determinant, the next terms is accordingly singly, doubly, triply and so on excited determinants, which are formed by replacing occupied molecular orbitals in the Hartree-Fock determinant by unoccupied molecular orbitals. In the case of a closed shell system with even number of electrons, the number of the unoccupied molecular orbitals is determined by the difference between the number of basis functions, used to expand the molecular orbitals, and half the number of treated electrons. The number of replaced orbitals determine the order of the excitation. Expansion coefficients are obtained variationally, by the requirement that the energy should be a minimum. If all possible excited configurations are included, the method

gives the exact solution within the space spanned by a given basis set[49], and is known as full configuration interaction (FCI). It is often used as benchmark for the calibration of approximate correlation techniques[49].

FCI computations are bearable only for very small systems, since expansion 1.37 exponentially grows with the increase system size[49]. In practice calculation limited only to single and double excitation (CISD).

Multi-configuration self-consistent field (MCSCF)[50] method can be considered as an extension to CI method. According to this method in the process of computation not only coefficient of expansion 1.37 are varied, but also the basis functions in molecular orbitals. MCSCF method does not recover much of correlation energy, the CI method, which keeps molecular orbitals fixed, is more efficient for this purpose[51]. However, MCSCF wave function may be used as reference wave function for CI method, that means that electrons are excited not only out single determinant, but out all considered by MCSCF determinants. This approach is called multi-reference configuration interaction (MRCI) method[52].

The idea of adding the corrections to a reference wave function was ultimately developed with coupled clusters (CC)[53] methods. After defining the excitation operator $\hat{T}_i$ as those, that upon acting on reference wave function Ψ_0 produces all ith excited Slater determinants, the CC wave function can be defined as

$$\psi_{CI}(\{\vec{r}_i\}) = e^{\hat{T}}\psi_0(\{\vec{r}_i\}), \tag{1.38}$$

where

$$\hat{T} = \hat{T}_1 + \hat{T}_2 + \hat{T}_3 + ... \tag{1.39}$$

$\hat{T}_1$ is regarded as operator of all single excitations, $\hat{T}_2$ is regarded as operator of all double excitations, $\hat{T}_3$ is an operator of all triple excitations, and so on. Truncation of the expansion 1.39 with $\hat{T} = \hat{T}_2$ is referred as coupled clusters doubled (CCD) method and it gives the lowest possible refinement over the reference wave function. Using $\hat{T} = \hat{T}_1 + \hat{T}_2$ is known as coupled cluster singles doubles (CCSD) method and it scales as sixth order of the basis size[54]. Consecutive addition of excitement levels gives coupled cluster singles doubles and triples (CCSDT), coupled cluster singles doubles triples and quadruples (CCSDTQ) and so on methods.

Another family of methods which account for correlation energy are based on probability and statistics and dubbed quantum Monte-Carlo (QMC)[55,56] methods. The main idea is that a property, which can be written as an expectation value of the trial wave function and has a finite variance, can be found by averaging of a property values obtained on a random set of sampling points. If this property is energy than for a trial

wave function $\psi_0(\{\vec{r}_i\})$

$$E = \frac{\int d\vec{r}\ \psi_0^*(\{\vec{r}_i\})\hat{H}\psi_0(\{\vec{r}_i\})}{\int d\vec{r}\ \psi_0^*(\{\vec{r}_i\})\psi_0(\{\vec{r}_i\})} = \frac{\int d\vec{r}\ \left|\psi_0(\{\vec{r}_i\})\right|^2\left(\psi_0^{-1}(\{\vec{r}_i\})\hat{H}\psi_0(\{\vec{r}_i\})\right)}{\int d\vec{r}\ \left|\psi_0(\{\vec{r}_i\})\right|^2} = \int d\vec{r}\ E_{loc}(\vec{r})P(\vec{r}), \tag{1.40}$$

this energy can be calculated as the integral of the local energy function $E_{loc}(\vec{r}) = \psi_0^{-1}(\{\vec{r}_i\})\hat{H}\psi_0(\{\vec{r}_i\})$ weighted with the probability density[57]

$$P(\vec{r}) = \frac{\left|\psi_0(\{\vec{r}_i\})\right|^2}{\int d\vec{r}\ \left|\psi_0(\{\vec{r}_i\})\right|^2}. \tag{1.41}$$

The resulting total energy is an average of local energies over a set of sampling points. The optimal parameters $\{\vec{r}_i\}$ are obtained upon minimizing the total energy of the system, that is the heart of variational Monte Carlo (VMC)[58,59] method.

A trial function generally based on a Slater determinant, produced either in the framework of the Hartree-Fock theory or in the framework of the LDA approximation to the Kohn-Sham DFT theory. To include correlation effects it multiplies by a suitable correlation function, often taken as Jastrow factor $U(\vec{r})$

$$U(\vec{r}) = \sum_{i>j} u(r_{ij}), \tag{1.42}$$

where $u(r_{ij})$ is a two-body function with the form similar to the potential energy function. Its parameters are variationally optimized during the QMC procedure.

An important extension of the VMC method is the diffusion Monte Carlo (DMC)[12,60,61] method, that deals with the time-dependent Schrödinger equation. In its framework a generalized diffusion equation

$$i\frac{\delta\Psi(\{\vec{r}_i\},t)}{\delta t} = -\frac{1}{2}\frac{\delta^2\Psi(\{\vec{r}_i\},t)}{\delta\{\vec{r}_i\}} + V(\{\vec{r}_i\})\Psi(\{\vec{r}_i\},t). \tag{1.43}$$

is solved. The starting wave function $\Psi(\{\vec{r}_i\},t)$ relates to the complete set of stationary eigenfunctions and eigenenergies of the Hamiltonian 1.3 as

$$\Psi(\{\vec{r}_i\},t) = \sum_k c_k\psi_k(\{\vec{r}_i\})e^{-iE_kt}, \tag{1.44}$$

where c_k are expansion coefficients.

Other QMC approaches include: auxiliary-field Monte Carlo (AFQMC)[62], that seeks for the wave function over a space of single Slater determinants, corresponding to dif-

ferent external potentials (auxiliary filed configurations); path integral Monte Carlo (PIMC)[63,64], that allows for quantum calculations at non-zero temperature; and many others generally based on discussed above methods and improving them[65–72].

The main disadvantage of the QMC methods is the statistical error in the calculated results, that decays with the inverse of square root of the number of sampling points. And statistical uncertainty makes it difficult to calculate nuclear forces and second derivatives[57].

Chapter 2

Solid State Computations

In order to perform an electron structure calculation for atomic or molecular systems one needs to expand the Kohn-Sham wave functions in some suitable basis set. The property of periodicity, which is inherent for solid state systems, restrains the form of one-particle basis sets to a linear combination of Bloch functions:

$$\psi_{\vec{k}}(\vec{r}) = \phi_{\vec{k}}(\vec{r})\ u_{\vec{k}}(\vec{r}). \tag{2.1}$$

Here $u_{\vec{k}}(\vec{r})$ represents some function which bears the same periodic properties as the crystal lattice, and $\phi_{\vec{k}}(\vec{r})$ is a phase factor dependent on the wave vector $\vec{k}$ which generally takes the form of the exponential function $e^{i\vec{k}\vec{r}}$. There are two possible ways to represent the function $u(\vec{r})$ - through combination of localized functions, that leads to a number of approaches such as the Linear Combination of Atomic Orbitals (LCAO) method[73] and the Numerical Atomic Orbitals (NAO) method[74], or through a plane-wave expansion $\sum_{\vec{G}} c_{\vec{k},\vec{G}} e^{i\vec{G}\vec{r}}$, where $\vec{G}$ is a reciprocal lattice vector and $c_{\vec{k}\vec{G}}$ is a set of plane-wave expansion coefficients. In the latter case the wave function (2.1) is rewritten to the form:

$$\psi_{\vec{k}}(\vec{r}) = \sum_{\vec{G}} c_{\vec{k},\vec{G}} e^{i(\vec{k}+\vec{G})\vec{r}}. \tag{2.2}$$

A plane-wave basis set possesses some advantages - it has a simple form, thus the construction of the Hamiltonian matrix is generally much faster than its diagonalization; it is unbiased, thus the resulted wave functions is independent of atom location and do not suffer from the basis set superposition error; its set of expansion coefficients can be easily transformed from reciprocal space to real space and back via the Fast Fourier-Transform (FFT) algorithm. Nevertheless the size of a plane-wave basis set, which is required for adequate description of a given system, is much bigger than in the case of using of localized orbitals and may comprise several ten thousands single plane-waves. The next problem is the failure to describe the high oscillating behavior of a wave function

in the vicinity of nuclei in terms of plane waves. In order to deal with this issue the fact that chemical properties of a compound are strongly dependent only on valence electrons is exploited. That allows one to divide the space in the vicinity of nuclei onto the core electron region and the valence electron region (frozen-core approximation), where the second contains the smooth part of the wave function and can be easily described by a moderate-size set of plane waves. The core electron region comprises all oscillations and can be described either in terms of pseudopotentials or with a method that allows to reproduce multinodal structure of core and valence electron wave functions.

2.1 Pseudopotential Methods

The main idea of the pseudopotential methods is to replace a true atomic potential with a pseudopotential which is capable to reproduce the effects of core electrons on valence states. The rules for construction of a "good" pseudopotential were given by Hamann, Schlüter and Chiang[75,76]:

• The valence all-electron eigenvalues should be equal to their pseudopotential counterparts for all angular momenta

$$\tilde{\epsilon}_l = \epsilon_l. \tag{2.3}$$

• The normalized atomic radial pseudo wave function should coincide with the normalized all-electron wave function $\psi(\vec{r})$ outside the core region, that is characterized by the cutoff radius r_c.

• The logarithmic derivatives of the all-electron and pseudo wave functions agree at r_c.

• The first energy derivative of logarithmic derivatives for the all-electron and pseudo wave functions should agree at r_c as well.

• A true valence charge density should be equal to the pseudo charge density, associated with the given pseudopotential, inside r_c:

$$\int_0^{r_c} dr\ r^2 |\tilde{\psi}_l(\vec{r})|^2 = \int_0^{r_c} dr\ r^2 |\psi_l(\vec{r})|^2. \tag{2.4}$$

The last condition implies the equality of the corresponding wave functions norms, thus it is known as norm-conservation condition. The pseudopotentials which satisfy it are called norm-conserving pseudopotentials[77].

Since the most of the conditions are imposed on a pseudo wave function it is reasonable to construct it first and then the associated pseudopotential. There are a number of available schemes for such constructions – it can be achieved via a fully numerical approach[75,78] or via an almost analytic approach[79]. Once the radial pseudo wave function $\tilde{\psi}_{R,l}(r)$ is ready the total pseudopotential can be constructed via inversion of the radial

Schrödinger equation

$$\tilde{V}_{sc,l}(r) = \epsilon_l - \frac{l(l+1)}{2r^2} + \frac{1}{2r\tilde{\psi}_{R,l}(r)} \frac{d^2}{dr^2}\Big(r\tilde{\psi}_{R,l}(r)\Big), \tag{2.5}$$

where spherical symmetry of the pseudopotential is assumed. The last is often referred as screened pseudopotential, since it bears the screening effect of valence electrons. Finally the "unscreened" pseudopotential, or in other words the bare ionic pseudopotential, is obtained by removing of the exchange-correlation contribution and the contribution due to Coulomb interaction, calculated for the pseudo wave function from the given screened pseudopotential[80,81]. The last is necessary in order to make the given pseudopotential transferable.

At present the most common method for generating norm-conserving pseudopotentials for solids is the one proposed by Troullier and Martins[82,83]. The problem with norm-conserving pseudopotentials arises from the fact that the choice of r_c also has an influence on transferability - the lower the given cutoff the better transferability can be achieved. However r_c could not be lower than the outermost node of the all-electron wave function, otherwise the number of plane waves increase drastically and the pseudopotential becomes much more harder.

Another approach was suggested by Vanderbilt and co-workers[84–86]. Here the condition of norm-conservation is sacrificed to a greater flexibility in the construction of the pseudo wave function. According to this approach the total energy of N valence electrons, described by wave function $\psi_j(\vec{r})$, is given as:

$$E = \sum_i \langle\tilde{\psi}_i|T + V^{NL}|\tilde{\psi}_i\rangle + \int d\vec{r}\; V^L_{ion}(\vec{r})n(\vec{r}) + J[n(\vec{r})] + E_{XC}[n(\vec{r})], \tag{2.6}$$

where T is the kinetic energy operator, V^L is the local (not l-dependent) and V^{NL} is the non-local (l-dependent) components of the pseudopotential.

The scheme for pseudopotential generation, as it described in Ref. (51) and Ref. (53), begins with the generation of a screened all-electron pseudopotential ($V^{AE}(\vec{r})$). Then the Schrödinger equations for each angular momentum at a chosen set of reference energies $\epsilon_{l,j}$, were j is a number of energies in each of such sets, are solved:

$$[T + V^{AE}(\vec{r})]\psi_{l,j}(\vec{r}) = \epsilon_{l,j}\psi_{l,j}(\vec{r}). \tag{2.7}$$

The pseudo wave functions $\tilde{\psi}_{l,i}(\vec{r})$ than is constructed to be as smooth as possible with the only constraint that they join smoothly to $\psi_{l,i}(\vec{r})$ at $r_{c,l}$. In the same time a smooth local potential $V^L(\vec{r})$, which smoothly matches to $V^{AE}(\vec{r})$ at another distance r^L_c, is generated.

From this point a set of specific local orbitals are introduced

$$|\chi_{lj}(\vec{r})\rangle = \Big(\epsilon_{lj} - T - V^L(\vec{r})\Big)|\tilde{\psi}_{lj}(\vec{r})\rangle, \tag{2.8}$$

which allow to define a matrix

$$B_{lj,l'j'} = \langle\tilde{\psi}_{lj}|\chi_{l'j'}\rangle, \tag{2.9}$$

which in turn serves for the construction of another set of local orbitals

$$|\beta_{lj}\rangle = \sum_{l'j'}(B^{-1})_{l'j',lj}|\chi_{l'j'}\rangle. \tag{2.10}$$

The last are the projectors of the nonlocal operator:

$$V^{NL} = \sum_{lj,l'j'} D_{lj,l'j'}|\beta_{lj}\rangle\langle\beta_{l'j'}|, \tag{2.11}$$

where

$$D_{lj,l'j'} = B_{lj,l'j'} + \epsilon_{l'j'}\int d\vec{r}\, Q_{lj,l'j'}(\vec{r}). \tag{2.12}$$

$Q_{lj,l'j'}(\vec{r})$ represents the difference between the true charge density and the pseudo charge density

$$Q_{lj,l'j'}(\vec{r}) = \int d\vec{r}\, \psi^*_{lj}(\vec{r})\psi_{l'j'}(\vec{r}) - \int d\vec{r}\, \tilde{\psi}^*_{lj}(\vec{r})\tilde{\psi}_{l'j'}(\vec{r}), \tag{2.13}$$

and should be equal to 0 in the case of retaining the norm-conservation requirement.

Finally the unscreening procedure, analogous to the unscreening procedure of norm-conserving pseudopotentials described above, is used for obtaining local ionic pseudopotential $V^L_{ion}(\vec{r})$. The unscreened nonlocal pseudopotential is obtained by substitution to the eq. 2.11 the unscreened form of operator $D_{lj,l'j'}$:

$$D^0_{lj,l'j'} = D_{lj,l'j'} - \int d\vec{r}\, V^L_{ion}(\vec{r})Q_{lj,l'j'}(\vec{r}). \tag{2.14}$$

The Vanderbilt procedure, through its complexity, allows one to chose relatively big r_c without worsening the transferability of the constructed pseudopotential. Due to the really moderate number of plane waves required for the calculation with Vanderbilt pseudopotentials, they are also labeled as ultra-soft.

The general problem of the pseudopotential approach is a complete loss of the all-electron wave function nodal structure in the vicinity of nuclei. This issue can be avoided by using other approaches such as one from the family of augmented plane wave methods (APW) or the projector augmented wave (PAW) method.

2.2 Augmented Plane Wave Methods

The whole family stems fromthe original augmented plane wave (APW) method, developed by Slater long ago[87,88]. According to it the space is divided into spheres around each atom α with radius R_α (muffin tin spheres, M) and the interstitial region (I). Then the all-electron wave function adopts the following form:

$$\psi_{\vec{k}}(\vec{r}) = \begin{cases} \frac{1}{\sqrt{V}} \sum_{\vec{G}} c_{\vec{k}+\vec{G}}\ e^{i(\vec{k}+\vec{G})\vec{r}}, & \vec{r} \in I \\ \sum_{lm} A_{lm}^{\alpha,\vec{k}+\vec{G}} u_l^\alpha(r, \epsilon_{l,\vec{k}}) Y_m^l(\hat{r}), & \vec{r} \in M \end{cases} \tag{2.15}$$

Thus the all-electron wave function is represented with plane waves in the interstitial region and via a spherical-harmonics expansion within the muffin tin spheres. The u_l^α is the solution to the atomic radial Schrödinger equation for some energy $\epsilon_l^{\vec{k}}$ while $A_{lm}^{\alpha,\vec{k}+\vec{G}}$ is a $\vec{k}$-dependent parameter. This parameter can be determined from the requirement that plane waves outside muffin tin spheres should match with wave function inside those spheres over all muffin tin spheres surface. For that purpose plane waves can be expanded in terms of spherical harmonics about the origin of the sphere:

$$c_{\vec{k}+\vec{G}}\ e^{i(\vec{k}+\vec{G})\vec{r}} = \frac{4\pi}{\sqrt{V}} c_{\vec{k}+\vec{G}}\ e^{i(\vec{k}+\vec{G})\vec{r}_\alpha} \sum_{lm} i^l j_l\big(|\vec{k}+\vec{G}|R_\alpha\big)\big(Y_m^l(\hat{k+G})\big)^* Y_m^l(\hat{r}), \tag{2.16}$$

where j_l is the Bessel function of order l. Then

$$A_{lm}^{\alpha,\vec{k}+\vec{G}} = \frac{4\pi i^l\ c_{\vec{k}+\vec{G}}\ e^{i(\vec{k}+\vec{G})\vec{r}_\alpha}}{\sqrt{V} u_l^\alpha(R_\alpha, \epsilon_{l,\vec{k}})} j_l\big(|\vec{k}+\vec{G}|R_\alpha\big)\big(Y_m^l(\hat{k+G})\big)^*. \tag{2.17}$$

The main problem with the APW method is the necessity to determine u_l^α for each energy $\epsilon_{l,\vec{k}}$, which in turn are the searched eigenenergies of the problem. This difficulty was mitigated by the Linearized Augmented Plane Wave ((L)APW) method[89], where in the case when $u_{l,0}^\alpha$ is already calculated for some energy ϵ_l^0 all other parameters for nearby energies could be estimated via Taylor expansion:

$$u_l^\alpha(r, \epsilon_{l,\vec{k}}) = u_l^\alpha(r, \epsilon_l^0) + \big(\epsilon_l^0 - \epsilon_{l,\vec{k}}\big) \frac{\partial u_l^\alpha(r, \epsilon_{l,\vec{k}})}{\partial \epsilon_{l,\vec{k}}}\Big|_{\epsilon_{l,\vec{k}}=\epsilon_l^0} + O\big(\epsilon_l^0 - \epsilon_{l,\vec{k}}\big)^2. \tag{2.18}$$

Thus all-electron wave function (2.15) takes the next form:

$$\psi_{\vec{k}}(\vec{r}) = \begin{cases} \frac{1}{\sqrt{V}} \sum_{\vec{G}} c_{\vec{k}+\vec{G}}\ e^{i(\vec{k}+\vec{G})\vec{r}}, & \vec{r} \in I \\ \sum_{lm} \Big(A_{lm}^{\alpha,\vec{k}+\vec{G}} u_l^\alpha(r, \epsilon_l^0) + B_{lm}^{\alpha,\vec{k}+\vec{G}} \frac{\partial u_l^\alpha(r, \epsilon_{l,\vec{k}})}{\partial \epsilon_{l,\vec{k}}}\Big|_{\epsilon_{l,\vec{k}}=\epsilon_l^0}\Big) Y_m^l(\hat{r}), & \vec{r} \in M \end{cases} \tag{2.19}$$

Further improvement may be made by adding to the basis local independent upon $\vec{k}$ orbitals, that leads to LAPW+LO method[90,91] and allows one to account for semi-core states – states, which have the same angular momentum as high lying valence states, but a smaller principal quantum number, and which still contribute to the valence region. Indeed, in the framework of the unmodified (L)APW method it is hard to decide which of two states with the same angular momentum should be chosen as reference in order to make a choice for ϵ_l^0. Local orbitals are introduced as follows:

$$\phi_{lm}^{\alpha,LO}(\vec{r}) = \begin{cases} 0, & \vec{r} \in I \\ \Big(A_{lm}^{\alpha,LO} u_l^\alpha(r,\epsilon_l^0) + B_{lm}^{\alpha,LO} \frac{\partial u_l^\alpha(r,\epsilon_l^0)}{\partial \epsilon_l^0} \\ \qquad + C_{lm}^{\alpha,LO} u_l^\alpha(r,\epsilon_l^1)\Big) Y_m^l(\hat{r}), & \vec{r} \in M \end{cases} \tag{2.20}$$

The energy ϵ_l^0 is the same as in (L)APW basis set, and they are adjusted for the highest of two valence states. The energy ϵ_l^1 corresponds to the lower valence state. The coefficients are determined from the requirement that the local orbitals are normalized and have zero values and zero slope at the muffin-tin boundary[92].

Despite of the fact that the (L)APW method allows one to avoid the energy dependence from basis set, it suffers from larger basis sets. The APW-lo method[91] combines the advantages of APW and (L)APW methods. It is based on two kind of functions – the first one is the APW basis function (Eq. (2.15)), but constructed for some fixed energies, and the second one is another kind of local orbitals:

$$\phi_{lm}^{\alpha,lo}(\vec{r}) = \begin{cases} 0, & \vec{r} \in I \\ \Big(A_{lm}^{\alpha,lo} u_l^\alpha(r,\epsilon_l^0) + B_{lm}^{\alpha,lo} \frac{\partial u_l^\alpha(r,\epsilon_l^0)}{\partial \epsilon_l^0}\Big) Y_m^l(\hat{r}), & \vec{r} \in M \end{cases} \tag{2.21}$$

The energies, used in APW part of basis and local orbitals part of basis, are generally the same. The coefficients $A_{lm}^{\alpha,lo}$ and $B_{lm}^{\alpha,lo}$ are determined by normalization and by the equality to zero of local orbitals at the muffin-tin boundary.

2.3 Projector Augmented Plane Wave Method

The projector augmented plane wave (PAW)[93] method is an exact all-electron method, formally related to ultrasoft pseudopotentials, as it was shown by Kresse and Joubert[94]. The main idea is to reconstruct the nodal structure of the all-electron wave function near nuclei via linear transformation of the smooth corresponding plane wave function extracted from given plane wave calculations:

$$|\psi\rangle = \hat{\tau}|\tilde{\psi}\rangle. \tag{2.22}$$

The general expression for such a transformation has the following form:

$$\psi_{j\vec{k}}(\vec{r}) = \tilde{\psi}_{j\vec{k}}(\vec{r}) + \sum_a \sum_i \left(\varphi_i^a(\vec{r}) - \tilde{\varphi}_i^a(\vec{r})\right) \langle \tilde{p}_i^a(\vec{r}) | \tilde{\psi}_{j\vec{k}}(\vec{r}) \rangle. \tag{2.23}$$

Here index a refers to all atomic sites, i represents simultaneously the quantum angular momentum l, the magnetic quantum number m and the index n, which enumerates radial functions for a given site and angular momentum. $\varphi_i^a(\vec{r})$ is the all-electron partial function, $\tilde{\varphi}_i^a(\vec{r})$ is the pseudo partial function, and $\tilde{p}_i^a(\vec{r})$ is the projector function. All these functions act only within some spherically shaped augmentation region enclosing the corresponding atom, that is analogous to muffin-tin sphere in APW methodology. They can be written as a product of a radial part times a spherical harmonic function:

$$\varphi_i^a(\vec{r}) = \varphi_{nl}^a(r) Y_{lm}(\hat{r}), \tag{2.24a}$$

$$\tilde{\varphi}_i^a(\vec{r}) = \tilde{\varphi}_{nl}^a(r) Y_{lm}(\hat{r}), \tag{2.24b}$$

$$\tilde{p}_i^a(\vec{r}) = \tilde{p}_{nl}^a(r') Y_{lm}(\hat{r'}). \tag{2.24c}$$

The most natural choice for the all-electron partial function is the solution of the Schrödinger equation for isolated atom. The pseudo partial functions should coincide with corresponding all-electron partial functions outside the augmentation region and form a complete set. When those conditions are satisfied, one can choose pseudo partial functions as smooth as possible. The projector function should fulfill the condition $\langle \tilde{p}_i^a(\vec{r}) | \tilde{\varphi}_l^a(\vec{r}) \rangle = \delta_{il}$ and should be localized inside the augmentation region.

It is clear that infinite sets of basis functions can be constructed, however the accuracy of calculations is affected by their choice. The typical scheme for the generation of a "good" set of basis functions may be as follows[95]:

1. At first the Schrödinger equation for an isolated atom or ion is self-consistently solved

   $$H|\varphi_i^0(r)\rangle = \epsilon_i |\varphi_i^0(r)\rangle, \tag{2.25}$$

   that gives the all-electron partial function, which, however, is not orthogonalized, that is underlined by superscript 0.

2. The pseudo partial functions are found by self-consistent solving of another Schrödinger equation:

   $$(\tilde{H} - \epsilon_i)|\tilde{\varphi}_i^0(r)\rangle = C_i k(r) |\tilde{\varphi}_i^0(r)\rangle, \tag{2.26}$$

   where ϵ_i is the same eigenvalues found in Eq.(2.25) and C_i coefficients are adjusted so that $\tilde{\varphi}_i^0(r)$ has a correct number of nodes for a given angular momentum and satisfies the boundary condition, according to which the pseudo partial function

and the all-electron partial function should match outside the augmentation region r_c. The Hamiltonian $\tilde{H}$ has the form:

$$\begin{aligned} \tilde{H} &= T+\tilde{v}_L(r) + J[\tilde{n}(r) + n'(r)] + E_{XC}[\tilde{n}(r)], \\ \tilde{n}(r) &= \sum_i \theta_i \frac{|\tilde{\varphi}_i^0(r)|^2}{4\pi r^2}. \end{aligned} \tag{2.27}$$

θ_i denotes the occupancy of a given orbital, $n'(r)$ is a compensation charge density, aimed to correct the total atomic charge. $v^L(r)$ is the local potential that vanishes outside the augmentation region. It can take the form $\nu_0 k(r)$, where nu_0 is some amplitude, and $k(r)$ is a shape function that can take a number of forms. One of the possible choices is the sinc function:

$$k(r) = \begin{cases} [\frac{\sin(\pi r/r_c)}{\pi r/r_c}]^2 & r < r_c, \\ 0 & r \geq r_c. \end{cases} \tag{2.28}$$

3. The projector functions can be formed via relation:

$$|\tilde{p}_i^0(r)\rangle = \frac{k(r)|\tilde{\varphi}_i^0(r)\rangle}{\langle\tilde{\varphi}_i^0(r)|k(r)|\tilde{\varphi}_i^0(r)\rangle} \tag{2.29}$$

4. The final set of basis functions are formed by a Gram-Schmidt orthogonalization procedure of the functions $|\varphi_i^0(r)\rangle$, $|\tilde{\varphi}_i^0(r)\rangle$ and $|\tilde{p}_i^0(r)\rangle$ [93].

If one opens the braces in equation (2.23) and makes substitutions

$$\chi^a_{j\vec{k},i}(\vec{r}) = \varphi^a_i(\vec{r})\langle\tilde{p}^a_i(\vec{r})|\tilde{\psi}_{j\vec{k}}(\vec{r})\rangle, \tag{2.30a}$$

$$\tilde{\chi}^a_{j\vec{k},i}(\vec{r}) = \tilde{\varphi}^a_i(\vec{r})\langle\tilde{p}^a_i(\vec{r})|\tilde{\psi}_{j\vec{k}}(\vec{r})\rangle, \tag{2.30b}$$

it becomes clear that the all-electron wave function is represented as the algebraic sum of three independent components

$$\psi_{j\vec{k}}(\vec{r}) = \tilde{\psi}_{j\vec{k}}(\vec{r}) + \sum_a \sum_i \chi^a_{j\vec{k},i}(\vec{r}) - \sum_a \sum_i \tilde{\chi}^a_{j\vec{k},i}(\vec{r}). \tag{2.31}$$

In the PAW method it is possible to represent any semilocal observable quantity as the sum of three independent components, completely analogously to the expression (2.31).

Chapter 3

Chemical Bonding Analysis of Solids and Molecules

The aim of chemical-bonding analysis is to reveal the peculiarities of interatomic interactions within the investigated compound, thus connecting them to physical and chemical properties. It is obvious that while talking about chemical-bonding analysis the concepts of chemical bonds and their order will inevitably be touched.

The first definition of the chemical bond by Lewis is dated back to 1916[96], when he also has suggested the formula for representation of covalent bonds, know as Lewis structure. Localized between two atoms, bonds were represented as a pair of electrons placed between bonded atoms, the number of pairs determined the order of a bond. Popular even until nowadays, this consideration of chemical bonding allows one to make only qualitative predictions and overlooks lone pairs. The last is covered with valence shell electron pair repulsion (VSEPR) theory[97,98], in the framework of which the tendency of valence electron pairs to repel each other is considered. However both technique do not account for bonding in metals and in conjugated systems.

With the advent of quantum chemistry the concepts of chemical bond and bond order were connected to the concept of molecular orbitals. Indeed, in the simple case of a two-center molecular orbital $|\psi\rangle = c_1|\chi_1\rangle + c_2|\chi_2\rangle$ one can get the picture of the electron distribution by taking the square of a given wave function:

$$\int |\psi|^2 d\tau = c_1^2 + c_2^2 + 2P_{12}. \tag{3.1}$$

$P_{12} = S_{12}D_{12} = c_1^* c_2 \langle\chi_1|\chi_2\rangle$ is called an overlap population and obviously describes the degree of interaction between the two given centers. In the general case, for a set of multi-center molecular orbitals, one should deal with the set of P_{ij} elements which form the matrix. Terms S_{ij} and D_{ij} are called correspondingly overlap and density matrices.

According to Mayer[99] the bond order can be determined with the equation:

$$B_{R_1R_2} = \sum_{i\in R_1}\sum_{j\in R_2}(SD)_{ij}(SD)_{ji}, \tag{3.2}$$

where the summation is carried out for all basis orbitals centered on atoms R_1 and R_2.

In chemical bonding analysis, a widely used concept is the n-order reduced density matrices

$$\Gamma^n(\vec{r}_1,...\vec{r}_n;\vec{r}'_1,...\vec{r}'_n) = \binom{N}{n}\int d\vec{r}_{i>n}\ \sum_\sigma \psi^{\sigma *}(\vec{r}'_1,...,\vec{r}'_n,\vec{r}_{n+1},...\vec{r}_N) * \psi^\sigma(\vec{r}_1,...,\vec{r}_n,...\vec{r}_N). \tag{3.3}$$

on the basis of which the n electron density can be defined as

$$\rho^n(\vec{r}_1,...\vec{r}_n) = \Gamma^n(\vec{r}_1,...\vec{r}_n;\vec{r}_1,...\vec{r}_n). \tag{3.4}$$

It evaluates to the probability of finding n electrons at positions $\vec{r}_1$,..$\vec{r}_n$ while all other electrons have arbitrary positions.

It is a widely discussed question which interactions should be regarded as chemical bonds, and which not. Weak interactions, like van der Waals forces, are not considered by many as chemical bonds, however, there is an opinion, that such definition of a chemical bond is "too restrictive and does not account for the physics underlying the processes of atomic and molecular interactions"[100].

Moreover from the quantum mechanical point of view, there is no such thing as "chemical bond", since there is no operator associated with that. There is no qualitative way to separate one kind of interaction from another and one should govern only with the quantitative picture of an electron distribution.

However, the concepts of covalent, ionic and metallic bonding are found to be still useful and will be used for underlying of the main particularities of particular interatomic interaction, such as the amount of electrons involved into it, the degree of their localization in between participating atoms, the number of atomic sites and so on.

3.1 Orbital Based Methods

In the framework of orbital based methods, electrons are associated with orbitals, centered on corresponding nuclei. Such point of view is especially useful for molecular systems, where atomic centered basis functions are used. In solid systems, the orbitals based chemical bonding analysis is generally performed in conjunction with a linear

combination of atomic orbitals.

3.1.1 Natural orbital analysis

It is worth to mention the family of methods which aim to represent the charge distribution in terms of orbitals, inspired by the concept of natural orbitals (NOs), which are defined as eigenfunctions of the first-order reduced density operator[101]:

$$\rho^1(\vec{r}_1, \vec{r}_1') = \int \psi^*(\vec{r}_1', \vec{r}_2, ...\vec{r}_N)\psi(\vec{r}_1, \vec{r}_2, ...\vec{r}_N)d\vec{r}_2...d\vec{r}_N, \tag{3.5}$$

that is the probability of finding an electron in position $\vec{r}_1$ while all other electrons have arbitrary positions. The corresponding eigenfunctions, which form a complete orthonormal set, are determined during the process of its diagonalization.

On the basis of the NO concept other techniques, aiming to prescribe electrons to atomic and molecular orbitals, are build. One of the representative is the concept of natural atomic orbitals (NAOs), which are constructed from atomic angular symmetry subblocks of the density matrix, localized on a particular atom[102−104]. Thus diagonalization is performed not over the whole reduced density matrix, but over specific subblocks, each comprising only those functions, which are centered at specific atomic sites. Orbitals, which are derived in such a way, are called the pre-orthogonal NAOs (PNAOs). They are orthogonal to each other within the parent atomic site, but non-orthogonal to orbitals, centered at other atomic sites. PNAOs may be used for the investigation of chemical-bonding peculiarities, since the information concerning interatomic interaction can be accessed via the overlap integrals between PNAOs that are belong to the atoms of interest. However, general non-orthogonality of the resulting orbitals violates the process of prescribing charges to specific atoms - the resulting charge from summation of PNAOs occupancies may be different from the initial number of electrons. Thus it is necessary to continue the process of diagonalization and extend the orthogonality condition to PNAOs which originate at different atomic sites. The resulting set of orbitals is referred as NAOs. Those orbitals possess occupations between 0 and 2 and sum up to well defined atomic charges. Generally highly occupied NAOs (>1.90) recover 99% of the total electron population, thus taking into account only those orbitals a Lewis-like electron pairs picture can be drawn.

The concept of natural bond orbitals (NBOs)[102, 105] is inseparable from NAOs. They are localized, few-center orbitals that describe molecular bonding pattern of electron pairs. Formally the NBO between two atomic centers A and B is represented in terms of two directed valence hybrids (NHOs) h_A, h_B with the corresponding polarization

coefficients c_A, c_B:

$$\sigma_{AB} = c_A h_A + c_B h_B, \tag{3.6}$$

where each NHO being an optimized linear combination of NAOs on the given center - $h_A = \sum_k a_k \theta_k^A$, and coefficients c_A and c_B satisfying $c_A^2 + c_B^2 = 1$. Two limiting conditions $c_A = c_B$ and $c_A \gg c_B$ correspond respectively to covalent and ionic limits. The procedure of generating of NBOs includes at first the removal from the density matrix core and lone pairs the NAOs contributions (in other words all orbitals with occupancy higher than 1.90) with further diagonalization of two-by-two subblocks (i.e. blocks which corresponds to pairs of atoms) of the density matrix. The criteria for accepting the NBO can vary until the sum of occupation number for bond, core and lone pairs orbitals will not sum up to the total number of electrons. Once NBOs are determined they may be written as the combination of NAOs, giving a picture which atomic orbitals are participating in the bonding[106].

Further development leads to the concept of natural localized molecular orbitals (NLMOs)[107], which resemble NBOs but are able to capture delocalization peculiarities caused by the chemical environment. Generally lone pair and core NBOs possess occupancy slightly lower than 2 thus reflecting some order of delocalization. This delocalization rate is captured by other NBOs with generally low occupancy. The combination of well occupied NBO σ_i with corresponding low occupied NBOs σ_j forms NLMO:

$$\omega_i = \eta(\sigma_i + \sum_j \sigma_j). \tag{3.7}$$

Here η refer to the normalizing constant. The resulting NLMOs have occupation number very close to 2 and can adopt the characteristic bonding pattern.

Finally the concept of NBOs can be extended to the multicenter two-electron bonds with adaptive natural density partitioning (AdNDP)[108] approach in the framework of which the diagonalization of n-atomic subblocks is performed. The resulting set of eigenvectors with occupancies higher than predetermined threshold is accepted as n-center 2-electron bonds.

3.1.2 Energy-resolved partitioning

While dealing with crystalline compounds it is useful to determine the contribution to the overlap population of each individual crystal orbital. The concept of crystal orbital overlap population (COOP)[109,110] provides one with such quantities, which can be extracted for each atom pairs. The COOP may be regarded as "weighted" density of states (DOS): in the particular energy range the total DOS is weighted by the contribution to

the overlap population made by the crystal orbital of interest. Representing a wave function as linear combination of atomic centered orbitals $|\psi_j\rangle = \sum_{R_l} c_{R_l j}|\chi_{R_l}\rangle$, where R_l denotes both atomic sites in the primitive cell and the orbitals defined by quantum numbers l and m, and introducing the DOS matrix[111]

$$P_{R_l R'_l}(E) = \sum_j f_j \delta(\epsilon - \epsilon_j) c^*_{R_l j} c_{R'_l j}, \tag{3.8}$$

COOP is defined as

$$COOP_{R_l R'_l} = P_{R_l R'_l}(E) D_{R_l R'_l}, \tag{3.9}$$

f_j is the electron occupation of the band j, and $D_{R_l, R'_l} = \langle \chi_{R_l} | \chi_{R'_l} \rangle$ is the overlap matrix. The integration of the COOP curve for a particular atom pair should reveal the total overlap population between those atoms, which is scaled to the bond order[110]. COOP is negative for antibonding states, positive for bonding ones and equal to zero in the case of nonbonding interactions[110,111].

In a similar way the crystal orbital Hamiltonian population (COHP)[112] concept could be introduced. COHP is determined via the equation:

$$COHP_{R_l R'_l} = P_{R_l R'_l}(E) H_{R_l R'_l}, \tag{3.10}$$

from which it is clear, that the only difference from equation (3.9) is substitution of density matrix elements with Hamiltonian matrix elements. COHP determines the level to which a given covalent bond contributes to the total binding energy in crystal. Opposite to COOP negative, a sign of the COHP indicates a bonding contribution, while positive - an antibonding one.

Two main problems arise from such analysis. The first one is prescribed to COHP and concerns its non-invariance regarding to the shift of electrostatic potential for extended systems[112,113]. For finite systems the electrostatic potential is dependent on boundary conditions. When an infinite system is constructed from a given finite one the contribution to the total electrostatic potential from the boundary conditions (sometimes called the termination constant) is not universe, but different for different systems. Thus setting the electrostatic potential to zero – that is the usual thing for a majority of density functional calculations for periodic systems – can result in different, but not unique, energy shifts for different systems. The second problem concerns both COOP and COHP: both concepts are basis dependent and tend to give good results only for methods that use minimal and well localized basis sets.

In order to expand COOP concept to less localized basis sets the balanced crystal overlap population (BCOOP)[114] technique was introduced. In its framework the COOP

is additionally weighted by the balanced overlap population:

$$BCOOP_{R_lR'_l} = \sum_j f_j\delta(\epsilon-\epsilon_j)\frac{\sum_{\alpha\in R_l}\sum_{\alpha'\in R'_l} c^*_{\alpha j}c_{\alpha' j}D_{\alpha\alpha'}}{\sum_{R_l}\sum_{\beta,\beta'\in R_l} c^*_{\beta j}c_{\beta' j}D_{\beta\beta'}}, \tag{3.11}$$

where α and β represent a set of quantum numbers for a specific atomic center R.

To use the COOP/COHP concepts one need to have atomic-centered basis set. However it was shown that the usage of a plane wave basis set is also possible. For that propose plane waves should be projected onto the corresponding local orbitals, that is made in the framework of the projected crystal orbital Hamiltonian population (pCOHP)[115] technique. pCOHP assumes that the band wave function $\psi_{j\vec{k}}(\vec{r})$ may be approximately written as a combination of atom-centered, orthonormal one-electron functions (local orbitals) $\phi_\mu(\vec{r})$

$$\psi_{j\vec{k}}(\vec{r}) \approx c_{j\vec{k}R_l}\phi_{R_l}(\vec{r}) + c_{j\vec{k}R'_l}\phi_{R'_l}(\vec{r}) + ... \tag{3.12}$$

Thus the set of overlap elements (called by authors "transfer matrix") between band wave functions and local orbitals can be calculated:

$$T_{j\vec{k},R_l} = \langle\psi_{j\vec{k}}|\phi_{R_l}\rangle, \tag{3.13}$$

and the projected density matrix can be constructed:

$$P^{proj}_{j\vec{k},R_lR'_l} = T^*_{j\vec{k},R_l}T_{j\vec{k},R'_l}, \tag{3.14}$$

which should bear the same chemical information as the density-matrix for a local atomic-centered basis. Further rewriting the Hamiltonian matrix elements in terms of local orbitals leads to the expansion of the plane wave Hamiltonian:

$$H^{proj}_{\vec{k},R_lR'_l} = \langle\phi_{R_l}|H^{pw}|\phi_{R'_l}\rangle = \sum_j \epsilon_j T^*_{j\vec{k},R_l}T_{j\vec{k},R'_l}. \tag{3.15}$$

Finally the pCOHP is written as follow:

$$pCOHP_{\vec{k},R_lR'_l} = \sum_j f_j\delta(\epsilon-\epsilon_j)\Re\Big[P^{proj}_{j\vec{k},R_lR'_l}H^{proj}_{\vec{k},R_lR'_l}\Big]. \tag{3.16}$$

The concept of COOP/COHP and its derivatives are recommended well for a number of complex compounds, however, one should keep in mind the above expressed limitations and be careful.

3.1.3 Wannier functions

Another type of chemical bonds description is based on Wannier functions[116] and naturally developed for crystalline compounds described in plane wave basis set:

$$w_0(\vec{r}) = \frac{V}{(2\pi)^3} \int_{BZ} d\vec{k}\ \psi_{n\vec{k}}(\vec{r}). \tag{3.17}$$

It is possible to construct from in such a way determined Wannier functions the localized Wannier orbitals (LWOs), which form an orthonormal set of orbitals, localized at a given site $\vec{R}$. Despite seeming simplicity, there are several difficulties. The first one is the smoothness of initial plane wave set – since Wannier functions are determined via Fourier transformations, truly localized results may be achieved only from a very smooth plane wave based wave function, that is generally not the case. Bloch functions can be made smooth due to their gauge freedom – any Bloch functions $\psi_{n\vec{k}}(\vec{r})$ can be replaced with the expression $e^{i\phi_n(\vec{k})}\psi_{n\vec{k}}(\vec{r})$, where $\phi_n(\vec{k})$ any real function that is periodic in reciprocal space. But here the second difficulty emerges – different choices of gauge form lead to different sets of Wannier functions with different shapes and spread[117].

One way to construct reliable Wannier orbitals was purposed by Marzari and Vanderbilt, and was called maximally localized Wannier functions (MLWF) method[118]. Here $\phi_n(\vec{k})$ represented in the form of matrix and is found by an iterative minimization procedure of the localization functional[119]

$$\Omega = \sum_n \left[\langle u_{n0}|r^2|u_{n0}\rangle - \langle u_{n0}|r|u_{n0}\rangle^2\right], \tag{3.18}$$

which measures the sum of the quadratic spreads of the Wannier functions in the home unit cell around their centers.

The problems with Wannier functions begin to emerge when one deals with the systems, in which bands are not separated from each other by energy gaps, but extensively overlap and hybridize with other bands. In this case it is difficult to chose an appropriate states from which Wannier functions should be generated. The procedures for overcoming of this problem include the choice of a subspace, where it is possible to form an isolated sets of bands from a linear combination of the given states[117,120]. But the whole procedure is may be regarded as some state of the art and requires a lot of accuracy from the researcher when a chemically meaningful results are desired.

3.2 Real Space Methods

Contrary to the orbital based methods, the real space methods are concentrated on the analysis of a real space property field, where atoms are defined as regions of space via the topology of this field. A lot of those methods are based on the analysis of the pair density. The latter can be written in terms of two independent particle densities plus a wave function dependent correlation part:

$$\rho_2^{\sigma_1\sigma_2}(\vec{r}_1,\vec{r}_2) = \rho^{\sigma_1}(\vec{r}_1)\rho^{\sigma_2}(\vec{r}_2) - |\sum_i \psi_i^{\sigma_1 *}(\vec{r}_1)\psi_i^{\sigma_2}(\vec{r}_2)|^2, \tag{3.19}$$

or, alternatively, with introducing the correlation factor $f^{\sigma_1\sigma_2}(\vec{r}_1,\vec{r}_2)$:

$$\rho_2^{\sigma_1\sigma_2}(\vec{r}_1,\vec{r}_2) = \rho^{\sigma_1}(\vec{r}_1)\rho^{\mu}(\vec{r}_2) - \rho^{\sigma_1}(\vec{r}_1)\rho^{\sigma_2}(\vec{r}_2)f^{\sigma_1\sigma_2}(\vec{r}_1,\vec{r}_2). \tag{3.20}$$

The importance of the last can be underlined by introducing the concept of *conditional probability*, which determine the probability of finding electron at the position $\vec{r}_2$ while the second electron is certainly located at the position $\vec{r}_1$:

$$\rho_c^{\sigma_1\sigma_2}(\vec{r}_1,\vec{r}_2) = \frac{\rho_2^{\sigma_1\sigma_2}(\vec{r}_1,\vec{r}_2)}{\rho^{\sigma_1}(\vec{r}_1)}. \tag{3.21}$$

If there are totally N electrons in a given system, than the conditional probability (3.21) should integrate to $N-1$ [121]. The difference between conditional probability and the probability of finding an electron at the position $\vec{r}_2$ leads to the concept of *exchange-correlation hole*:

$$h_{XC}^{\sigma_1\sigma_2}(\vec{r}_1,\vec{r}_2) = \frac{\rho_2^{\sigma_1\sigma_2}(\vec{r}_1,\vec{r}_2)}{\rho^{\sigma_1}(\vec{r}_1)} - \rho^{\sigma_2}(\vec{r}_2) = \rho^{\sigma_2}(\vec{r}_2)f^{\sigma_1\sigma_2}(\vec{r}_1,\vec{r}_2). \tag{3.22}$$

Exchange-correlation hole can be split on two parts - the one which accounted for same spin electrons, and the one which accounted for different spin electrons:

$$h_{XC}^{\sigma_1\sigma_2}(\vec{r}_1,\vec{r}_2) = h_X^{\sigma_1=\sigma_2}(\vec{r}_1,\vec{r}_2) + h_C^{\sigma_1\neq\sigma_2}(\vec{r}_1,\vec{r}_2). \tag{3.23}$$

The first part is called *Fermi hole*, while the second - *Coulomb hole*.

3.2.1 Quantum theory of atoms in molecules

Quantum theory of atoms in molecules (QTAIM) [122] is based on the topological analysis of the electron density, that allows to partition the whole space into spacial domains and

provides with chemically viable definitions of atoms and bonds between them.

QTAIM relays on the fact, that taking at some point the gradient vector of a scalar property field directs towards the increase of the a given property in value. Thus building a gradient vector trajectory it is possible to recover a point with the maximum value of a given property (attractor). In QTAIM the role of such a scalar property field plays an electron density, that is following the electron density gradient vector trajectory one should end up at the point characterized by maximum of the charge density, which generally should coincide with the position of a nucleus. In the framework of QTAIM a region of space, which comprises all trajectories that terminates at a given nucleus, is called basin, and the union of a basin and its attractor defines an atom. In a polyatomic molecule each atom is separated from other adjoining atoms by zero flux surface - a surface where the boundary condition

$$\vec{\nabla}\rho(\vec{r})\vec{n}(\vec{r}) = 0 \tag{3.24}$$

is satisfied. The special meaning is attributed to points, where the first derivative of the electron density vanishes - the so-called critical points. The type of a critical point could be determined from the analysis of the second derivative of the electron density at this point, that results in the Hessian matrix with nine individual components. After its diagonalization only three non-zero diagonal elements remain $\{\partial^2\rho/\partial x^2, \partial^2\rho/\partial y^2, \partial^2\rho/\partial z^2\}$. Different combinations of their sings give rise to four types of critical points:

- all three negative: local maximum of $\rho(\vec{r})$ - nuclear critical point;
- two negative values and one positive: local maximum of $\rho(\vec{r})$ in the plane defined by corresponding eigenvectors but minimum along the line perpendicular to this plane - bond critical point;
- one negative value and two positive: local minimum of $\rho(\vec{r})$ in the plane defined by corresponding eigenvectors but maximum along the line perpendicular to this plane - ring critical point;
- all three positive: local maximum of $\rho(\vec{r})$ - cage critical point.

Nuclear critical points are defined above attractors and generally they are associated with nuclei, although there are some cases with non-nuclear attractors[123]. Bond critical points generally appear at zero flux surfaces, and electron density gradient trajectories drawn from this points to nuclei of the corresponding adjoining basins generally form a line which is called bond path. Ring critical points always placed within the ring, formed by bonded atoms. Cage critical points generally appear within regions, enclosed by several atom rings.

It is worth to note that the presence of a bond path between two atoms indicates that

they are bonded with each other in QTAIM sense[124], but does not imply the forming of chemical bond, defined in traditional way (for example, on the basis of Lewis or VSPER models)[100,125]. One way to look a bond path is to consider it as a privileged exchange energy channel[126].

Thus QTAIM provides with the unambiguous method for partitioning of a whole space into chemically meaningful properties additive domains with its own definition of chemical bonding. However such definition does not give answer to the question how strong the interaction between directly bonded and non-bonded atoms is, and it fails in the case of multicenter bonding[127].

3.2.2 Two electron domain space partitioning: Electron localization function and electron localizability indicators.

Conditional probability function bears information about how the known location of one electron affect on the probability of finding another electron elsewhere in the space. In other words, if the conditional probability function for same spin electrons experienced minimum at some region, it means, that within this region one electron is already well localized and due to the Pauli principle there is no place for a second electron. Therefore, analyzing the short-range behavior for a position $\vec{r}_2$ approaching the reference position $\vec{r}_1$, electron localization domains could be revealed. With this aim a conditional probability (3.21) could be expressed via the Taylor expansion[128]:

$$\begin{aligned}\rho_c^{\sigma\sigma}(\vec{r}_1,\vec{r}_2) &\approx \Big(1+\vec{s}\,\vec{\nabla}_{\vec{r}_2}+\frac{1}{2}(\vec{s}\,\vec{\nabla}_{\vec{r}_2})^2+...\Big)\rho_c^{\sigma\sigma}(\vec{r}_1,\vec{r}_2)|_{\vec{r}_2\to\vec{r}_1}\\ &\approx e^{\vec{s}\,\vec{\nabla}_{\vec{r}_2}}\rho_c^{\sigma\sigma}(\vec{r}_1,\vec{r}_2)|_{\vec{r}_2\to\vec{r}_1}.\end{aligned} \tag{3.25}$$

Here $\vec{s}=\vec{r}_2-\vec{r}_1$ and the gradient acts only on the coordinates $\vec{r}_2$.

After considering only the spherically average case (that is the exchange-correlation hole is assumed to be spherical) and limiting themselves only with the second order term, Becke[128] derived the final expression of the equation (3.25) for the one-determinant wave function:

$$\overline{\rho}_c^{\sigma\sigma}(\vec{r},s)=\rho_c^{\sigma\sigma}(\vec{r}_1,\vec{r}_2)|_{\vec{r}_2\to\vec{r}_1}+\frac{1}{6}\Big(\vec{\nabla}^2\rho^\sigma(\vec{r})-2\tau^\sigma(\vec{r})+\frac{1}{2}\frac{|\vec{\nabla}\rho^\sigma(\vec{r})|^2}{\rho^\sigma(\vec{r})}\Big)s^2+... \tag{3.26}$$

The first term is equal to zero, since the probability of finding an electron at some position, where the other electron with the same spin is already placed, is equal to 0.

Lately Becke and Edgecombe[129] have taken the expression

$$g^{\sigma}_{ELF}(\vec{r}) = \tau^{\sigma}(\vec{r}) - \frac{1}{4}\frac{|\vec{\nabla}\rho^{\sigma}(\vec{r})|^2}{\rho^{\sigma}(\vec{r})} \tag{3.27}$$

as a measure for analyzing the electron localization information. The lower the value of $D^{\sigma}(\vec{r})$ for a given region, the stronger the localization of electrons within it. The authors proposed the definition of the electron localization function (ELF):

$$\gamma^{\sigma}(\vec{r}) = \Big(1 + \big(\frac{g^{\sigma}_{ELF}(\vec{r})}{g^{\sigma}_{0}(\vec{r})}\big)^2\Big)^{-1}, \tag{3.28}$$

where $g^{\sigma}_{0}(\vec{r}) = \frac{3}{5}(6\pi^2)^{2/3}\big(\rho^{\sigma}(\vec{r})\big)^{5/3}$ is defined for the uniform electron gas with the same electron density, as in the system. ELF (3.28) is defined between 0 and 1 and "reverse" regarding to the expression (3.27), that is it has not low but high values (close to 1) within well localized regions.

Another formulation of ELF was proposed by Savin at al[130]. They used the fact, obtained by Tal and Bader[131], that kinetic energy density cannot exceed the threshold value $\frac{1}{8}\frac{|\vec{\nabla}\rho(\vec{r})|^2}{\rho(\vec{r})}$. They introduced a kinetic energy density $\tau^{\sigma}(\vec{r}) = \sum_i |\vec{\nabla}\psi^{\sigma}_i(\vec{r})|^2$ and redefined g_{ELF} as

$$g_{ELF}(\vec{r}) = \tau(\vec{r}) - \frac{1}{8}\frac{|\vec{\nabla}\rho(\vec{r})|^2}{\rho(\vec{r})}. \tag{3.29}$$

This definition bears the same qualitative information concerning electron localization properties. Note, this equation deals with the total electron density as well as with the kinetic energy density for both spins, assuming the close-shell system under consideration. The minimum value occurs only when the orbitals are proportional to the quadratic square of electron density and that is possible no more than for two orbitals. The main advantage of such formulation is in fact that now ELF is independent from the spin and can be used in the framework of DFT, for which pair density is not explicitly defined and thus the first formulation is not workable.

ELF provides meaningful and understandable chemical information. It is particularly good for revealing atomic shell structures[129,132] and provides a pictorial representation of bonding and lone pairs regions[133].

Electron localizability indicators (ELI)[134–139] propose another possibility for atomic shell and bonding analysis. The main idea of ELI is to divide the whole space into a number of non overlapping domains, each of them contains the same predetermined value of some quantity μ (control property). The integration of an other quantity ν (sampling property) over these domains leads to the discrete distribution of ν. In initial formulation of ELI (named ELI-q[134]) a charge of σ-spin electrons was chosen as a control

property, while the place of a sampling property was taken by the pair density. With such a choice of control and sampling properties the integral of the pair density

$$D_{2,q}^{\sigma\sigma}(\Omega) = \int_{\Omega}\int_{\Omega} \rho_2^{\sigma\sigma}(\vec{r}_1, \vec{r}_2) d\vec{r}_1 d\vec{r}_2 \tag{3.30}$$

determines the same-spin electron localization degree within every space domain Ω, or alternatively, in each point of space if domains were chosen so small and compact, that they could be referenced by a single point. Indeed, the amount of charge q^σ within the space domain Ω depends on the probability of finding some number of σ-spin electrons within that domain. If $q^\sigma < 1$ and it originates from only one σ-spin electron, then, in the case of perfectly localized σ electron and consequently a highly correlated motion of σ-spin electrons, $D_{2,q}^{\sigma\sigma}(\Omega)$ should be equal to zero. In the case of totally uncorrelated motion of electrons, when each σ-spin electron contributes equally to q^σ within domain Ω, $D_{2,q}^{\sigma\sigma}(\Omega) = (q^\sigma)^2/2$.

Kohout[134] introduced ELI-q as reverse value to the integrated pair density, similarly to the definition of ELF as reverse to the integrated conditional probability,

$$\gamma_q^\sigma(\vec{r}) = \frac{1}{1 + \left(c_q D_{2,q}^{\sigma\sigma}(\Omega, \vec{r})\right)^2}. \tag{3.31}$$

Since the value of $D_{2,q}^{\sigma\sigma}(\Omega)$ depends on chosen spin charge q^σ, a variable c_q was introduced aiming to remove this dependency. It was shown[134] that this variable is proportional to $(q^\sigma)^{8/3}$. The dependence of $D_{2,q}^{\sigma\sigma}(\Omega)$ from $\vec{r}$ in expression (3.31) indicates the point around which the space region Ω was build and to which this domain should be referenced.

In another variation of ELI (named ELI-D[135,137,138]) the same-spin electron pairs (3.30) were used as the control property, that is the space was divided into small domains, each of which contains some fixed fraction of same-spin electron pairs. A sampling property is then the spin density. Integrating it over the defined domains yields a discrete distribution of charge of σ-spin electrons. Thus, ELI-D actually represents a discrete distribution of values $\gamma_D^\sigma(\vec{r}_1), \gamma_D^\sigma(\vec{r}_2), \gamma_D^\sigma(\vec{r}_3), ...$ proportional to the determined spin charges.

It was shown[135] that the amount of spin charge contained within small domain is approximated by

$$Q^\sigma(\vec{r}) \approx \left(D_2^{\sigma\sigma}\right)^{3/8} \left(12 \frac{\left(\rho^\sigma(\vec{r})\right)^{8/3}}{g^\sigma(\vec{r})}\right)^{3/8}, \tag{3.32}$$

where g^{σ}_{ELI} is the Fermi hole curvature[140] and has rather similar form to the key component in definition of ELF (3.27):

$$g^{\sigma}(\vec{r}) = \rho^{\sigma}(\vec{r})\tau(\vec{r}) - \frac{1}{4}\left|\vec{\nabla}\rho^{\sigma}(\vec{r})\right|^2. \tag{3.33}$$

ELI-D is taken as same-spin pair independent part of equation (3.32):

$$\gamma^{\sigma}_{D}(\vec{r}) = \rho^{\sigma}(\vec{r})\Big(\frac{12}{g^{\sigma}(\vec{r})}\Big)^{3/8}. \tag{3.34}$$

Other variations of ELI include extensions to antiparallel-spin pairs (ELIA)[136] or tripled-coupled electrons[139].

Generally ELI is able to recover the same atomic shell structures and bonding pictures as ELF, but it is free from somewhat artificial references to uniform electron gas and extendable to correlated wave functions.

3.2.3 Localization and delocalization indices and domain averaged Fermi hole analysis

Localization and delocalization indices[141,142] allow to evaluate how many electrons are localized inside some basin and how many electrons are delocalized from a given basin to another basin. In the present context, the term "electron delocalization" means the measure of the amount of electrons that shared between the two chosen space domains.

To understand the concept of the localization index $\lambda(\Omega)$ one needs to investigate the double integral of the pair density over the domain Ω, that gives the average amount of electron pairs within this domain:

$$D^{\sigma\sigma}_{2}(\Omega) = \int_{\Omega}\int_{\Omega}\rho^{\sigma\sigma}_{2}(\vec{r}_1,\vec{r}_2)d\vec{r}_1 d\vec{r}_2 = \Big(\big(N^{\sigma}(\Omega)\big)^2 + F^{\sigma\sigma}(\Omega,\Omega)\Big)/2. \tag{3.35}$$

Here and further only same-spin electrons will be considered. Unlike to space domains in Eq. (3.30), in the present equation Ω represents the atom in QTAIM sense. The division by 2 is performed since the only one kind of spin is considered. $N^{\sigma}(\Omega)$ is the electron population of a given atom, while $F^{\sigma\sigma}(\Omega,\Omega)$ is an integrated over space domain Ω Fermi hole. Formally the latter insures that the pair density will integrate to the correct number of electrons by removing the self-pairing contribution. If Ω covers all space, then $F^{\sigma\sigma}(\Omega,\Omega) = -N^{\sigma}$ and $D^{\sigma\sigma}_{2}(\Omega) = N(N-1)/2$. For a given atom, if $F^{\sigma\sigma}(\Omega,\Omega)$ is equal to the limiting number of electrons $-N^{\sigma}(\Omega)$, then all electrons should be considered as perfectly localized within the corresponding atomic basin. From this consideration it is clear that the magnitude of $F^{\sigma\sigma}(\Omega,\Omega)$ could be taken as a measure

of electron localization - and that is the definition of the localization indices. For the one-determinant Ansatz based on orbitals $\{\psi_i^\sigma(\vec{r})\}$, localization indices are expressed via overlap integrals $S_{ij}^{\sigma\sigma}(\Omega)$:

$$\begin{aligned} \lambda^\sigma(\Omega) &= 2\sum_{i,j} n(\theta_i^\sigma)n(\theta_j^\sigma)S_{ij}^{\sigma\sigma}(\Omega)S_{ji}^{\sigma\sigma}(\Omega), \\ S_{ij}^{\sigma\sigma}(\Omega) &= \int_\Omega \psi_i^{\sigma*}(\vec{r})\psi_j^\sigma(\vec{r})d\vec{r}. \end{aligned} \tag{3.36}$$

$n^\sigma(\theta)$ is the function from electron population θ_j^σ of a given orbital. In the Angyan formulation[143] it equals simply to the orbital electron population, while in the Fulton formulation[144] it equals to the square root of the orbital electron population.

Delocalization indices are determined from the expression analogous to equation (3.36), with the exception that the integration is performed for two distinct atomic basins:

$$\delta^{\sigma\sigma}(\Omega,\Omega') = \sum_{i,j} n(\theta_i^\sigma)n(\theta_j^\sigma)S_{ij^{\sigma\sigma}}(\Omega)S_{ji}^{\sigma\sigma}(\Omega'). \tag{3.37}$$

That expression serves as a measure of a number of electron pairs shared between two atoms. In order to find how many electrons are shared by some atom with all another atoms, the difference between atomic basin average population and the corresponding localization index should be determined:

$$\sigma^{\sigma 2}(\Omega) = N^\sigma(\Omega) - \lambda^\sigma(\Omega) = \frac{1}{2}\sum_{\Omega\neq\Omega'} \delta^{\sigma\sigma}(\Omega,\Omega'). \tag{3.38}$$

The values of the delocalization indices can be connected to the bond order between two considered atoms, that is, for triple covalent bonds $\delta^{\sigma\sigma}(\Omega,\Omega')$ shows values close to three (or, at least, larger than two), for double covalent bonds - close to two, and for single covalent bonds - close to one[142,99]. For closed shell interactions (ionic bonds, hydrogen bonds, van der Waals interaction) one expects to get low values of DI - pretty close to 0[145], while for a metal bonding DI vary from 0.1-0.2 for simple monoatomic metals to values higher then 1 for multiple bonds[146,147].

An important feature of the localization/delocalization indices concept is that it is applicable for any level of electron structure calculation. Even in the case of DFT, with not well defined pair density, the use of a pair density, that is approximated on the basis of Kohn-Sham orbitals, is valid and brings the values very close to those obtained at the Hartree-Fock level[148]. It is worth mentioning that delocalization indices obtained on the DFT and Hartree-Fock levels are systematically higher compared to those obtained from correlated wave functions (for example, configuration interaction (CI) wave functions), but this difference not so large and generally does not affect the chemical

correctness[148,149].

Another technique is the domain average Fermi hole (DAFH)[150,151] analysis, which, although it belongs to the class of real-space methods, enables molecular orbital representation. In the very heart of the method is the attempt to make the definition for conditional probability (3.21) compatible with the quantum mechanics, particularly with the uncertainty principle[150], that is do not fix the position of a reference electron, but allow it to move within the spatial domain Ω:

$$\rho_{c,\Omega}(\vec{r}_2) = \frac{\int_\Omega \rho_2(\vec{r}_1, \vec{r}_2) d\vec{r}_1}{\int_\Omega \rho(\vec{r}_1) d\vec{r}_1} \tag{3.39}$$

If such spatial domain comprises not one, but two or more atomic basins, the localized orbitals associated with individual bonds between considered atoms could be recovered. However, it is more convenient to perform such an analysis in relation to another quantity - the "integrated" Fermi hole:

$$g_\Omega^{\sigma\sigma}(\vec{r}_2) = \int_\Omega h_X^{\sigma\sigma}(\vec{r}_1, \vec{r}_2) d\vec{r}_1, \tag{3.40}$$

that is the DAFH definition. Direct relevance to localization and delocalization indices can be found immediately - the integration of $g_\Omega(\vec{r}_2)$ over the same domain Ω results in the corresponding localization index, while the integration over a different domain Ω' should recover the half of the corresponding delocalization index.

For one-determinant Hartree-Fock-like wave function:

$$g_\Omega^{\sigma\sigma}(\vec{r}) = \sum_{ij} S_{ij}^{\sigma\sigma}(\Omega) \psi_i^\sigma(\vec{r}) \psi_j^{\sigma *}(\vec{r}) n(\theta_i^\sigma) n(\theta_j^\sigma). \tag{3.41}$$

The diagonalization of the corresponding overlap matrix makes the resulting one-electron functions orthogonal to each other within the domain. The new resulting eigenvectors $\{\phi_i(\vec{r})\}$ would remain orthonormal, and their corresponding eigenvalues (occupations) would sum up to the total domain population.

Constructed in such a way DAFH orbitals provide highly visual and understandable pictures of chemical-bonding patterns. The only disadvantage of the DAFH analysis as well as the localization and delocalization indices concepts is the necessity to compute domain overlap matrix elements $S_{ij}(\Omega)$ that is a quite demanding procedure even for medium size systems. Nevertheless, the limits of DAFH analysis applicability is currently expanding, including extensions to solids[152] and correlated wave functions[153].

3.2.4 Other methods

The above described methods are probably the most popular ones, however there are a lot of other methods and it is worth to briefly underline at least some of them.

An alternative way to describe electron localization regions, based on the analysis of the Laplacian of the electron density, was proposed by Bader at al[154]. The value of the Laplacian of the electron density should be below zero in the regions where charge is accumulated, and above zero in regions where it is depleted. Thus in principal the function

$$L(\vec{r}) = -\vec{\nabla}^2\rho(\vec{r}) \tag{3.42}$$

could mapped out the same atomic shell structure as it is done by ELF. Nevertheless ELF proved to be stricter, since $\vec{\nabla}^2\rho(\vec{r})$ despite giving the same qualitative picture, quantitatively often fails, providing wrong numbers of electrons for defined atomic shells[155]. Also, in the case of single covalent bonds, the Laplacian of the electron density tends to allocate separate regions for each participating atom, while ELF yields a shared domain[156], that is more useful for chemical bonding analysis.

The idea of finding n-centers electron bonds ultimately developed with the concept of natural adaptive orbitals (NADOs)[157], which, as well as methods from section 3.2.3, is based on the space partitioning into well defined domains. With this approach a n-center electron population within a domain is defined:

$$< N_{ab...n} >= \int_{\Omega_a} d\vec{r}_1 \int_{\Omega_b} d\vec{r}_2 ... \int_{\Omega_n} d\vec{r}_n \rho_C^n(\vec{r}_1, \vec{r}_2, ...\vec{r}_n), \tag{3.43}$$

where a, b,... n refer to a set of domains into which a whole space is divided, $\rho_C^n(\vec{r}_1, \vec{r}_2, ...\vec{r}_n)$ is the n-th order cumulant density, that bears the information concerning n-body correlation. For instance, in the case of a reduced pair density the comulant density is equal to the correlation parts of equations 3.19 and 3.20. The sum of all N_i contributions should recover the total domain population. Analogously, the 1-order density matrices could be partitioned over n domains:

$$\rho^1_{ab..n}(\vec{r}_1, ...\vec{r}_n; \vec{r}'_1, ...\vec{r}_n) = \int_{\Omega_a} d\vec{r}_2 \int_{\Omega_b} d\vec{r}_3 ... \int_{\Omega_n} d\vec{r}_{n+1} \rho_C^{n+1}(\vec{r}_1, \vec{r}_2, ...\vec{r}_{n+1}). \tag{3.44}$$

After the diagonalization of such domain partitioned density matrices, a set of eigenfunctions with the corresponding eigenvalues is obtained, which could be considered as the set of n-center orbitals with associated occupancy numbers. For $n = 1$ such a procedure restores DAFH orbitals, thus NADOs could be considered as a generalized case of DAFH analysis.

Finally an original method to partition of space into non-overlapping atomic areas is the Voronoi deformation density method[158,159]. In its framework all space that is closer to a given atomic site than to any other atomic sites is defined as the corresponding atomic region; such a region is customarily called the Voronoi cell[160] of an atom. The amount of charge contained within such a Voronoi cell of atom A is calculated as

$$Q_A^{VDD} = -\int_{Voronoi\ cell} d\vec{r}\left(\rho_{mol}(\vec{r}) - \sum_B \rho_B(\vec{r})\right), \tag{3.45}$$

where $\rho_{mol}(\vec{r})$ is a true electron density of the molecule, and $\rho_B(\vec{r})$ is the spherically-symmetrized density of an isolated atom B.

The bonding peculiarities can be investigated by considering a change in the atomic electron population upon the formation of a new molecular complex. Thereby, if $Q_{A\ mol}^{VDD}$ is the amount of charge contained within the Voronoi cell of atom A for a separate molecular fragment, and $Q_{A\ complex}^{VDD}$ is the amount of charge contained within the Voronoi cell of atom A when this molecular fragment is a part of a molecular complex, then the difference

$$\Delta Q_A^{VDD} = Q_{A\ complex}^{VDD} - Q_{A\ mol}^{VDD} \tag{3.46}$$

measures the degree to which atom A contributes to the bonding in a given complex. However, it was shown that such analysis gives poor results in the case of weak intermolecular interactions like hydrogen bonding[159]. In the last case it is preferred to use such charge decomposition in combination with techniques that provide bond energy decomposition[159].

Chapter 4

Chemical Bonding Analysis from the PAW Method

The projector augmented-wave (PAW) method offers a good alternative to other established methods, giving results comparable in accuracy with those obtained with the (L)APW method or finite grid calculations[161,162], but with greater computational efficiency[163]. From this point of view the extension of the PAW method to methods of chemical-bonding analysis is looking very perspective, since that can open an access to up to this date unattainable complex solids with large unit cells and low symmetries.

The current chapter is concentrated on real-space methods, such as localization and delocalization indices, domain average Fermi hole orbitals and electron localizability indicators from the PAW method, and on the technical aspects of their implementation.

The corresponding derivations are presented only for the case without spin-coupling, thus only same-spin terms will be considered and the spin indicator σ will be omitted for brevity.

4.1 Electron Density

Charge density is vital for all above mentioned real-space methods, thereby deriving the corresponding formalism from the PAW method should begin with the derivation of the explicit expression for the electron density.

As have been previously stated, in the framework of the PAW method any quantity defined as expectation value of a semilocal operator on the basis of a given all electron wave function can be expressed as the algebraic sum of three independent terms. Each of them represents the expectation value of this operator on the base of three functions - pseudo wave function ($|\tilde{\psi}\rangle$), all-electron partial wave function ($|\chi\rangle$) and pseudo partial

wave function ($|\tilde{\chi}\rangle$):

$$\langle A\rangle = \langle\tilde{\psi}|A|\tilde{\psi}\rangle + \sum_a \big(\langle\chi^a|A|\chi^a\rangle - \langle\tilde{\chi}^a|A|\tilde{\chi}^a\rangle\big). \tag{4.1}$$

Thus an expression for the charge density, represented as the real-space projector operator $|r\rangle\langle r|$, should be given as[93]

$$\begin{aligned}\rho(\vec{r}) = \sum_{j\vec{k}}^{occ} \Big(&\langle\tilde{\psi}_{j\vec{k}}|r\rangle\langle r|\tilde{\psi}_{j\vec{k}}\rangle + \sum_a\sum_i \big(\langle\tilde{\psi}_{j\vec{k}}|\tilde{p}^a_i\rangle\langle\chi^a_i|r\rangle\langle r|\chi^a_i\rangle\langle\tilde{p}^a_i|\tilde{\psi}_{j\vec{k}}\rangle \\ &- \langle\tilde{\psi}_{j\vec{k}}|\tilde{p}^a_i\rangle\langle\tilde{\chi}^a_i|r\rangle\langle r|\tilde{\chi}^a_i\rangle\langle\tilde{p}^a_i|\tilde{\psi}_{j\vec{k}}\rangle\big)\Big) \\ &= \tilde{\rho}(\vec{r}) + \sum_a \big(\rho^a(\vec{r}) - \tilde{\rho}^a(\vec{r})\big).\end{aligned} \tag{4.2}$$

The first term is build up from plane waves and has the form

$$\tilde{\rho}(\vec{r}) = \frac{1}{V}\sum_{j\vec{k}}^{occ}\theta_{j\vec{k}}\sum_{\vec{G}\vec{G}'} c^*_{j\vec{k},\vec{G}}c_{j\vec{k},\vec{G}'}\ e^{i(\vec{G}-\vec{G}')\vec{r}}, \tag{4.3}$$

where V is primitive cell volume and $\theta_{j\vec{k}}$ is the occupation number of a given band. Further, for simplicity, the occupation numbers will be considered equal to 1 and will be omitted.

The explicit form of the second and third terms dependent on the integral $\langle\tilde{p}^a_{nlm}|\tilde{\psi}_{j\vec{k}}\rangle$ that is the product of the function expressed as multipole expansion and the function expressed as a sum of plane waves. Clearly this integral is not equal to zero only inside muffin-tins since the projector function is defined only within them. In order to compute it the exponential part of the plane wave function is projected on the point grid where the projector function is defined, that is made by it representation via Rayleigh equation in terms of spherical expansion around the center $\vec{R}$ of the corresponding muffin-tin:

$$e^{i(\vec{k}+\vec{G})\vec{r}} = 4\pi e^{i(\vec{k}+\vec{G})\vec{R}}\sum_{l_1m_1} i^{l_1} j_{l_1}(|\vec{k}+\vec{G}|r)Y_{l_1m_1}(\hat{r})Y^*_{l_1m_1}(\hat{k+G}), \tag{4.4}$$

where $j_{l_1}(|\vec{k}+\vec{G}|r)$ is the spherical Bessel function. Therefore the product of projector function and pseudo wave function takes the form

$$\begin{aligned}\langle\tilde{p}^a_{nlm}|\tilde{\psi}_{j\vec{k}}\rangle = &\int d\vec{r}\ \tilde{p}^a_{nlm}(r)Y^*_{lm}(\hat{r})* \\ &4\pi\sum_{\vec{G}} c_{j\vec{k},\vec{G}}e^{i(\vec{k}+\vec{G})\vec{R}}\sum_{l_1m_1} i^{l_1}J_{l_1}(|\vec{k}+\vec{G}|r)Y_{l_1m_1}(\hat{r})Y^*_{l_1m_1}(\hat{k+G}),\end{aligned} \tag{4.5}$$

which is convenient to consider in spherical coordinates:

$$\begin{aligned}\langle\tilde{p}^a_{nlm}|\tilde{\psi}_{j\vec{k}}\rangle = \int_0^{2\pi}\int_0^{\pi}\int_0^{r_m} r^2 \sin\hat{r}_\theta dr d\hat{r}\ \tilde{p}^{a*}_{nlm}(r)Y^*_{lm}(\hat{r})* \\ 4\pi\sum_{\vec{G}} c_{j\vec{k},\vec{G}} e^{i(\vec{k}+\vec{G})\vec{R}} \sum_{l_1m_1} i^{l_1} J_{l_1}(|\vec{k}+\vec{G}|r) Y_{l_1m_1}(\hat{r}) Y^*_{l_1m_1}(\hat{k+G}).\end{aligned} \tag{4.6}$$

After regrouping spherical and radial parts

$$\begin{aligned}\langle\tilde{p}^a_{nlm}|\tilde{\psi}_{j\vec{k}}\rangle = 4\pi\sum_{\vec{G}}\sum_{l_1m_1} i^{l_1} c_{j\vec{k},\vec{G}} Y^*_{l_1m_1}(\hat{k+G}) e^{i(\vec{k}+\vec{G})\vec{R}}* \\ \int_0^{2\pi}\int_0^{\pi} d\hat{r}\ Y^*_{lm}(\hat{r}) Y_{l_1m_1}(\hat{r}) \sin\hat{r}_\theta \int_0^{r_m} dr\ r^2 \tilde{p}^a_{nlm}(r) J_{l_1}(|\vec{k}+\vec{G}|r)\end{aligned} \tag{4.7}$$

and considering known normalization condition for spherical harmonics[164]

$$\int\int d\hat{r}\ Y^*_{lm}(\hat{r}) Y_{l_1m_1}(\hat{r}) \sin\hat{r}_\theta = \delta_{ll_1}\delta_{mm_1} \tag{4.8}$$

it is seen that the summation over angular and magnetic momenta l_1 and m_1 vanished.

Thereby the present integral is reduced to the following form:

$$\langle\tilde{p}^a_{nlm}|\tilde{\psi}_{j\vec{k}}\rangle = 4\pi i^l \sum_{\vec{G}} c_{j\vec{k},\vec{G}} Y^*_{lm}(\hat{k+G}) e^{i(\vec{k}+\vec{G})\vec{R}} \int_0^{r_m} dr\ r^2 \tilde{p}^a_{nlm}(r) J_l(|\vec{k}+\vec{G}|r). \tag{4.9}$$

The knowing of the explicit expression of those integrals gives direct access to the all-electron partial function and pseudo partial function contributions to the total valence electron density, since they are just squares of the corresponding functions $\chi^a_{j\vec{k},nlm}(\vec{r})$ and $\tilde{\chi}^a_{j\vec{k},nlm}(\vec{r})$ (2.30) multiplied by the occupation numbers of the corresponding bands.

4.2 Domain Overlap Matrices

Like the expression for electron density (4.2), the expression for domain overlap matrix elements is given as the algebraic sum of three independent components:

$$S_{j\vec{k},j'\vec{k}'}(\Omega) = \int d\vec{r}\ \zeta^\Omega(\vec{r})\psi^*_{j\vec{k}}(\vec{r})\psi_{j'\vec{k}'}(\vec{r}) = S^{\tilde{\psi}}_{j\vec{k},j'\vec{k}'}(\Omega) + S^{\chi}_{j\vec{k},j'\vec{k}'}(\Omega) - S^{\tilde{\chi}}_{j\vec{k},j'\vec{k}'}(\Omega). \tag{4.10}$$

Here the integration over the domain of interest Ω is substituted by the integration over a whole space, but the new function (further will be referred as shape function) is

introduced $\zeta^{\Omega}(\vec{r})$:

$$\zeta^{\Omega}(\vec{r}) = \begin{cases} 1, & \vec{r} \in \Omega \\ 0, & \vec{r} \notin \Omega. \end{cases} \tag{4.11}$$

Further the contributions to the domain overlap matrix elements stemming from plane wave and muffin-tins parts will be considered separately.

4.2.1 Domain Overlap Matrices: Plane Wave Part

The simple form of plane waves (2.2) implies the quite simple form of the corresponding contribution to the domain overlap matrix elements:

$$\begin{aligned} S^{\tilde{\psi}}_{j\vec{k},j'\vec{k}'}(\Omega) &= \int d\vec{r}\; \zeta^{\Omega}(\vec{r})\tilde{\psi}^{*}_{j\vec{k}}(\vec{r})\tilde{\psi}^{*}_{j\vec{k}}(\vec{r}) \\ &= \sum_{\vec{G}\vec{G}'} c^{*}_{j\vec{k},\vec{G}} c_{j'\vec{k}',\vec{G}'} \int d\vec{r}\; \zeta^{\Omega}(\vec{r}) e^{-i(\vec{k}+\vec{G})\vec{r}} e^{i(\vec{k}'+\vec{G}')\vec{r}}, \end{aligned} \tag{4.12}$$

which in turn is quite demanding to evaluate. Indeed, the direct evaluation of the double sum of plane waves coefficient products is already an $O(N^2)$ complexity process, which is further exacerbated by the necessity of computation the integral $\int d\vec{r}\; \zeta^{\Omega}(\vec{r}) e^{-i(\vec{k}+\vec{G})\vec{r}} e^{i(\vec{k}'+\vec{G}')\vec{r}}$ at each step. Taking into account that for large systems the typical number of plane waves per wave function associated only with one band is larger than 10000, the arising task becomes formidable. The next considerations allow to reduce the cost of computations significantly.

At first, the integral part under the double summation will be considered:

$$\int d\vec{r}\; \zeta^{\Omega}(\vec{r}) e^{-i(\vec{k}+\vec{G})\vec{r}} e^{i(\vec{k}'+\vec{G}')\vec{r}} = \int d\vec{r}\; \zeta^{\Omega}(\vec{r}) e^{-i\Delta\vec{k}\vec{r}} e^{-i\Delta\vec{G}\vec{r}}. \tag{4.13}$$

After introducing of new function $h^{\Omega}_{\Delta\vec{k}}(\vec{r}) = \zeta^{\Omega}(\vec{r}) e^{-i\Delta\vec{k}\vec{r}}$, that is the product of shape function and $\vec{k}$-dependent part of the exponential function, it becomes evident that the given integral is the Fourier transform of the just introduced function $h_{\Delta\vec{k}}(\vec{r})$, which can be defined on a point grid ΔG:

$$\int d\vec{r}\; \zeta^{\Omega}(\vec{r}) e^{-i\Delta\vec{k}\vec{r}} e^{-i\Delta\vec{G}\vec{r}} = \int d\vec{r}\; h^{\Omega}_{\Delta\vec{k}}(\vec{r}) e^{-i\Delta\vec{G}\vec{r}} = H^{\Omega}_{\Delta\vec{k}}(\Delta\vec{G}). \tag{4.14}$$

Thus the equation (4.12) is rewritten to the form

$$S^{\tilde{\psi}}_{j\vec{k},j'\vec{k}'}(\Omega) = \sum_{\vec{G}\vec{G}'} c^{*}_{j\vec{k},\vec{G}} c_{j'\vec{k}',\vec{G}'} H^{\Omega}_{\Delta\vec{k}}(\Delta\vec{G}). \tag{4.15}$$

Further it is convenient to look at plane wave coefficients not as at some set of complex numbers, but rather at as some discrete function dependent on $\vec{G}$:

$$S^{\tilde{\psi}}_{j\vec{k},j'\vec{k}'}(\Omega) = \sum_{\vec{G}\vec{G}'} C^*_{j\vec{k}}(\vec{G}) C_{j'\vec{k}'}(\vec{G}') H^{\Omega}_{\Delta\vec{k}}(\Delta\vec{G}). \tag{4.16}$$

After changing variables $\vec{G}' = \vec{G} - \Delta\vec{G}$ and separating the summation over $\vec{G}$, this relation is rewritten to the form:

$$S^{\tilde{\psi}}_{j\vec{k},j'\vec{k}'}(\Omega) = \sum_{\Delta\vec{G}} \Big[\sum_{\vec{G}} C^*_{j\vec{k}}(\vec{G}) C_{j'\vec{k}'}(\vec{G} - \Delta\vec{G}) \Big] H^{\Omega}_{\Delta\vec{k}}(\Delta\vec{G}). \tag{4.17}$$

The expression in the square brackets is just a cross-correlation of two functions $C_{j\vec{k}}(\vec{G})$ and $C_{j'\vec{k}'}(\vec{G})$, which is equal to the product of their individual backward Fourier transforms - $f^0_{j\vec{k}}(\vec{r}_G)$ and $f^0_{j'\vec{k}'}(\vec{r}_G)$. The resulting function

$$f_{jj',\vec{k}\vec{k}'}(\vec{r}_G) = f^0_{j\vec{k}}(\vec{r}_G) f^0_{j'\vec{k}'}(\vec{r}_G) \tag{4.18}$$

is defined in real space on the point grid $\vec{r}_G$, which is the real space analogy to the point grid $\vec{G}$ defined in momentum space. It is essential to bring this function back to reciprocal space in order to compute its product with the there defined function $H^{\Omega}_{\Delta\vec{k}}(\Delta\vec{G})$, that is accomplished by an other Fourier transformation:

$$F_{jj',\vec{k}\vec{k}'}(\Delta\vec{G}) = \sum_{\Delta\vec{r}_G} f_{jj',\vec{k}\vec{k}'}(\Delta\vec{r}_G) e^{2\pi i \Delta\vec{r}_G \Delta\vec{G}/n_{\Delta\vec{G}}}. \tag{4.19}$$

Note, the transformation should be performed on another point grid $\Delta\vec{r}_G$, which is analogous to the point grid $\Delta\vec{G}$, in order to achieve the matching of the resulting function with $H^{\Omega}_{\Delta\vec{k}}(\Delta\vec{G})$.

Finally the expression (4.12) takes the form:

$$S^{\tilde{\psi}}_{j\vec{k},j'\vec{k}'}(\Omega) = \sum_{\Delta\vec{G}} F_{jj',\vec{k}\vec{k}'}(\Delta\vec{G}) H^{\Omega}_{\Delta\vec{k}}(\Delta\vec{G}). \tag{4.20}$$

Taking into account that Fourier transformation could be efficiently made by fast Fourier transformation (FFT) procedure (that is a $O(N \log N)$ complexity process), one can estimate the complexity of the equation (4.20) as follows:

$$N = a_{shape} n_{\vec{G}} + 2n_{\vec{G}} \log(n_{\vec{G}}) + 2n_{\vec{G}} \log(2n_{\vec{G}}) + a_{shape} n_{\vec{G}} \log(a_{shape} n_{\vec{G}}), \tag{4.21}$$

where the first term stems from the single summation over the resampled grid points $\Delta\vec{G}$, the second term stems from the two FFT procedures that bring the plane wave coefficients functions $C_{j\vec{k}}(\vec{G})$ and $C_{j'\vec{k}'}(\vec{G})$ to real space, the third term stems from the FFT procedure with the help of which the function $F_{jj',\vec{k}\vec{k}'}(\Delta\vec{G})$ is determined, and the fourth term is responsible for evaluation of function $H^{\Omega}_{\Delta\vec{k}}(\Delta\vec{G})$. The coefficient a_{shape} determines in how many times for the shape expansion coefficients the point grid $\Delta\vec{G}$ is finer than the initial point grid $\vec{G}$. Note, that point grid $\Delta\vec{G}$ for the function $H^{\Omega}_{\Delta\vec{k}}(\Delta\vec{G})$ should be at least twice finer than the point grid $\vec{G}$, thus coefficient a_{shape} should take values from 2 and larger. On the other hand the point grid for the function $F_{jj',\vec{k}\vec{k}'}(\Delta\vec{G})$ can be resampled no more than in 2 times and is not depended on how dense is the grid for the shape expansion coefficients, which is controlled, as it was stated above, by the parameter a_{shpae}.

In principle, if the analytic Fourier transforms of the shape function $H^{\Omega}_{\Delta\vec{k}}(\Delta\vec{G})$ is known, the corresponding plane waves domain overlap matrix elements $S^{\tilde{\psi}}_{j\vec{k},j'\vec{k}'}(\Omega)$ can be computed exactly. In reality this function is sampled on a discrete grid. As it known from the Nyquist-Shannon sampling theorem, only those functions, which are perfectly band limited to a bandwidth f_0 (continuous signals), can be sampled at a discrete grid with the sample rate greater than $2f_0$ without loss of information[165,166]. Since the domain shape functions correspond to QTAIM basins, they are discontinuous and have unlimited bandwidth, and thus one can get only approximated Fourier expansion coefficients. It is anticipated, that the value of a_{shape} should be directly bonded to the accuracy of the obtained results. This dependence will be traced lately.

Nevertheless, the main point is that the initially quadratic complex procedure of the relation (4.12) is reduced to the combination of linear and logarithmic complexity processes $O(N + N\log N)$ of the relation (4.20). Though the final results formally are not exact, it will be demonstrated that the error is small and does not affect the final conclusions concerning the investigated bonding patterns.

4.2.2 Domain Overlap Matrices: Muffin-tin part

The explicit form of the contributions from partial waves to the domain overlap matrix elements can be deduced based on the fact, which states that, since partial waves act only within some build around the nuclei spherical augmented regions, the shape function also has to act only within those regions and can be expressed as a radial part times a spherical part - in other words, analogously to the partial waves, it can be expressed as a multipole expansion. Thereby, considering at first the all-electron partial wave function,

the next relation arises:

$$\begin{aligned} S^{\chi}_{j\vec{k},j'\vec{k}'}(\Omega) &= \int d\vec{r}\; \zeta^{\Omega}(\vec{r}) \sum_{alm} \chi^{a}_{j\vec{k}lm}(r) Y^{*}_{lm}(\hat{r}) \sum_{al'm'} \chi^{a}_{j'\vec{k}'l'm'}(r) Y_{l'm'}(\hat{r}) \\ &= \int d\vec{r} \sum_{l^0m^0} \zeta^{\Omega}_{l^0m^0}(r) Y_{l^0m^0}(\hat{r}) \sum_{alm} \chi^{a}_{j\vec{k}lm}(r) Y^{*}_{lm}(\hat{r}) \sum_{al'm'} \chi^{a}_{j'\vec{k}'l'm'}(r) Y_{l'm'}(\hat{r}). \end{aligned} \tag{4.22}$$

After changing the coordinate system into the spherical one and separating radial and spherical parts, this relation takes the following form:

$$\begin{aligned} S^{\chi}_{j\vec{k},j'\vec{k}'}(\Omega) = &\sum_{a} \sum_{l^0m^0} \sum_{lm} \sum_{l'm'} \int_0^{r_m} dr\; r^2 \zeta^{\Omega}_{l^0m^0}(r) \chi^{a}_{j\vec{k}lm}(r) \chi^{a}_{j'\vec{k}'l'm'}(r) \\ &* \int_0^{2\pi} \int_0^{\pi} d\hat{r}\; \sin\hat{r}_\theta Y_{l^0m^0}(\hat{r}) Y^{*}_{lm}(\hat{r}) Y_{l'm'}(\hat{r}). \end{aligned} \tag{4.23}$$

Spherical harmonics form a orthonormal basis set, thereby the product of two spherical harmonics can be expressed in terms of a linear combination of a higher order spherical harmonics. The coefficients of such representation can be found by computing the corresponding Wigner 3-j symbols:

$$\begin{aligned} Y_{l_1m_1}(\hat{r}) Y_{l_2m_2}(\hat{r}) = &\sum_{lm} \sqrt{\frac{(2l_1+1)(2l_2+1)(2l_3+1)}{4\pi}} \\ &* \begin{pmatrix} l_1 & l_2 & l_3 \\ 0 & 0 & 0 \end{pmatrix} Y^{*}_{lm}(\hat{r}) \begin{pmatrix} l_1 & l_2 & l_3 \\ m_1 & m_2 & m_3 \end{pmatrix}. \end{aligned} \tag{4.24}$$

It can be shown that an integrated product of three spherical harmonics is expressed in a similar manner[167]:

$$\begin{aligned} &\int d\hat{r}\; \sin\hat{r}_\theta Y_{l_1m_1}(\hat{r}) Y_{l_2m_2}(\hat{r}) Y_{l_3m_3}(\hat{r}) = \\ &\qquad \begin{pmatrix} l_1 & l_2 & l_3 \\ 0 & 0 & 0 \end{pmatrix} \begin{pmatrix} l_1 & l_2 & l_3 \\ m_1 & m_2 & m_3 \end{pmatrix} \sqrt{\frac{(2l_1+1)(2l_2+1)(2l_3+1)}{4\pi}}. \end{aligned} \tag{4.25}$$

After substituting of the relation (4.25) into the equation (4.23) the final expression for AE partial waves contribution to domain overlap matrix elements appears:

$$\begin{aligned} S^{\chi}_{j\vec{k},j'\vec{k}'}(\Omega) = &\sum_{a} \sum_{l^0m^0} \sum_{lm} \sum_{l'm'} (-1)^m \int_0^{r_m} dr\; r^2 \zeta^{\Omega}_{l^0m^0}(r) \chi^{a}_{j\vec{k}lm}(r) \chi^{a}_{j'\vec{k}'l'm'}(r) \\ &\sqrt{\frac{(2l^0+1)(2l+1)(2l'+1)}{4\pi}} \begin{pmatrix} l^0 & l & l' \\ 0 & 0 & 0 \end{pmatrix} \begin{pmatrix} l^0 & l & l' \\ m^0 & -m & m' \end{pmatrix}. \end{aligned} \tag{4.26}$$

The expression for PS partial waves contribution to domain overlap matrix elements is deduced completely analogously and have the same form:

$$S^{\tilde{\chi}}_{j\vec{k},j'\vec{k}'}(\Omega) = \sum_a \sum_{l^0m^0} \sum_{lm} \sum_{l'm'} (-1)^m \int_0^{r_m} dr\ r^2 \zeta^{\Omega}_{l^0m^0}(r) \tilde{\chi}^a_{j\vec{k}lm}(r) \tilde{\chi}^a_{j'\vec{k}'l'm'}(r) \sqrt{\frac{(2l^0+1)(2l+1)(2l'+1)}{4\pi}} \begin{pmatrix} l^0 & l & l' \\ 0 & 0 & 0 \end{pmatrix} \begin{pmatrix} l^0 & l & l' \\ m^0 & -m & m' \end{pmatrix}. \tag{4.27}$$

4.3 Realization peculiarities

For a proper and accurate representation of an electron density a dense enough real space point grid should be chose. Generally even for coarse calculations the distance between two adjusting points should not exceed 0.1 Bohr, that leads to the total number of points in the range from several hundred thousands to several millions points depending on the size of a chosen box. The computation of the pseudo density straightforwardly from Eq. 4.3 is a $O(n^2_{\vec{G}})$ process. To avoid this, the standard procedure for recovering the electron density from a plane wave basis is used[168, 169]. Pseudo wave functions for each k-point and each band can be calculated via Fourier transformation to real space:

$$\tilde{\psi}_{j\vec{k}}(\vec{r}) = e^{i\vec{k}\vec{r}} \sum_{\vec{G}} c_{j\vec{k},\vec{G}} e^{i\vec{G}\vec{r}}, \tag{4.28}$$

that is a $n_{\vec{G}} \log n_{\vec{G}}$ complexity task due to fast Fourier transformation procedure. Then they are squared and summed up, that is a $n_{\vec{G}}$ complexity procedure. Finally the output function, which describes the electron density field, is represented in reciprocal space, that is done by backward Fourier transformation of obtained real space representation:

$$\tilde{\rho}(\vec{G}) = \frac{2}{n_{\vec{k}}} \sum_{\vec{r}} \tilde{\rho}(\vec{r}) e^{-i\vec{G}\vec{r}}. \tag{4.29}$$

Here factor 2 is introduced to account for spin degeneracy, $n_{\vec{k}}$ is the number of $\vec{k}$-points.

The summation in the square brackets can be efficiently computed with the FFT procedure, avoiding the direct computation of the $e^{2i\vec{k}\vec{r}}$ for each $\vec{k}$-point at every point $\vec{r}$. Thus the summation over $\vec{G}$ vectors with corresponding evaluation of the exponential function at each point $\vec{r}$ should be performed only once, irrelevant from the number of $\vec{k}$-points and the number of occupied bands.

For the evaluation of the partial waves electron densities:

$$\rho^a(\vec{r}) = \sum_{lm} \sum_{n} \sum_{j\vec{k}} |\chi^a_{j\vec{k},nlm}(r) Y_{lm}(\hat{r})|^2, \tag{4.30a}$$

$$\tilde{\rho}^a(\vec{r}) = \sum_{lm} \sum_{n} \sum_{j\vec{k}} |\tilde{\chi}^a_{j\vec{k},nlm}(r) Y_{lm}(\hat{r})|^2, \tag{4.30b}$$

at each point $\vec{r}$ some previous calculations are also made - that is the evaluation of the integrals $\langle \tilde{p}^a_{nlm} | \tilde{\psi}_{j\vec{k}} \rangle$ (4.9). For this purpose at first the expression for each $\vec{G}$ and $\vec{k}$

$$B^{a,nlm}_{j\vec{k}}(\vec{G}) = c_{j\vec{k},\vec{G}} Y^*_{lm}(k \hat{+} G) \int_0^{r_m} dr' \; r'^2 \tilde{p}^a_{nlm}(r') J_l(|\vec{k} + \vec{G}|r'), \tag{4.31}$$

is evaluated, since in that case the integrals $\int_0^{r_m} dr' \; r'^2 \tilde{p}^a_{nlm}(r') J_l(|\vec{k}+\vec{G}|r')$ are calculated not for every atom inside the unit cell, but for every type of atom. The use of r' underlines the difference between the radial point grid where the projector function is defined and the point grid $\vec{r}$. Further the sets of integrals (4.9) for each atom are received after the multiplication of $B^{a,nlm}_{j\vec{k}}(\vec{G})$ by the exponential function $e^{i(\vec{k}+\vec{G})\vec{R}}$ and the summation over all $\vec{G}$. The number of such sets is clearly dependent on the value of orbital momentum for the given atom, each comprises $N_{\vec{k}} N_j$ values.

It is essential that the partial waves electron density as well as the partial waves functions can be represented in the form of multipole expansions. Thus, instead of the set of $N_{\vec{k}} N_j$ multipole expansions for each atom only one has to be constructed, which coefficients equal to the sum of the squares over all $\vec{k}$-points and occupied bands of the radial parts of partial waves functions $\chi^a_{j\vec{k},nlm}(r)$, expanded on the set of spherical harmonics with the doubled angular momentum $l^0 = 2l$:

$$\rho^a(\vec{r}) = \sum_{lm} \Big[\sum_{n} \sum_{j\vec{k}} |\chi^a_{j\vec{k},nlm}(r)|^2 \Big] |Y_{lm}(\hat{r})|^2 = \sum_{l^0 m^0} \chi^a_{l^0 m^0}(r) Y_{l^0 m^0}(\hat{r}), \tag{4.32a}$$

$$\tilde{\rho}^a(\vec{r}) = \sum_{lm} \Big[\sum_{n} \sum_{j\vec{k}} |\tilde{\chi}^a_{j\vec{k},nlm}(r)|^2 \Big] |Y_{lm}(\hat{r})|^2 = \sum_{l^0 m^0} \tilde{\chi}^a_{l^0 m^0}(r) Y_{l^0 m^0}(\hat{r}). \tag{4.32b}$$

The subsequent topological analysis of the electron density - finding first and higher order derivatives, critical points and division into basins, - is performed with routines initially integrated into DGrid.

The implementation of the scheme for the evaluation of plane waves contributions to the domain overlap matrix elements is rather straightforward and presented at fig. 4.1. At the first step the evaluation of the function $H^{\Omega}_{\Delta\vec{k}}(\Delta\vec{G})$ is performed not for the each pair of $\vec{k}$-points, but for the each unique distance between them, since this function is dependent not on the coordinates of $\vec{k}$-points but on the difference between them.

In order to choose the parameter a_{shape} from eq. 4.21, that controls the precision of the domain overlap matrix elements evaluation, the contribution from plane waves were calculated for different values of a_{shape}. As can be seen from table 4.1 the given

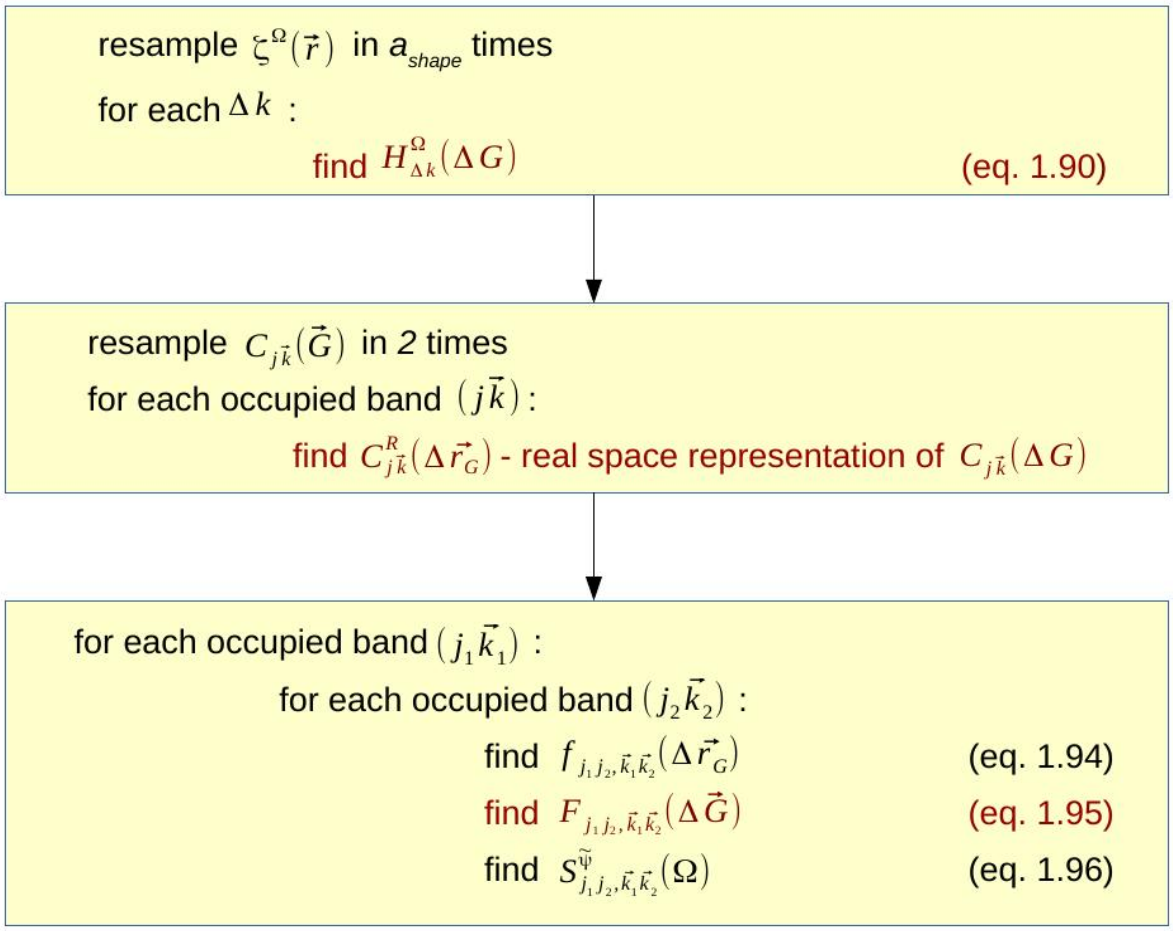

Figure 4.1: The scheme for the calculation of plane wave contributions to domain matrix overlap elements, implemented to the ABINIT module for the program DGrid. Steps, at which FFT procedure is performed, are highlighted in red.

contributions remain almost unchanged and the assignment of a lowest possible value of 2 to a_{shape} is reasonable in most of the cases.

One type of problem can arise when the properties related to a specific basin are calculated with the help of integration over a finite set of points. When dealing with a highly symmetrical system, it may happen that a number of mesh points will be placed just at the edge along which two adjacent atom basins are contacted. The main issue than is to which basin those points should be prescribed. Prescribing them exclusively to one of the given basins may result in artificial increase of charge density, comprising within it, with consequent bad evaluation of localization and delocalization indices. The case of MgB_2 may serve as a vivid example (Fig. 4.2). Here a number of points can fall at a demarcation edge between two boron basins. Prescribing of all points to one of the boron basins leads to unsymmetrical charge densities inside those basins, while in reality this atoms are equitable and should possess the same amount of charge.

Table 4.1: Dependence of plane wave contributions to delocalization indices upon the value of parameter a_{shape}.

Compound	Atoms	a_{shape}				
	$A-B$	2	4	6	8	10
1HD	$H-H$	0.4230	0.4232	0.4232	0.4232	0.4232
3HD	$H-H$	0.1226	0.1226	0.1226	0.1226	0.1226
Diamond	$C-C$	0.8414	0.8413	0.8415	0.8416	0.8416
MgB_2	$B-B$	0.9490	0.9536	0.9528	0.9536	0.9534
	$Mg-B$	0.0662	0.0620	0.0616	0.0608	0.0606
NaCl	$Na-Cl$	0.0654	0.0662	0.0658	0.0654	0.0654
	$Cl-Cl$	0.0523	0.0518	0.0520	0.0521	0.0521

Table 4.2: Dependence of charges of boron basins in MgB_2 upon the value of parameter a_{shape}.

Atom	a_{shape}						
	2	4	6	8	10	12	14
B1	5.905	5.856	5.829	5.821	5.813	5.808	5.804
B2	5.625	5.702	5.728	5.742	5.751	5.756	5.760

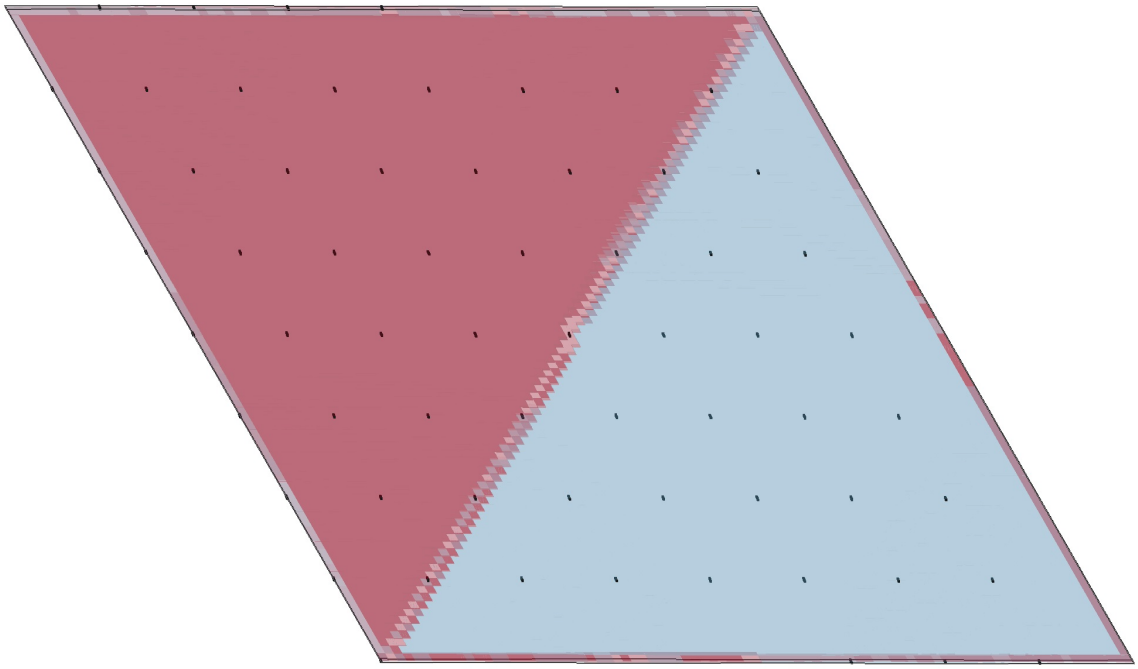

Figure 4.2: $\vec{k}$-point mesh (8×8×8, represented as black dots) within MgB_2 primitive cell. QTAIM boron basin are colored with light blue and red.

Two possible solutions exist - the first one is to increase the number of integration points thus reducing the fraction of problem points and, consequently, reducing the error, and the second one is to divide equally the contributions that stem from problem points among adjacent basins. The first solution is directly related to the value of parameter a_{shape}, but has the disadvantage that it will not eliminate the error completely. The second solution has the disadvantage of loose justification of a such procedure. Nevertheless, both possible solutions were implemented to the module, but in present investigation the increase of parameter a_{shape} was used. Imposing the value of 10 to a_{shape} is resulted in reduction of error to the acceptable value of around 0.05 electrons (table 4.2). Further, when such problem will arise, the localization and deloclaization indices will be evaluated with $a_{shape} = 10$, while for the rest of the tasks $a_{shape} = 2$ will be used.

The evaluation of partial waves contributions to domain overlap matrix elements (4.26, 4.27) begins with the evaluation of the corresponding Wigner 3-j symbols. They obey the so-called selection rules ($m_1 + m_2 = m_3$, "triangular inequality")[170], therefore only a few of them will be nonzero. Further it is necessary to recall that the radial functions $\chi^a_{j\vec{k}lm}(r)$ and $\tilde{\chi}^a_{j\vec{k}lm}(r)$ are the linear combinations of $j, \vec{k}$-independent functions $\varphi^a_{nlm}(r)$ and $\tilde{\varphi}^a_{nlm}(r)$, and $j, \vec{k}$-dependent coefficients $\langle \tilde{p}^a_{nlm} | \tilde{\psi}_{j\vec{k}} \rangle$. Therefore, taking as example an all electron partial wave function, after the regrouping the dependent on r

and the independent on it terms:

$$\begin{aligned}
&\int_0^{r_m} r^2 dr\ \zeta_{l^0m^0}(r)\chi^a_{j\vec{k}lm}(r)\tilde{\chi}^a_{j\vec{k}lm}(r) = \\
&\int_0^{r_m} r^2 dr\ \zeta_{l^0m^0}(r)\sum_n \varphi^a_{nlm}(r)\langle\tilde{p}^a_{nlm}|\tilde{\psi}_{j\vec{k}}\rangle \sum_{n'} \varphi^a_{n'l'm'}(r)\langle\tilde{p}^a_{n'l'm'}|\tilde{\psi}_{j'\vec{k}'}\rangle = \\
&\sum_n\sum_{n'}\langle\tilde{p}^a_{nlm}|\tilde{\psi}_{j\vec{k}}\rangle\langle\tilde{p}^a_{n'l'm'}|\tilde{\psi}_{j'\vec{k}'}\rangle \int_0^{r_m} r^2 dr\zeta_{l^0m^0}(r)\varphi^a_{nlm}(r)\varphi^a_{n'l'm'}(r),
\end{aligned} \tag{4.33}$$

it becomes clear that there is no need to perform the radial integration for all occupied bands and $\vec{k}$-points. Instead the radial integrals

$$\int_0^{r_m} r^2 dr\zeta_{l^0m^0}(r)\varphi^a_{nlm}(r)\varphi^a_{n'l'm'}(r) \tag{4.34}$$

can be precomputed only for all combinations of three given orbital momenta and the number of projectors per given atom - excluding, of course, those, for which Wigner 3-j coefficients are equal to zero. Thereafter, when partial waves contributions through double loop over all occupied bands would be computed, those precomputed values simple are substituted to the main relation.

The implementation of the PAW method for ELF/ELI concepts is rather straightforward. In accordance with the PAW feature to express any semilocal property operator in the form of the sum of three independent terms, the key components for ELI and ELF, $\rho(\vec{r})$, $\tau(\vec{r})$ and $\vec{\nabla}\rho(\vec{r})$, should be computed in advance in the same way:

$$\begin{aligned}
\rho_{tot}(\vec{r}) &= \tilde{\rho}(\vec{r}) + \sum_a \big(\rho^a(\vec{r}) - \tilde{\rho}^a(\vec{r})\big), \\
\vec{\nabla}\rho_{tot}(\vec{r}) &= \vec{\nabla}\tilde{\rho}(\vec{r}) + \sum_a \big(\vec{\nabla}\rho^a(\vec{r}) - \vec{\nabla}\tilde{\rho}^a(\vec{r})\big), \\
\tau_{tot}(\vec{r}) &= \tilde{\tau}(\vec{r}) + \sum_a \big(\tau^a(\vec{r}) - \tilde{\tau}^a(\vec{r})\big).
\end{aligned} \tag{4.35}$$

Further these obtained values are substituted to the corresponding expressions of ELF (3.28) or ELI (3.34).

The last issue concerns the way how the derivatives from the electron density and the Kohn-Sham wave functions should be computed.

The part that stems from pseudo wave function is the simpler one. Since it is represented as a plane wave expansion, the resulting first derivatives is the same plane wave expansions, only with the coefficients multiplied by the corresponding $\vec{G}$ coordinates and

imaginary unit. For example:

$$\begin{aligned}\vec{\nabla}\tilde{\psi}_{j\vec{k}}(\vec{r}) &= \sum_{\vec{G}} \Big(i(\vec{k}+\vec{G})c_{j\vec{k},\vec{G}}\Big)e^{i(\vec{k}+\vec{G})\vec{r}},\\ \vec{\nabla}\tilde{\rho}(\vec{r}) &= \sum_{\vec{G}\vec{G}'} \Big(i(\vec{G}'-\vec{G})c^{*}_{j\vec{k},\vec{G}}c_{j\vec{k},\vec{G}'}\Big)e^{i(\vec{G}'-\vec{G})\vec{r}}.\end{aligned} \tag{4.36}$$

The parts which stem from muffin-tins are more complicated, since they require the computing of multipole expansion derivatives. The corresponding derivatives can be also represented via multipole expansions up to the $(l+1)$ orbital momentum, where l is the orbital momentum of the initial multipole expansion. The radial part of a new multipole expansion is obtained with the procedure, that is used in Elk[171]. Thus for this purpose the following formula is used[171]:

$$\begin{aligned}F_{lm}(r)Y_{lm}(\hat{r}) = &\sqrt{\frac{l+1}{2l+3}}C(l\ m\ 1\ \mu|l+1\ m+\mu)Y_{l+1m+\mu}(\hat{r})\Big(\frac{d}{dr}-\frac{l}{r}\Big)f_{lm}(r)\\ &-\sqrt{\frac{l}{2l-1}}C(l\ m\ 1\ \mu|l-1\ m+\mu)Y_{l-1m+\mu}(\hat{r})\Big(\frac{d}{dr}+\frac{l+1}{r}\Big)f_{lm}(r),\end{aligned} \tag{4.37}$$

where $F_{lm}(r)$ are radial expansion coefficients for the new multipole expansion, $f_{lm}(r)$ are radial expansion coefficients for the initial multipole expansion. μ relates to the spherical unit vectors $\hat{e}_{\mu}$

$$\begin{aligned}\hat{e}_{+1} &= -\frac{\hat{x}+i\hat{y}}{\sqrt{2}},\\ \hat{e}_{0} &= \hat{z},\\ \hat{e}_{-1} &= -\frac{\hat{x}-i\hat{y}}{\sqrt{2}}.\end{aligned} \tag{4.38}$$

C are Clebsch-Gordon coefficients and they are related to Wigner 3-j symbols via relation[173]

$$C(l_1\ m_1\ l_2\ m_2|L\ M) = (-1)^{l_1-l_2+M}\sqrt{2L+1}\begin{pmatrix} l_1 & l_2 & L\\ m_1 & m_2 & -M\end{pmatrix} \tag{4.39}$$

Radial expansion coefficient $f_{lm}(r)$ for partial and pseudo partial wave functions are known from the procedure of PAW basis function generation and sampled on a discrete radial grid. The required radial derivatives are obtained with the cubic spline interpolation procedure[172].

4.4 Implementation details

The implementation of chemical-bonding analysis from PAW method was realized in the form of the C++ module to the program DGrid[174]. Wave functions from solid-state DFT calculations with the program package ABINIT[175,176] were utilized. In order to construct required property field plane wave expansion coefficients are read from the binary *WFK* file and the radial parts of atomic PAW datasets are read from text files generated with ATOMPAW code[95]. The corresponding data collected into single text file, that afterwards used as DGrid basis file. All subsequent calculations are governed with standard DGrid commands and control files[177].

The topological analysis and basin partitioning are performed with the embedded to DGrid program discreet grid technique[177,178]. Fast Fourier transform and matrix diagonalization procedures are performed with the fast Fourier transform function library[179] and linear algebra package (LAPACK) routine *zheev*[180] from Intel math kernel library (MKL)[181] respectively.

The additional localization procedure of DAFH eigenvectros (Eq. 3.41) employing the isopycnic transformation[182] is performed in order to symmetrize the eigenvectros and eigenvalues.

The parallelization over a number of bands of developed module were performed with OpenMp interface[183]. Current implementation of parallelization procedure allow one to get 14-16th time speed up in evaluation of domain overlap matrix elements with 24 processors.

Chapter 5

Simple Compounds

Projectors and partial functions for atomic PAW datasets, generated using the local spin density approximation with the Perdew-Wang exchange-correlation functional[13], have been taken from the official ABINIT site[184].

Several simple inorganic solids have been selected to test the algorithm and compare its performance and results of the evaluation of delocalization indices and domain-average Fermi hole orbitals with the results obtained from the previous implementation of these chemical-binding indicators for the (L)APW method[147]. These are 1D and 3D hydrogen lattices, diamond, sodium chloride and magnesium diboride. Those compounds contain at most three atoms in the primitive cell. For the 1D hydrogen lattice (further 1DH lattice) the row of 8 equidistant atoms were taken, while for the 3D hydrogen lattice (further 3DH lattice) a cube with 4 equidistant atoms along each edge was chosen. The computation details are collected to the tables 5.1 and 5.2.

5.1 Delocalization indices and DAFH orbitals

All results are collected to the table 5.3. The comparison of localization and delocalization indices produced by (L)APW and PAW methods reveals a great agreement between those methods. Generally, with exception of metallic compounds, differences between the values computed by the PAW and the (L)APW methods appeared only in the third digit after the comma.

5.1.1 Hydrogen lattices

The hydrogen lattices are simplest model structures with a single electron per atom. Due to their simplicity, they are among the most convenient structures for testing of developed approaches.

Table 5.1: Calculation details for ABINIT. Simple compounds.

Compound	Cell (a.u.)	E_{cut}(Ha)	r_{cut}(a.u.)	core orbitals	k-point mesh
1DH	2.50	15.0	0.90	none	1× 1× 64
3DH	2.50	15.0	0.90	none	8× 8× 8
Al	7.65	16.0	1.90	[Ar]	8× 8× 8
Fe	10.85	32.0	3.72	[Ar]	8× 8× 8
Diamond	6.75	16.0	1.12	1s	8× 8× 8
NaCl	10.66	18.0	1.80 (Na) 1.50 (Cl)	1s [Ne]	8× 8× 8
MgB_2	$a = b$ =5.83 c =6.65	10.0	1.90 (Mg) 1.50 (B)	1s 1s	8× 8× 8

Table 5.2: Calculation details for Elk. Simple compounds. Cell parameters and k-point meshes are the same as in table 5.1.

Compound	RGk_{max}^{APW}	G_{max}^{V}	l_{max}^{APW}	l_{max}^{V}	core orbitals
1DH	6.0	13.0	8	7	none
3DH	6.0	13.0	8	7	none
Al	7.0	12.0	8	7	[Ar]
Fe	7.0	12.0	8	7	[Ar]
Diamond	8.0	12.0	11	11	1s
NaCl	11.0	12.05	8	7	[Ne](Na) [Ne](Cl)
MgB_2	7.0	12.0	8	7	[Ne](Mg) 1s(B)

APW: expansion cut-offs for wave functions; V: expansion cut-offs for potential and density. Fine logarithmic radial mesh (Elk keyword *lradstp*) was used in all calculations.

Table 5.3: Localization and delocalization indices for QTAIM basins of chosen simple compounds.

Compound	Method	Atom	$N(A)$	$\sigma^2(A)$	$\lambda(A)$	$A-B$	$\delta(A,B)$
1DH	PAW	H	1.00	0.548	0.452	H-H (1)	0.426
						H-H (2)	0.034
	LAPW	H	1.00	0.546	0.443	H-H (1)	0.417
						H-H (2)	0.032
3DH	PAW	H	1.00	0.697	0.303	H-H (1)	0.121
						H-H (2)	0.022
	LAPW	H	1.00	0.701	0.299	H-H (1)	0.121
						H-H (2)	0.023
Al	PAW	Al	13.00	1.950	11.050	Al-Al (1)	0.257
						Al-Al (2)	0.010
	LAPW	Al	13.00	2.000	11.000	Al-Al (1)	0.260
						Al-Al (2)	0.010
Fe(ferr)	PAW	Fe	26.00	2.875	10.196(↑)	Fe-Fe (1)(↑)	0.309
						Fe-Fe (2)(↑)	0.114
					12.929(↓)	Fe-Fe (1)(↓)	0.184
						Fe-Fe (2)(↓)	0.079
	LAPW	Fe	26.00	2.985	10.082(↑)	Fe-Fe (1)(↑)	0.312
						Fe-Fe (2)(↑)	0.115
					12.933(↓)	Fe-Fe (1)(↓)	0.185
						Fe-Fe (2)(↓)	0.077
Diamond	PAW	C	6.00	2.191	3.810	C-C (1)	0.913
						C-C (2)	0.035
	LAPW	C	6.00	2.188	3.812	C-C (1)	0.914
						C-C (2)	0.039
NaCl	PAW	Na	10.13	0.216	9.924	Na-Cl	0.070
		Cl	17.87	0.508	17.346	Cl-Cl	0.047
	LAPW	Na	10.15	0.221	9.923	Na-Cl	0.072
		Cl	17.85	0.514	17.340	Cl-Cl	0.048
MgB_2	PAW	Mg	10.42	0.466	9.955	Mg-B	0.062
		B	5.79	2.221	3.565	B-B	0.936
	LAPW	Mg	10.40	0.454	9.949	Mg-B	0.064
		B	5.80	2.118	3.611	B-B	0.984

The hydrogen lattices show a gradual transition from a weakly correlated metallic state to an insulating state with strong correlation when increasing the distance between adjacent atoms[186–188]. It was shown that for hydrogen clusters a metal-insulator transition occurs at interatomic distances in the range of 2.8 – 3.8 a. u.[188]. The interatomic distance, chosen for the present investigation, was 2.5 a.u. and should correspond to the metallic case in both 1DH and 3DH systems.

The values of localization and delocalization indices for hydrogen atoms in 1DH lattice show a significant degree of electron sharing between given a QTAIM basin and its neighbors. The increase of the system dimension (in other words, the transition from 1DH system to 3DH system) leads to the decrease of localization/delocalization indices and, consequently, to the increase of fluctuation in electron population. The reason is in necessity for one-site electron population to "spread out" among a much larger number of basins, than it was in the 1DH lattice situation where one hydrogen atom has only two direct neighbors. For the 3DH lattice the number of direct neighbors is increased to 6 - here a basin is considered as a direct neighbor if it shares the same face with initially given basin. Taking the results from the PAW calculations, it is seen, that the delocalization index between basins with a shared face is equal to 0.121, thereby, the degree of electron pairs shared by one atom with all his direct neighbors is evaluated as $6 * 0.121 = 0.726$ in 3DH lattice, while for 1DH lattice this value is equal to $2 * 0.426 = 0.852$. The degree of electron pairs which are shared by this atom with more distant basins is evaluated as $2 * 0.697 - 0.726 = 0.668$ for 3DH lattice and as $2 * 0.548 - 0.852 = 0.244$ for 1DH lattice. The former value is almost in three times smaller than the first one, that is in nice agreement with increase of dimension form 1 to 3. The (L)APW method gives almost the same results[147], the greatest deviation concerns localization indices for 1DH system and do not exceed 0.01.

The isosurfaces of DAFH orbitals for the 1DH and the 3DH systems are presented at Fig. 5.1 and 5.2 correspondingly. For the 1DH lattice the occupation of the given orbital is equal to 0.95, while only 47.5% of its norm is localized within the native basin, 42.4% is localized within two closest neighbors and the remaining 10.1% is localized at second and higher order neighbors. The contribution of the DAFH orbital in the 3DH lattice to the population of the native basin is equal to 0.77 electrons, while the contributions from all other orbitals are small and do not exceed 0.07 electrons. 38.6% of this DAFH orbital is localized inside native basin, while 36.6% of it is localized within adjoining basins which share with the given one a face, and 5.3% of it is localized within basins which share with the given one an edge. The remaining 19.5% of the norm of this DAFH orbital is localized within distant basins. Such prominent delocalization of the investigated orbitals underlines the metallic nature of the considered model compounds.

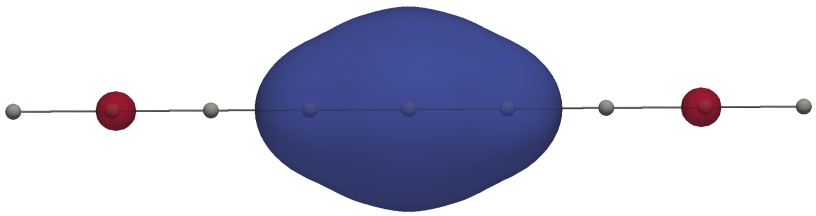

Figure 5.1: DAFH orbital from DFT calculation for 1DH lattice. The basin of the corresponding DAFH orbital is attributed to the central atom of the given chain. The isosurface of orbital amplitude is equal to 0.01. The change in color corresponds to the change in phase.

5.1.2 Metallic bonding

Generally metallic bonding is characterized by non-negligible electron sharing not only between adjoining basins, but also between distant basins, thus revealing a substantial degree of long-range delocalization[147].

In the case of aluminum the PAW method evaluates the fluctuation in the aluminum basin (Fig. 5.3a) population as equal to 1.950 electrons. Assuming 12 direct neighbors, the average amount of electron pairs shared between the given basin and the first coordination shell neighbors is equal to $12 * 0.257 = 3.084$, that lives $2 * 1.950 - 3.084 = 0.816$ (20.9% of the total amount of delocalized electron pairs) electron pairs shared between distant basins. The former two values are evaluated by (L)APW method as being equal correspondingly to $12 * 0.260 = 3.120$ and $2 * 2.000 - 3.120 = 0.880$ electron pairs.

The set of DAFH orbitals (table 5.4) reveals four orbitals with the occupancy higher than 0.1, one of which has the shape similar to s-orbitals and thus can be attributed to the 3s state (further s-like DAFH orbital), and the rest three orbitals have p-like shapes and can be attributed to the 3p states (further p-like DAFH orbitals) of the aluminum atom. It appears that the s-like DAFH orbital is quite diffuse, since its occupancy number is equal to 1.12 electrons and it localizes within native basin only by 66%. The rest of the norm is equally distributed among the 12 neighboring aluminum basins, within every of which the given DAFH orbital localizes by approximately 2.6%. Each of the p-like DAFH orbitals (Fig. 5.3b) have occupancy of 0.46 electrons and localize within native basin by 33%. The sum of the norms, which each of the 12 direct neighbors receive from

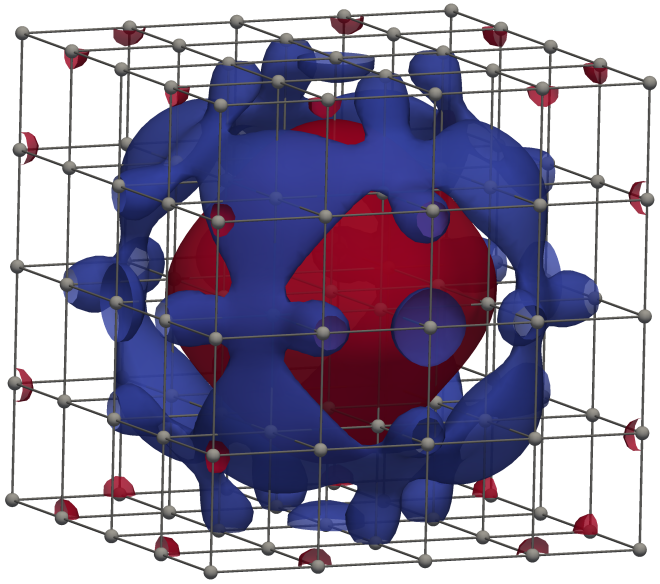

Figure 5.2: DAFH orbital from DFT calculation for 3DH lattice. The basin of the corresponding DAFH orbital is attributed to the central atom. The isosurface of orbital amplitude is equal to 0.01. The change in color corresponds to the change in phase.

p-like DAFH orbitals, is equal approximately to 15%, however the contributions to this sum from the distinct p-like DAFH orbitals are not equal due to the spatial form of the 3p states. Thus, among 12 direct neighbors two sorts can be distinguished – the one, that gets 12% of the norm from one of the p-like DAFH orbitals and 1.5% from other two, and the one, that gets 7% of the norm from the two p-like DAFH orbitals and 1% from the remaining one. Totally 3p DAFH orbitals contribute $2*0.460*0.150 = 0.138$ electron pairs (or 53%) to the delocalization index between two neighboring aluminum basins. Since s-like DAFH orbital covers additionally $2 * 1.120 * 0.026 = 0.058$ electron pairs (22%) from the considered delocalization index, the remaining $0.262 - 0.138 - 0.058 = 0.066$ shared electron pairs are contributed by the higher lying states, which should be empty in the case of isolated aluminum atom. In the given analysis those higher states mainly represented by six DAFH orbitals with population of 0.07 electrons each (Fig. 5.3c).

The analysis of *bcc* ferromagnetic iron requires a separate consideration of different spins. The two considered spin states (further "spin-up" and "spin-down" states) give unequal contributions to the total amount of shared electron pairs. To the value of the delocalization index between two neighboring basins "spin-up" electrons contribute 0.309 (62.7%) electron pairs, while "spin-down" electrons contribute the rest 37.3%. Thus the contribution of "spin-up" electrons to the covalent interaction with the first-coordination shell is almost in 1.7 times higher than the contribution of "spin-down" electrons. However the relative contribution of two spin states to the covalent interaction

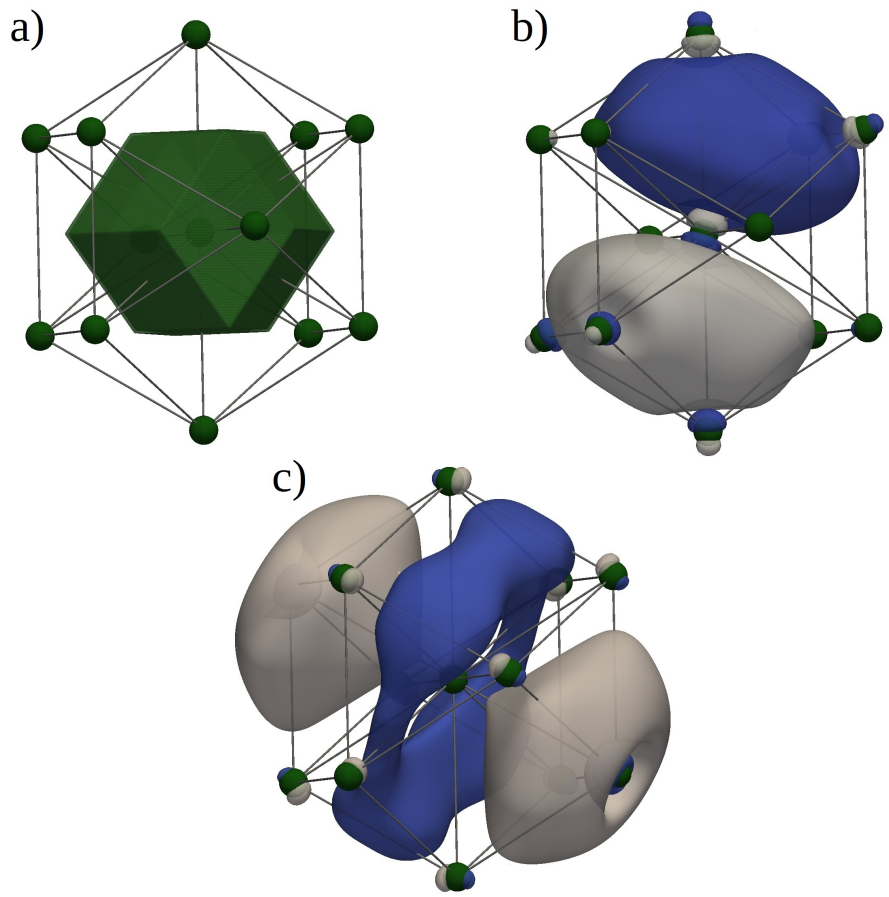

Figure 5.3: a) QTAIM basin of the central aluminum atom; b) DAFH orbital for the same aluminum atom with occupancy of 0.46 electrons; c)DAFH orbital for the same aluminum atom with occupancy of 0.07 electrons. The isosurfaces of orbital amplitudes are equal to 0.02. The change in color corresponds to the change in phase.

with the second-coordination shell becomes not so sharp - "spin-up" electrons contribute only in 1.4 times more shared electron pairs. Like in the case of aluminum the amount of distantly shared electron pairs is quite high and equal to $2 * 2.875 - 8 * (0.309 + 0.184) = 1.806$ (31.4%). The results from the (L)APW calculations confirm the previous conclusions, giving a bit higher number of distantly shared electron pairs – 1.994 (33.4%).

Two sets of DAFH orbitals for both spins reveal perfectly localized within native basin s and p-type DAFH orbitals which can be associated with 3s and 3p atomic orbitals respectively (table 5.4). However, the rest of DAFH orbitals are different. For "spin-up" set one can distinguish five d-like DAFH orbitals, which can be associated with 3d atomic orbitals, one s-like DAFH orbital, that can be attributed to 4s atomic orbital, and three p-like DAFH orbitals with occupations close to 0.1 electrons. Contrary, "spin-down" set comprises three sub-sets with three quite delocalized DAFH orbitals within each, which can not be unambiguously associated with any atomic orbital. However their number

Table 5.4: DAFH orbital analysis for simple metals. Only valence electrons are considered.

Compound	n_i^A[a]	$p_i^A(A)$[b]	DAFHo type	$\sum_i n_i^A$[c]
Al	1×1.12	0.66	s-type(3s)	2.85
	3×0.46	0.33	p-type(3p)	
	6×0.07	<0.1	mixed types	
Fe(ferr)		"spin-up"		
	1×1.00	1.00	s-type(3s)	8.97
	3×1.00	1.00	p-type(3p)	
	2×0.91	0.92	d-type(3d)	
	3×0.84	0.87	d-type(3d)	
	1×0.30	0.30	s-type(4s)	
	3×0.11	0.11	p-type(4p)	
		"spin-down"		
	1×1.00	1.00	s-type(3s)	6.82
	3×1.00	1.00	p-type(3p)	
	3×0.49	0.51	mixed types	
	3×0.32	0.33	mixed types	
	3×0.13	0.14	mixed types	

[a] DAFH orbital occupation.
[b] DAFH orbital norm in corresponding QTAIM basin.
[c] Sum of DAFH orbital occupations.

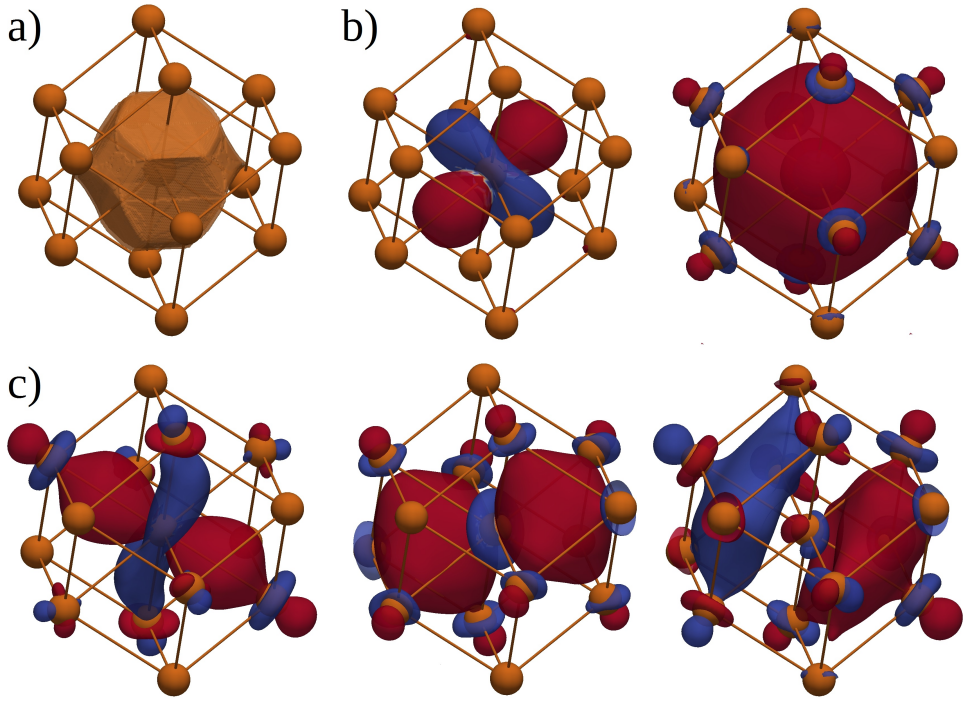

Figure 5.4: a) QTAIM basin of the central iron atom; b) DAFH orbitals for "spin-up" electrons: to the left - d-like DAFH orbital with occupancy of 0.84 electrons, to the right - s-like DAFH orbital with occupancy of 0.30 electrons ; c)DAFH orbitals for "spin-down" electrons: to the left - DAFH orbital with occupancy of 0.49 electrons, to the center - DAFH orbital with occupancy of 0.33 electrons, to the right - DAFH orbital with occupancy of 0.13 electrons. The isosurfaces of orbital amplitudes are equal to 0.04. The change in color corresponds to the change in phase.

– totally nine such DAFH orbitals – allows to suggest that they can be decomposed on contributions from five 3d, one 4s and three 3p atomic orbitals.

5.1.3 Covalent and ionic bonding

Diamond represents a solid with single order covalent bonds. Both methods estimate the delocalization indices between closest atoms as being a little less that 1. The PAW method predicts $4 * 0.913 = 3.652$ electron pairs shared with direct neighbors and $2 * 2.191 - 3.652 = 0.73$ (16.7%) pairs shared with distant basins. The (L)APW method stands for 3.656 and 0.72 electron pairs respectively.

There are four half localized DAFH orbitals (the localization norm is equal to 48.1%) with occupancy 0.94 electrons within one carbon basin (figure 5.5). Each of them is directed toward one of the adjoining carbon basins and almost all remaining part of their norms (39% – 40%) are localized there. Taking into account that there is one more orbital, which stems from the adjoining atom and is directed toward the given one with

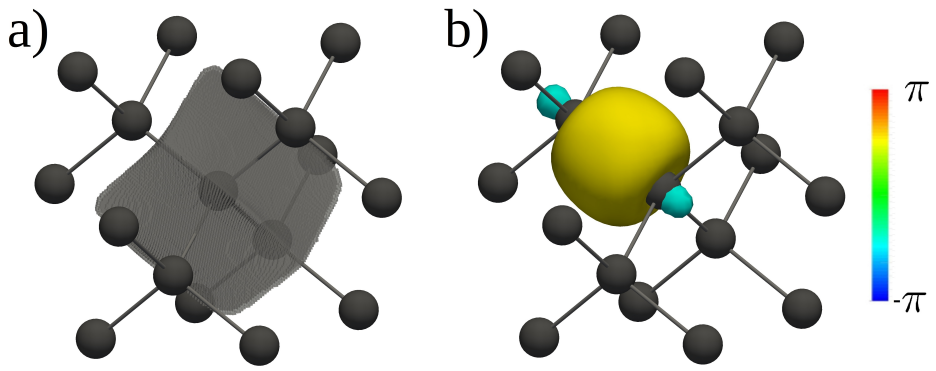

Figure 5.5: a) QTAIM basin of carbon atom in diamond; b) DAFH orbital for carbon atom in diamond. The amplitude of orbital isosurface is equal to 0.01.

the same occupancy due to symmetry, there are $2 * 0.94 = 1.88$ electrons participated in one chemical bond, that is close to 2 and corresponds to single order covalent bond.

Sodium cloride represents a crystal with ionic type of bonding, where atoms hold together mainly due to electrostatic forces. A part of the electron density is "transferred" from one atom (which is the cation) to another atom (which is the anion). As a result one should expect an increase in the anion QTAIM basin electron population and a decrease of the same amount in the cation QTAIM basin electron population (assuming that there are equal numbers of anions and cations). A great degree of electron pairs sharing between cations and anions is not expected thereby the fluctuation in electron populations should be rather small.

Indeed, the electron population of sodium basin is decreased by 0.87 electrons in the case of PAW method and by 0.85 electrons is the case of (L)APW method, while the electron population of the chlorine basins is increased by the same amount. The values of the delocalization indices are very low and do not exceed 0.1, while the localization indices are high and cover 95.35% for the sodium atom and 97.07% for the chlorine atom of total electron populations within those basins. The sodium basin shares $6 * 0.070 = 0.420$ electron pairs with adjoining chlorine basins (0.432 in the case of the (L)APW method) and a negligible small number of electron pairs with other sodium basins. Contrary, the chlorine basin shares $12 * 0.047 = 0.564$ electron pairs with nearest chlorine basins (0.576 in the case of the (L)APW method), that is even more than with the adjoining sodium basins.

DAFH orbitals – as example, for the chlorine basin (fig. 5.6b), – are almost completely localized. Considering only valence orbitals, there are p-like orbitals with occupancy 1.89 electrons (with 95% of their norm localized within given chlorine basin), that are analogous to 3p atomic orbitals, and one s-like orbital with occupancy 1.98 electrons (with 99% of it norm localized within given chlorine basin), that is analogous to a 3s

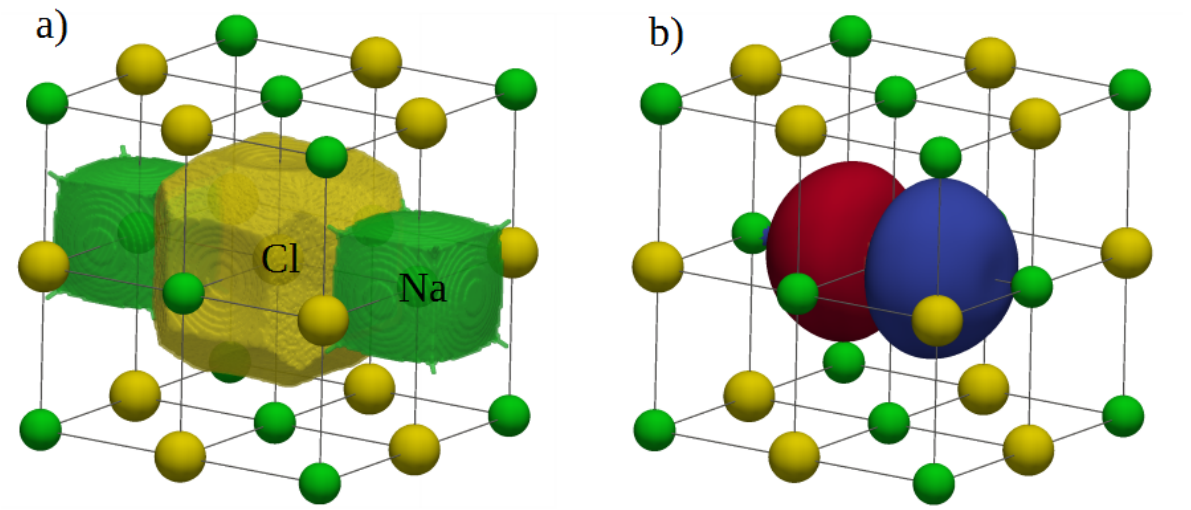

Figure 5.6: a) QTAIM basin of the chlorine and sodium atoms in NaCl; b) DAFH orbital for the chlorine atom, which associates with one of 3p atomic orbitals. The amplitude of the orbital isosurface is equal to 0.01. The change in color corresponds to the change in phase.

atomic orbital.

5.1.4 Magnesium Diboride

The crystal structure of MgB_2 is formed by alternating closed-packed hexagonal magnesium layers and honeycomb boron layers. The primitive cell comprises one magnesium atom and two boron atoms. MgB_2 is regarded as a metal and exhibits superconducting properties[189]. The investigation of electronic states reveals that those at the Fermi level are mainly due to σ- or π- bonding boron orbitals, with the σ-bonding states being confined to the boron layer[190]. This resembles the picture in in graphite, however in the case of MgB_2 the σ-bonding states are not fully occupied due to smaller number of electrons of the boron atom than the number of electrons in carbon atom.

The results given by the (L)APW and the PAW methods are similar and, despite some more clearly underlined differences than it was before for other compounds, lead to identical general conclusions. As expected the magnesium basin acts as a cation by transferring 1.58 electrons (1.60 electrons in the case of (L)APW method) to the two boron basins. Consistently, the boron basins experience an increase in their electron population by $1.58/2 = 0.79$ electrons. The analysis of basins shapes reveals a muffin-like structure, where sphere-like magnesium basins are strongly localized around magnesium nuclei and are not in direct contact with each other. The whole remaining space is filled

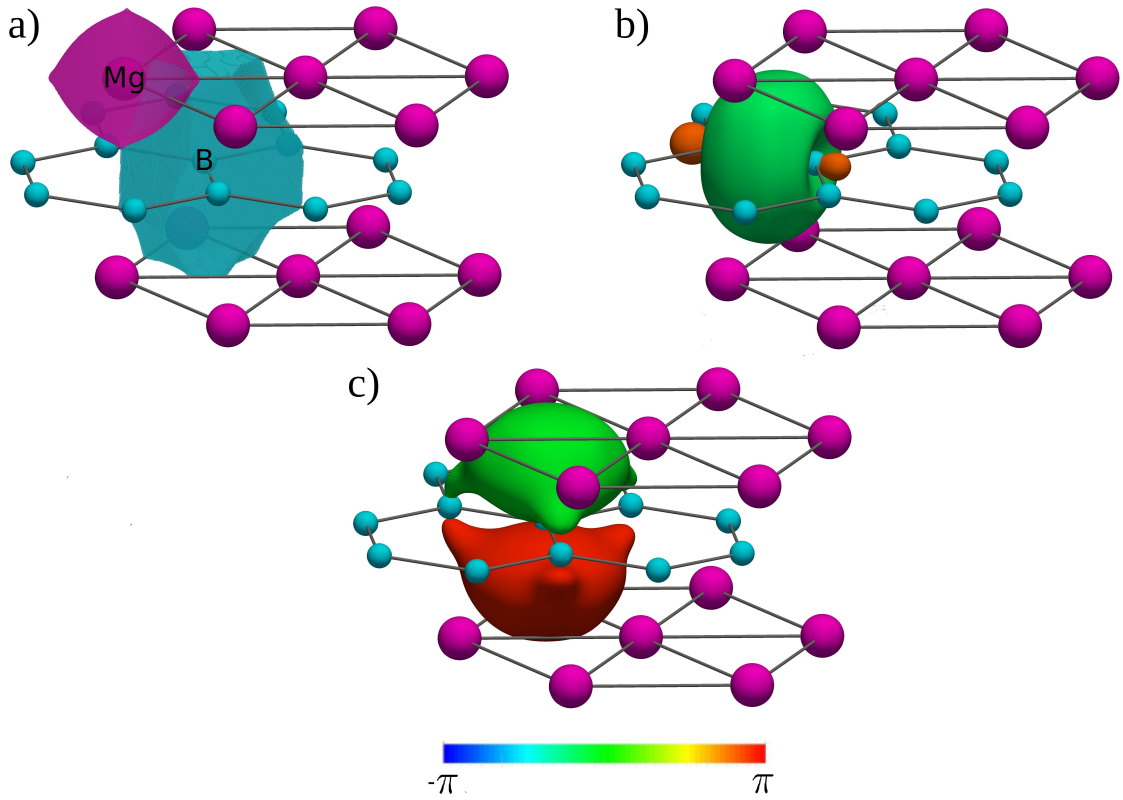

Figure 5.7: a) QTAIM basins of the magnesium and the boron atoms in MgB_2; b) DAFH orbital of the boron atom which is localized within boron layer; c) delocalized DAFH orbital of the boron atom. The amplitudes of orbital isosurfaces are equal to 0.05.

by boron basins. While the values of the localization and the delocalization indices for the magnesium basin are typically low as for ionic compounds, the respective values for the boron basins indicate a high degree of electron sharing. The PAW method predicts a slightly higher degree of electron pairs fluctuation within boron basins and slightly lower delocalization indices for adjacent boron basins than the (L)APW method. According to the PAW method there are $3*0.936 = 2.808$ electron pairs shared between a given boron basin and his direct boron neighbors, and $6*0.062 = 0.372$ electron pairs shared between it and closest magnesium basins. The remaining $2*2.221-2.808-0.372 = 1.262$ electron pairs of this basin are shared with distant basins. The (L)APW method estimates the number of electron pairs which are shared between distant basins and given boron basin as equal to $2 * 2.118 - 3 * 0.984 - 6 * 0.064 = 0.900$. Thus the PAW method predicts a higher degree of long-range delocalization.

From the shapes of the DAFH orbitals for the boron atoms it is easy to draw a conclusion that the orbital which is accountable for electron delocalization over whole crystal volume should be a π-type orbital. Three other valence orbitals are localized within boron layer and directed toward the closest boron neighbors giving a picture of

the electron distribution that resembles the graphite case[152]. The three DAFH orbitals that are localized within boron layer orbitals and posses occupancies close to 0.88, while the p-like orbital possesses a bit smaller occupancy – 0.84. Thereby together with the core 1s orbital they cover 5.48 (94.5%) from total population of 5.79 electrons for boron QTAIM basin. 42% of the p-like DAFH orbital norm is found inside the corresponding QTAIM basin. Approximately 33% is in the first coordination shell – 26.4% fall onto three boron neighbors and 8.4% fall onto six magnesium neighbors. In the case of the three localized within boron layer DAFH orbitals, 46% of their norms are localized within native basin. Almost all remaining norm (39.7%) is localized within adjoining boron basin in the direction of which given DAFH orbital is directed.

5.2 ELI-D

The PAW implementation of the ELI approach possesses its own advantage over using the (L)APW method. For the latter the most troublesome regions are muffin tin spheres surfaces, were the matching between the atomic-like wave functions from the muffin tins and the plane waves from the interstitial region should be satisfied. However, the perfect matching is available only for an infinite multipole expansion of the APW functions, which is not the case for real calculations. Thus, real-space properties that are derived from the (L)APW method, such as ELF and ELI, can suffer from discontinuities at the surfaces of muffin tin spheres[178]. Such artifacts have the tendency to reduce with the increase of the basis set size, however they do not disappear. Contrary, in the PAW method, upon the condition of using good partial waves dataset, the continuity of the real-space properties at the boundaries of muffin tin spheres is ensured. Indeed, as it seen from Fig. 5.8 the ELI-D function from the (L)APW method experiences an abrupt leap at the distance from nuclei that is equal to the radius of the muffin-tin sphere, while the ELI-D function from the PAW method is smooth over the whole space.

The resulting ELI-D field from the PAW method and is identical to the one obtained from the (L)APW method with only minor deviations, that will be demonstrated on the examples of *fcc*-aluminum and magnesium diboride.

In the case of aluminum (Fig. 5.9) the ELI-D field shows four types of regions with a heightened concentration of electron pairs – two types near the nucleus, one in the connecting line between aluminum atoms and one around the tetrahedral voids of the packing. The presence of the last is in line with the previous investigation of aluminum with ELF, where in addition to the ELF bonding attractors in the midpoint of the nearest aluminum atoms another ELF attractor with corresponding monosynaptic basin was detected[191].

The construction of ELI-D basins recovers two spherical-like basins around the alu-

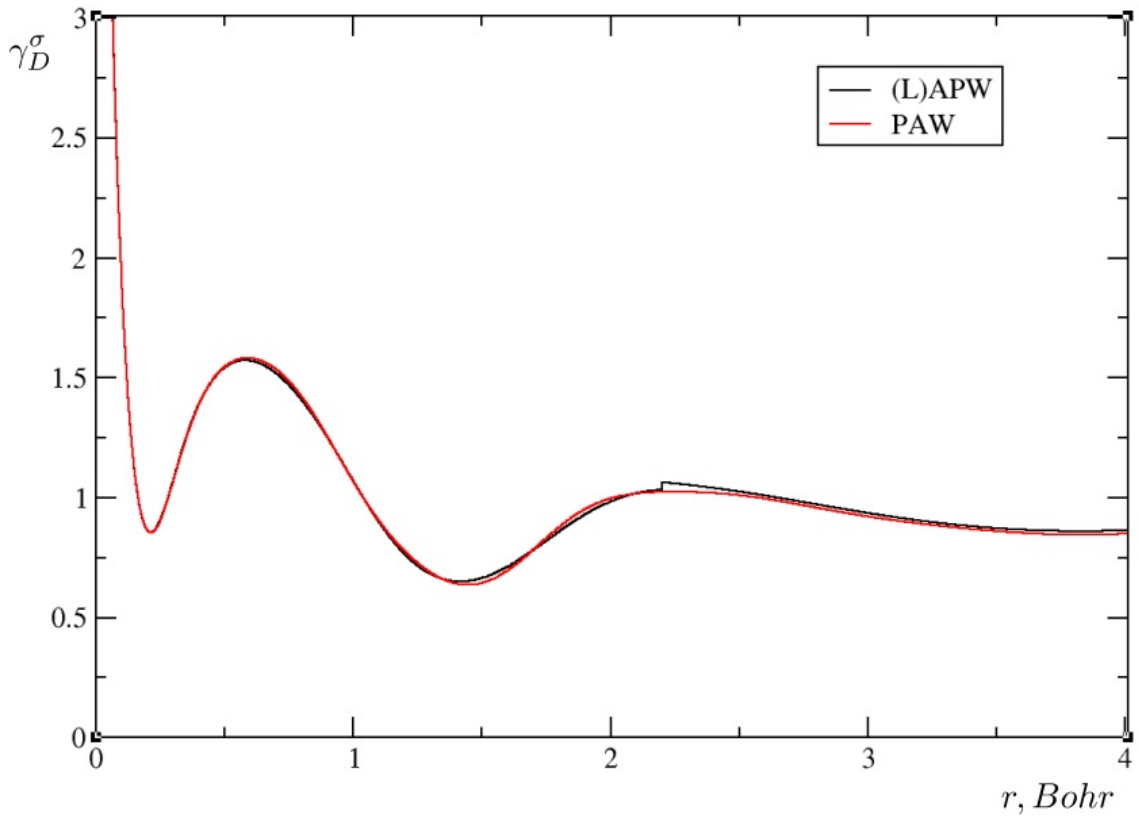

Figure 5.8: ELI-D field for aluminum from (L)APW and PAW calculations. Direction (1 0 0). Muffin-tin radius for the (L)APW calculation is equal to 2.2 Bohr, muffin-tin radius for the PAW calculation is equal to 1.9 Bohr

minum nuclei, the first of which is closer to the nucleus and comprises 2.17 electrons (2.18 in the case of the (LAPW) method) and is attributable to the first electron shell, and the second one encloses the first one and comprises 7.94 electrons (7.90 in the case of the (L)APW method) and is attributable to the second electron shell. Since for one atom there are twelve closest neighbors, the (L)APW method gives twelve ELI-D basins between atom pairs with 0.40 electrons inside. The PAW method gives in average 0.43 electrons within the analogous type of ELI-D basins (Fig. 5.9, basin number 2). Finally, both methods give eight basins for each aluminum atoms, associated with the attractors within the tetrahedral voids. The (L)APW methods predicts in average 0.07 electrons, while the PAW methods states on average occupation of 0.04 electrons(Fig. 5.9, basin number 3).

For magnesium diboride the ELI-D field reveals except the core shells for magnesium and boron atoms also high ELI-D values between boron atoms, thus revealing covalent bonds between them (Fig. 5.10). The corresponding basin penetrates the whole primitive cell and comprises approximately 2.59 electrons. Totally 3 such basins could be

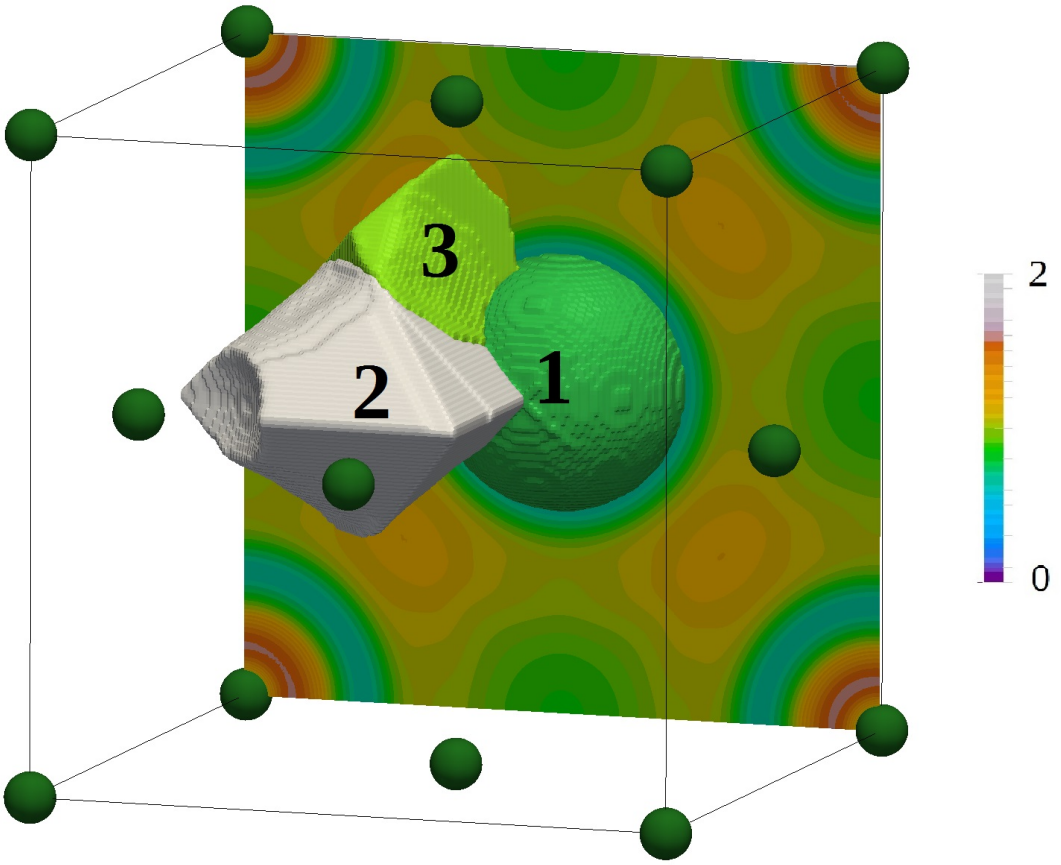

Figure 5.9: ELI-D field together with the domain between two neighboring atoms for aluminum from PAW calculation. 1 – ELI-D basin of second electron shell, population 7.94 electrons; 2 – ELI-D basin with population 0.43 electrons; 3 – ELI-D basin with population 0.04 electrons.

distinguished for one primitive cell. The rest of the primitive cell space is partitioning as follow – two basins with 2.09 electrons within, which enclose boron nuclei (boron first electron shells), one basin with 2.18 electrons within, that encloses magnesium nucleus (magnesium first electron shell), and one basin with 7.88 electrons within, that corresponds to the magnesium second shell. No special attractors between boron and magnesium atoms are detected, thus the magnesium atom is involved only in ionic-like interaction, donating almost 2 electrons (1.94) to the boron atoms. The (L)APW calculation gives the same partitioning of the primitive cell space and almost perfectly replicates the charges within those domains. According to the (L)APW method the first boron electron shell contains 2.09 electrons, the first magnesium electron shell contains 2.17 electrons, the second magnesium electron shell contains 7.89 electrons and the three interstitial domains contain 2.59 electrons each.

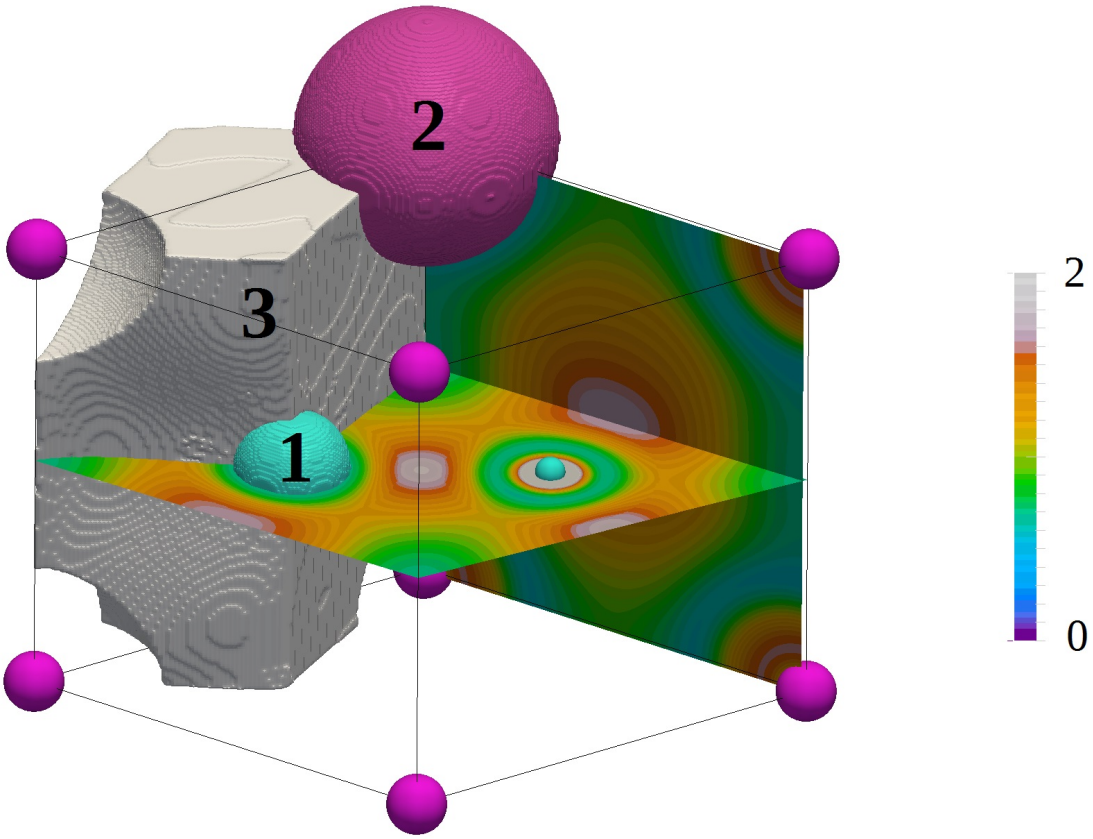

Figure 5.10: ELI-D field together with the ELI-D basins for MgB_2 from the PAW calculation. 1 - ELI-D basin of the boron first electron shell, population - 2.09 electrons; 2 - ELI-D basin of the magnesium second electron shell, population - 7.88 electrons; 3 - ELI-D basin in between boron atoms that represents B-B bonding, population - 2.59 electrons. Atoms are colored according to the Fig. 5.7.

5.3 Concluding Remarks Concerning Performance

The comparison of the current domain overlap matrix elements evaluation scheme implemented for the PAW method with the previous scheme implemented for the (L)APW method reveals a significant reduction of time and memory required for the complete calculation of overlap matrix. The degree of time reduction lies in a quite broad range – from 5 to 25 times depending on the compound, while the memory reduction is in the range from 1.5 to 3 times. Since the algorithm for the domain overlap matrix elements evaluation implemented for the (L)APW method also scales as a $O(N \log N)$ complexity procedure, the nature of such speedup is formed by specific peculiarities of the (L)APW and the PAW methods. As example, the muffin-tin part can be considered. In the framework of the (L)APW method multipole expansions within muffin-tins require the considering of very large orbital momenta, up to 30. That makes the computational costs required for evaluation of muffin-tin and plane wave interstitial parts comparable

Table 5.5: Time required for the evaluation of muffin-tin and plane wave contributions to the domain matrix overlap elements. Present results are taken for the individual basins as average of 5 independent calculations at single core with the clock frequency 2.4 GHz, processor type – Intel Core(TM) i7-3740QM.

Compound	Basin	Muffin-tin part (*sec*)	Plane wave part (*sec*)
Diamond	C	165	1280
MgB_2	Mg	848	7309
	B	878	7399
NaCl	Na	517	28661
	Cl	507	31188

with each other. The PAW method does not require such huge multipole expansions, the maximum size of multipole expansion is governed by the equation 4.26 and 4.27 and can not exceed the doubled maximum angular momentum, that makes the process of evaluation of a muffin-tin part much faster than the plane wave part.

That is why the addition of extra partial waves per angular moment in PAW datasets should not significantly increase the computational time. As seen from table 5.5, the relative part, which is required for the evaluation of muffin-tin contributions, is quite small, about 2 – 13 %. Moreover this relative part becomes even smaller with an increase of the complexity of the computations, i.e. with the increase of the number of plane waves per state. In our computations, the addition of one extra partial wave per angular momentum in the dataset for carbon atom results in the increase of the computational time of one minute, while the addition of one extra partial wave per angular momentum in the dataset for boron atom in the case of magnesium diboride results in the increase of the computational time of 22 minutes, that is less than 4%. The corresponding values of localization and delocalization indices do not experience any significant change, all changes do not exceed 0.01 electron pairs.

Chapter 6

Complex Compounds

As examples of complex compounds the niobium complex $Nb_2(Se_2)_2(AlCl_4)_4$[192], two rhodium chalcogenides $Rh_{17}S_{15}$ and $Cu_2Rh_{34}S_{30}$, and two akin bimetallic compounds Bi_8Ni_8S and $Bi_8Ni_8SI_2$[193] were chosen. All computational details are collected to the table 6.1. As for the simple compounds, for the complex ones projector and partial functions for the PAW datasets have been taken from the official ABINIT[184] site. The data sets for Al, Rh and S in the cases of rhodium chalcogenides were modified in order to avoid overlapping between atomic spheres. The modified ATOMPAW input files are presented in Appendix A. The LDA approximation with Perdew-Wang exchange-correlation functional[13] was used for the computation of Bi_8Ni_8S and $Bi_8Ni_8SI_2$, while for the computation of $Nb_2(Se_2)_2(AlCl_4)_4$ and rhodium chalcogenides the GGA approximation with Perdew-Burke-Ernzerhof functional[14] was used.

6.1 Niobium (IV) complex $Nb_2(Se_2)_2(AlCl_4)_4$

The ternary compound of the transition metal niobium shows diamagnetic and semiconducting properties and is build by discrete $Nb_2(Se_2)_2(AlCl_4)_4$ molecular fragments. The structure of the $Nb_2(Se_2)_2(AlCl_4)_4$ molecule together with QTAIM basins for consistent atoms are depicted at figure 6.1a. The unit cell of $Nb_2(Se_2)_2(AlCl_4)_4$ crystal comprises two molecules that leads to 52 atoms per unit cell, and, assuming the choice of core states and $\vec{k}$-point mesh (table 6.1), to over 4000 valence bands. The oxidation number of the niobium atom (+4) points towards the forming of Nb-Cl, Nb-Se and Nb-Nb covalent bonds, thus suggesting the dominant covalent bonding pattern holding the structure together.

According to the QTAIM charges the niobium basin loses 1.5 electrons, which are redistributed among four selenium and four closest chlorine basins. The quite moderate increase in electron population of selenium basins (at only 0.13 electrons per basin) indi-

Table 6.1: Calculation details for ABINIT. Complex compounds.

Compound	Cell (a.u.)	E_{cut}(Ha)	r_{cut}(a.u.)	core orbitals	k-point mesh
$Nb_2(Se_2)_2(AlCl_4)_4$	a=16.97	20.0	2.21 (Nb)	[Ar]3d	3×3×2
	b=18.73		2.10 (Se)	[Ar]	
	c=30.79		1.50 (Cl)	[Ne]	
	$\alpha = \gamma = 90.00$		2.20 (Al)	[Ne]	
	$\beta = 92.43$				
$Rh_{17}S_{15}$	a=b=c=18.72	18.0	2.27 (Rh)	[Ar]3d	2×2×2
	$\alpha = \beta =$		1.70 (S)	[Ne]	
	$=\gamma = 90.0$				
$Cu_2Rh_{34}S_{30}$	a=b=c=18.85	18.0	2.27 (Rh)	[Ar]3d	2×2×2
	$\alpha = \beta =$		1.70 (S)	[Ne]	
	$=\gamma = 90.0$		2.02 (Cu)	[Ne]	
Bi_8Ni_8S	a=33.07	18.0	2.91 (Bi)	[Xe]5d4f	2×3×3
	b=19.04		1.81 (Ni)	[Ne]	
	c=15.86		1.91 (S)	[Ne]	
	$\alpha = \beta =$				
	$=\gamma = 90.0$				
$Bi_8Ni_8SI_2$	a=18.76	18.0	2.91 (Bi)	[Xe]5d4f	3×2×3
	b=40.77		1.81 (Ni)	[Ne]	
	c=15.71		1.91 (S)	[Ne]	
	$\alpha = \beta =$		2.30 (I)	[Kr]4d	
	$=\gamma = 90.0$				

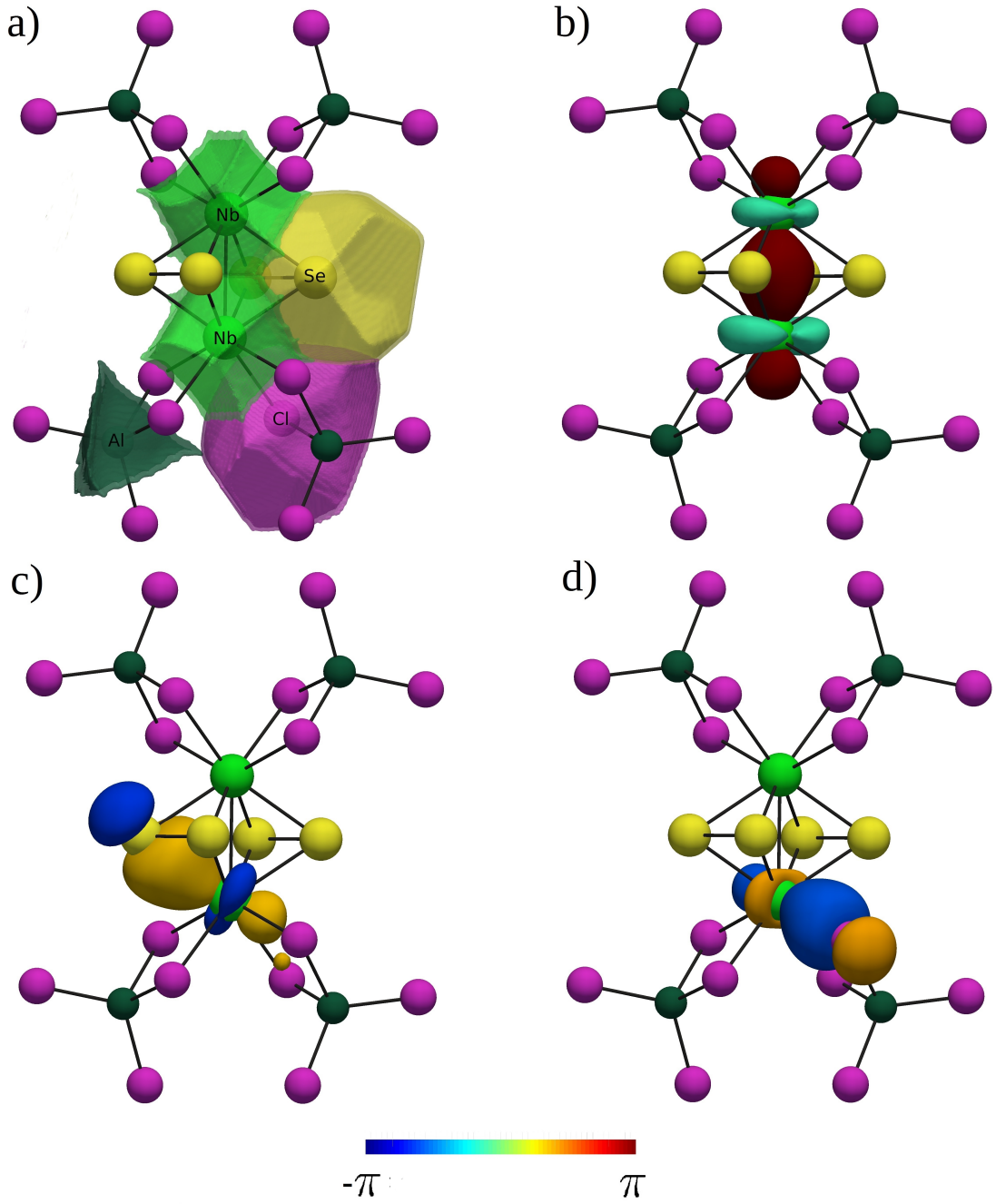

Figure 6.1: a) QTAIM basin for constituent atoms in the $Nb_2(Se_2)_2(AlCl_4)_4$ complex; b) DAFH orbital which represents Nb-Nb covalent bonding; c) DAFH orbital which represents Nb-Se polar covalent bonding; d) DAFH orbital which represents Nb-Cl polar covalent bonding. The amplitude of the orbital isosurface is equal to 0.06.

Table 6.2: Localization and delocalization indices for QTAIM basins in the niobium complex $Nb_2(Se_2)_2(AlCl_4)_4$.

Atom	$N(A)$	$\sigma^2(A)$	$\lambda(A)$	$A-B$	$\delta(A,B)$
Nb	39.50	2.643	36.857	Nb-Nb	0.594
				Nb-Se	0.707
				Nb-Cl	0.410
Se	34.13	1.720	32.410	Se-Se (4.31 a.u.)	1.244
				Se-Se (6.95 a.u.)	0.060
Cl	17.70	0.795	16.909	Cl-Cl (6.04 a.u.)	0.115
				Cl-Cl (6.06 a.u.)	0.172
Al	10.65	0.599	10.054	Al-Cl	0.237

Table 6.3: DAFH orbital analysis for niobium atom in the $Nb_2(Se_2)_2(AlCl_4)_4$ crystal structure.

Atom	n_i^A[a]	$p_i^A(A)$[b]	$p_i^A(B)$[c]	$\sum_i n_i^A$[d]
Nb	4×2.00	1.00	0.00	11.48
	1×0.88	0.45	0.30 (Nb)	
			0.16 (4Se)	
			0.08 (4Cl)	
	4×0.47	0.27	0.57 (Se)	
			0.16	
			(Nb+4Cl+3Se)	
	4×0.18	0.13	0.73 (Cl)	
			0.14 (3Cl+4Se)	

[a] DAFH orbital occupation.
[b] DAFH orbital norm in corresponding QTAIM basin.
[c] DAFH orbital norm in QTAIM basins of the coordination shell.
[d] Sum of DAFH orbital occupations.

cates that $1.50 - 2 * 0.13 = 1.24$ electrons are transferred to chlorine basins (0.31 per one basin). The values of the delocalization indices confirm the existence of chemical bonds not only between niobium and chlorine and selenium atoms, but also between the two niobium atoms. The last is important since not all methods can give a clear picture. For example, ELI-D analysis shows that the corresponding Nb-Nb bonding basin comprises only 0.26 electrons[192], that is not what one expects from a two-electron two-center covalent bond. From the total amount of electron pairs shared by the niobium basin with other basins $2.643 * 2 = 5.266$, 0.594 (11.3%) pairs drop to sharing with another niobium basin, $4 * 0.707 = 2.828$ (53.7%) pairs drop to sharing with four selenium atoms and $4 * 0.410 = 1.640$ (31.1%) pairs drop to sharing with four closest chloride basins. The remaining 3.9% of electron pairs are shared with distant basins.

The selenium atoms appear to be in strong interaction only with the two niobium atoms and the closest selenium neighbor. Despite the two unpaired electrons in 4p atomic orbitals of selenium atom, the double-bond rule[194], which says that multiple bonds are prohibited for the main group elements with principal quantum number greater than 2, seemingly not allow to form a double bond with the closest selenium neighbor. But the value of the Se-Se delocalization index (1.244) indicates the forming of a covalent Se-Se bond with the order greater than 1. It can not be regarded as a complete double bond, since the corresponding delocalization index value is much less than two, but can be viewed as the intermediate state between single and double order bond. In principle, such effect is not a complete novelty, since the deviations from the double-bond rule have already been discovered. As example the organic compound selenoketone ($R_2C{=}Se$)[195, 196] can be mentioned.

DAFH orbital analysis reveals 13 valence DAFH orbitals per one niobium atom with the occupancy greater then 0.01 (table 6.3), four of them are perfectly localized and correspond to one 4s and three 4p atomic orbitals. The Nb-Nb bond seemingly forms due to overlapping of d_{z^2} type of orbitals, 45% of corresponding DAFH orbital norm (Fig. 6.1b) is localized within native basin, while 30% is localized within second niobium basin. The occupancy of this orbital is equal to 0.88, and since there is the analogous DAFH orbital with the same occupancy for the second niobium basin, the formation of two-electron bond can be postulated. Moreover, this DAFH orbital covers $2 * 0.88 * 0.30 = 0.528$ (88.8%) from the Nb-Nb delocalization index, thus Nb-Nb interaction can be described almost completely just with these DAFH orbitals.

The DAFH orbitals, which are responsible for niobium-selenium (Nb-Se) and niobium-chlorine (Nb-Cl) bonds, look as some type of hybrid orbitals. Four DAFH orbitals (Fig. 6.1c), each with occupation of 0.47 electrons, describe Nb-Se bonding. The major part of the norm (57%) is confined within selenium QTAIM basin, while within native niobium basin there are 47% of its norm. This DAFH orbitals cover 75.8% of the Nb-Cl

delocalization index. These findings confirm the polar covalent character of Nb-Se bond. Four other DAFH orbitals (Fig. 6.1d) with the occupation of 0.18 electrons represent similar but more polar Nb-Cl bonding. The greater polarity is confirmed by the smaller number of the norm preserved within niobium QTAIM basin comparatively to the case of Nb-Se bonding. Corresponding DAFH orbitals cover 64.1% from the Nb-Cl delocalization index.

It also worth to mention a non negligible delocalization of all bonding DAFH orbitals. A quite significant part of their norms (up to 24% in the case of Nb-Nb bond) are localized within surrounding atoms.

Thus the present analysis allows to fully recover all covalent bonding patterns within the $[Nb_2(Se_2)_2]^{4+}$ group with establishing of several subtle peculiarities such as the somewhat mmulticenter character of bonds, which of Nb-Se and Nb-Cl bonds are more polar, and whether Nb-Nb bond is really formed.

6.2 Rhodium chalcogenides $Rh_{17}S_{15}$ and $Cu_2Rh_{34}S_{30}$

Rhodium sulfide $Rh_{17}S_{15}$ belongs to the class of noble metal chalcogenides characterized by high catalytic activity[197]. It has been found that this compound exhibits supeconductivity, caused, as believed, by strongly correlated 4d electrons of Rh[198,199]. As it seen from the structure (Fig. 6.2) the Rh atoms are arranged in cubic-like lattices with the voids in the centers, where different dopants can be placed. That is the way how $Cu_2Rh_{34}S_{30}$ is formed, since Cu atom takes the role of such dopant. However, despite the structure of $Cu_2Rh_{34}S_{30}$ is almost the same as $Rh_{17}S_{15}$, the first one is no longer exhibits superconductivity[200], thus the doping with Cu atoms ruins it. The main aim of the ensuing chemical-bonding analysis is to determine the electron distribution changes, that underlie such significant changes in physical properties.

The analysis of QTAIM charges of $Cu_2Rh_{34}S_{30}$ reveals a charge transfer from Cu atom to the Rh-S framework (Fig. 6.3, further atoms will be labeled according to this figure). That results in slight increase of negative charge at S atoms, whereas overall charge of Rh atoms become more positive.

The value of delocalization index between Cu and closest Rh atoms points towards the substantial degree of covalency in Cu-Rh interaction. Moreover the non-negligible degree of covalency is traced in Cu-S interaction, thus indicating that Cu atom shares electrons with the whole Rh-S framework. In the same time the value of Rh-S, Rh-S', Rh-Rh' and Rh-Rh" delocalization indices in $Cu_2Rh_{34}S_{30}$ is lower than in $Rh_{17}S_{15}$ (see table 6.4) that, together with above mentioned changes in QTAIM charges, points towards the increase of ionic character in Rh-S interactions and redistribution of Rh electrons in the favor of interaction with copper. The latter is appeared to be the reason for destroying

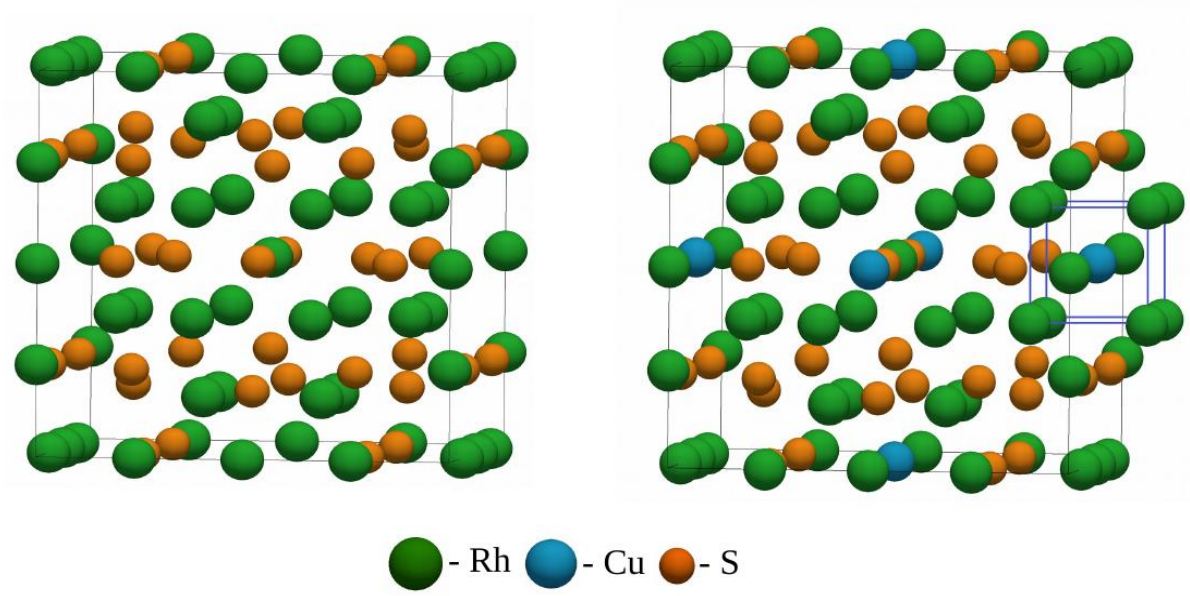

Figure 6.2: Structures of a) $Rh_{17}S_{15}$ and b) $Cu_2Rh_{34}S_{30}$.

the superconductivity. However from the shown numbers it is hard to make a conclusion which states are involved in such changes, that is the task for further DAFH analysis.

The set of DAFH orbitals for one of the Rh atoms, arranged in cubic-like formation, comprises 13 orbitals with occupancy higher than 0.1 electrons. From them 4 DAFH orbitals localize within native basin almost perfectly and can be associated with 4s and 4p states, that do not involved in bonding. Five DAFH orbitals have d-like shapes and among them there is one that significantly contributes to Rh-Rh" interaction in both compounds but in $Cu_2Rh_{34}S_{30}$ it partially reorients towards Cu atom and contributes less to the Rh-Rh" delocalization index. Thus in the case of $Rh_{17}S_{15}$ (Fig. 6.4a) it has occupancy of 1.47 electrons and localizes within neighboring Rh atom by 5% – it means that this DAFH orbital covers $1.47 * 0.05 * 2 = 0.147$ (42.0%) from $\delta(Rh - Rh'') = 0.349$. In the case of $Cu_2Rh_{34}S_{30}$ (Fig. 6.4b) the occupancy of analogous DAFH orbital drops to 1.43 electrons and its localization within neighboring Rh decreases to approximately 3%, that means that this DAFH orbital covers $1.43 * 0.03 * 2 = 0.086$ (33.0%) from $\delta(Rh - Rh'') = 0.264$. Moreover, this DAFH orbital localizes by 4% within Cu atom, thus contributing $1.43 * 0.04 * 2 = 0.114$ to $\delta(Cu - Rh) = 0.26$. Four remaining DAFH orbitals have occupancies below 1.0 electron and can be associated with 5s-5p states or mixture of them. Among these DAFH orbitals also can be found one, which contributes less to the Rh-Rh interaction upon doping with Cu atoms. In $Rh_{17}S_{15}$ (Fig. 6.4c) its occupancy is equal to 0.20 electrons and it localizes by 21% within Rh" basin, thus contributing 0.084 (24%) $\delta(Rh - Rh'')$. In $Cu_2Rh_{34}S_{30}$ (Fig. 6.4d) its occupancy is equal to 0.21 electrons but its localization degree within Rh" basin fall to 16%, thus it

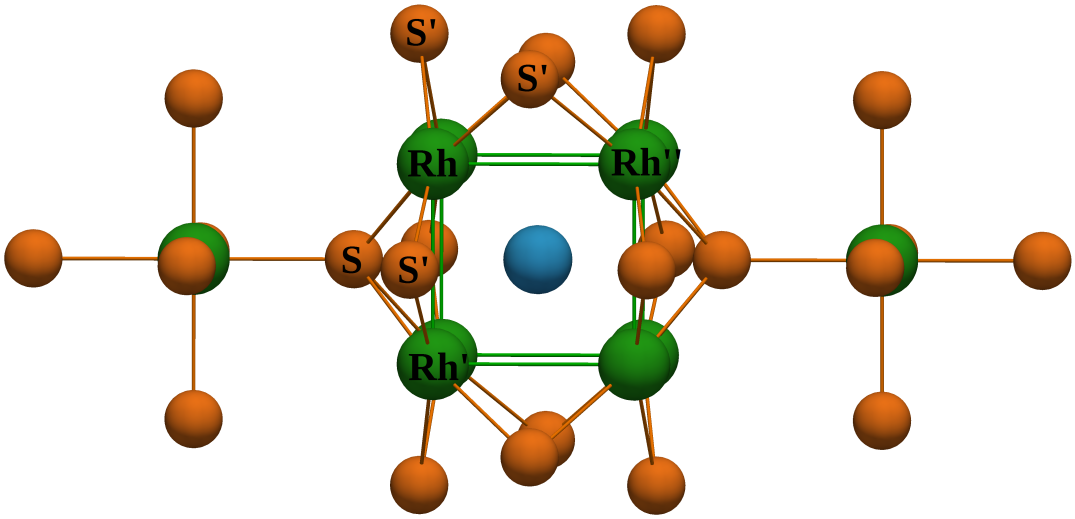

Figure 6.3: Rh-S framework in $Cu_2Rh_{34}S_{30}$.

Table 6.4: Localization and delocalization indices for QTAIM basins in rhodium chalcogenides $Rh_{17}S_{15}$ and $Cu_2Rh_{34}S_{30}$.

Atom[1]	$Rh_{17}S_{15}$				$Cu_2Rh_{34}S_{30}$			
	$N(A)$	$\lambda(A)$	$A-B$[1]	$\delta(A,B)$	$N(A)$	$\lambda(A)$	$A-B$[1]	$\delta(A,B)$
Rh	44.71	42.20	Rh-Rh"	0.349	44.66	42.18	Rh-Rh"	0.264
			Rh-Rh'	0.260			Rh-Rh'	0.202
			Rh-S'	0.790			Rh-S'	0.703
S	16.33	14.15	S-Rh	0.696	16.41	14.24	Rh-S	0.648
Cu					28.77	27.05	Cu-Rh	0.352
							Cu-S	0.151

[1] Atoms are labeled in accordance with the Fig. 6.3.

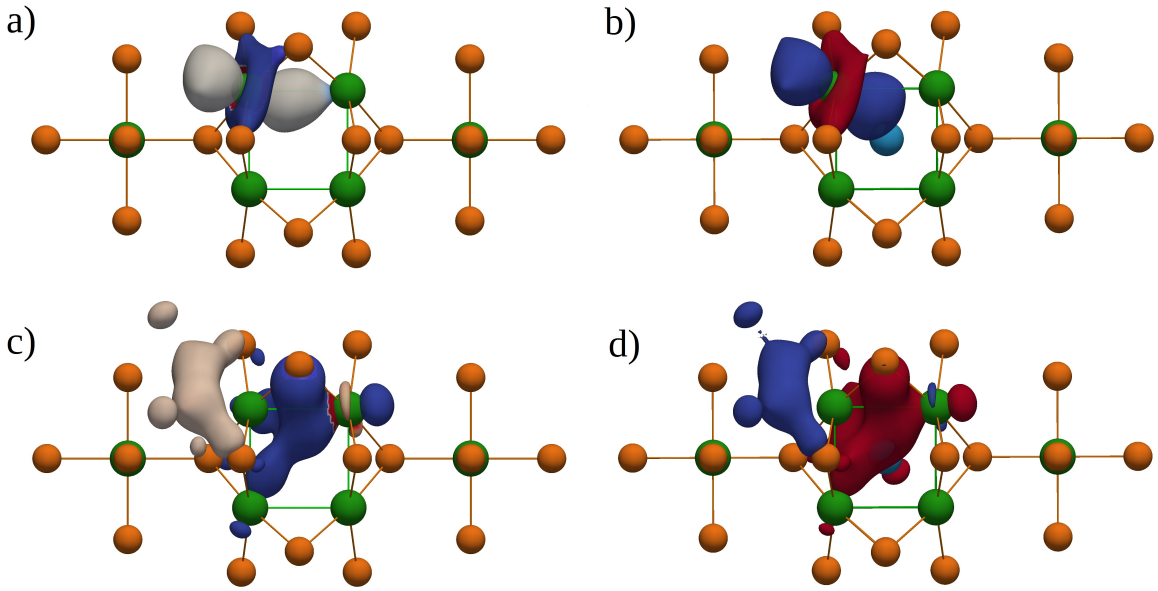

Figure 6.4: DAFH orbitals for Rh atom in $Rh_{17}S_{15}$ and $Cu_2Rh_{34}S_{30}$ crystal structures: a) d-like DAFH orbitals in $Rh_{17}S_{15}$ with occupancy 1.47 electrons, contributes 42.0% to $\delta(Rh - Rh'')$; b) d-like DAFH orbitals in $Cu_2Rh_{34}S_{30}$ with occupancy 1.43 electrons, contributes 33.0% to $\delta(Rh - Rh'')$; c) DAFH orbitals in $Rh_{17}S_{15}$ with occupancy 0.20 electrons, contributes 24.0% to $\delta(Rh - Rh'')$; d) DAFH orbitals in $Cu_2Rh_{34}S_{30}$ with occupancy 0.21 electrons, contributes 25.0% to $\delta(Rh - Rh'')$. The amplitude of orbital isosurfaces is equal to 0.04. The change in color corresponds to the change in phase.

contributes 0.067 (25%) $\delta(Rh - Rh'')$.

It is worth to underline that those two DAFH orbitals, which exhibit the decrease in number of electrons shared between Rh and Rh" basins, are mostly in charge for Rh-Cu interaction. Thus they can be regarded as a visual representation of a change in electron redistribution upon doping of Cu atoms, that causes the destruction of superconductivity. The d-like shape of one of those DAFH orbitals can serve as a confirmation for statement that 4d electrons of Rh atom plays a crucial role in this process.

The set of DAFH orbital for Cu atom in term of localization, occupancy and shape is rather typical to one, that was found for simple metals like *fcc*-Cu and *bcc*-Na[152] (table 6.6b). There are four DAFH orbitals with occupancies close to 2.0 electrons and localization degree within native basin close to 100%, which can be associated with low laying valence states 3s and 3p. The d-like DAFH orbitals (Fig. 6.5) which can be associated with 3d states have occupancies in the range 1.79-1.96 electrons and can be consider as well localized within native basin. Among four remaining DAFH orbitals there is one that has s-like shape (Fig. 6.5c), localizes within native basin only by 31% and end evenly localizes within first coordination shell – by 7% within each out of eight closest Rh QTAIM basins and by 3% within closest S QTAIM basins. Three other have

Table 6.5: DAFH orbitals for Rh atom in rhodium chalcogenides $Rh_{17}S_{15}$ and $Cu_2Rh_{34}S_{30}$.

Orbital type	$Rh_{17}S_{15}$			$Cu_2Rh_{34}S_{30}$		
	n_i^A[a]	p_i^A[b]	$p_i^A(B)$[c]	n_i^A[a]	p_i^A[b]	$p_i^A(B)$[c]
s-type(4s)	2.00	1.00	–	2.00	1.00	–
p-type(4p)	3×2.00	1.00	–	3×2.00	1.00	–
d-type(4d)	1.70	0.85	0.04(S')	1.71	0.85	0.05(S')
	1.69	0.84	0.05(S')	1.67	0.83	0.05(S')
						0.03(S)
	1.50	0.75	0.06(S')	1.54	0.77	0.04(S')
			0.05(Rh')			0.06(Rh')
	1.47	0.73	0.05(Rh")	1.43	0.72	0.03(Rh")
			0.03(S')			0.04(S')
						0.04(Cu)
	1.10	0.55	0.21(S)	1.10	0.55	0.09(S)
			0.12(S')			0.24(S')
mixed-types	2×0.31	0.18	0.49(S')	2×0.31	0.19	0.54(S')
			0.17(S)			0.03(S)
			0.06(Rh')			0.07(Rh')
	0.21	0.12	0.49(S)	0.20	0.11	0.47(S)
			0.17(S')			0.20(S')
			0.11(Rh')			0.08(Rh')
						0.03(Cu)
	0.20	0.11	0.38(S')	0.21	0.11	0.28(S')
			0.21(Rh")			0.16(Rh")
			0.11(Rh')			0.08(Rh')
						0.15(Cu)

[a] DAFH orbital occupation.
[b] DAFH orbital norm in corresponding QTAIM basin.
[c] DAFH orbital norm in QTAIM basins of the coordination shell.

Table 6.6: Comparison of DAFH orbitals in $Cu_2Rh_{34}S_{30}$ and *fcc* Cu.

Compound	Orbitals type	n_i^A[a]	p_i^A[b]
fcc Cu[1]	s-type	0.69	0.36
	p-type	0.24	0.14
	d-type	1.86-1.89	0.94-0.96
$Cu_2Rh_{34}S_{30}$	s-type	0.62	0.31
	p-type	0.18-0.22	0.09-0.13
	d-type	1.79-1.96	0.93-0.97

[a] DAFH orbital occupation.
[b] DAFH orbital norm in corresponding QTAIM basin.
[1] Results are taken from Ref. 152.

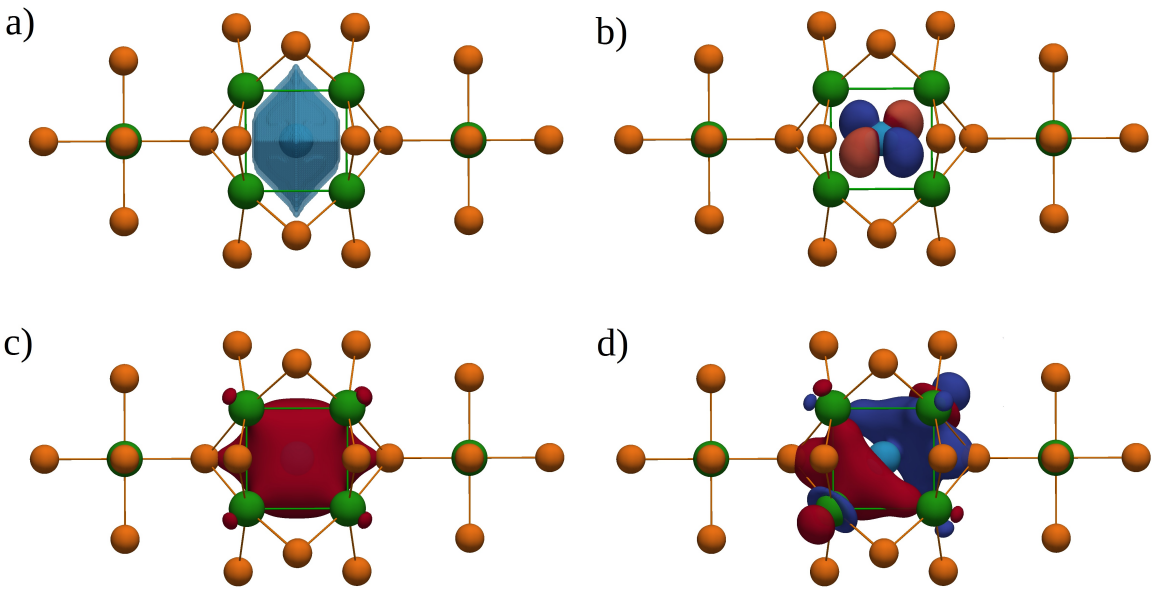

Figure 6.5: a) QTAIM basin for Cu atom in $Cu_2Rh_{34}S_{30}$ crystal structure; b) d-like DAFH orbital with occupancy of 1.82 electrons; c) s-like DAFH orbital with occupancy 0.62 electrons; d) p-like DAFH orbital with occupancy 0.20 electrons. The amplitude of orbital isosurfaces is equal to 0.04. The change in color corresponds to the change in phase.

p-like (Fig. 6.5d) shape and also characterized by comparatively low occupancy and localization within the Cu basin.

6.3 Bimetallic sulfides Bi_8Ni_8S and $Bi_8Ni_8SI_2$

The main building blocks for both compounds are two-layered rods, where nickel layer forms the inner shell and bismuth layer forms the outer shell. Sulfur atoms are confined within the inner voids and line up along central axis forming S_2 covalently-bonded units (fig. 6.6a). Those rods form a hexagonal packing with embedded iodide ions between them in the case of $Bi_8Ni_8SI_2$ (fig. 6.6b). Thus, the first question arises whether the interaction between I^- and $[Bi_8Ni_8S]^+$ completely ionic or bears some degree of covalency. In the original paper[193] ELI analysis has been not able to detect any disynaptic attractors, that was interpreted as an evidence of purely electrostatic interaction. The next problem is to evaluate the degree of interaction between bismuth atoms from neighboring rods, how strongly it decreases with the incorporation of iodide atoms and is it any change in the picture of electron distribution happens within the rods.

Detailed investigation of chemical bonding patterns will be started with Bi_8Ni_8S. The picture of electron distribution for bismuth atoms, that can be drawn from the

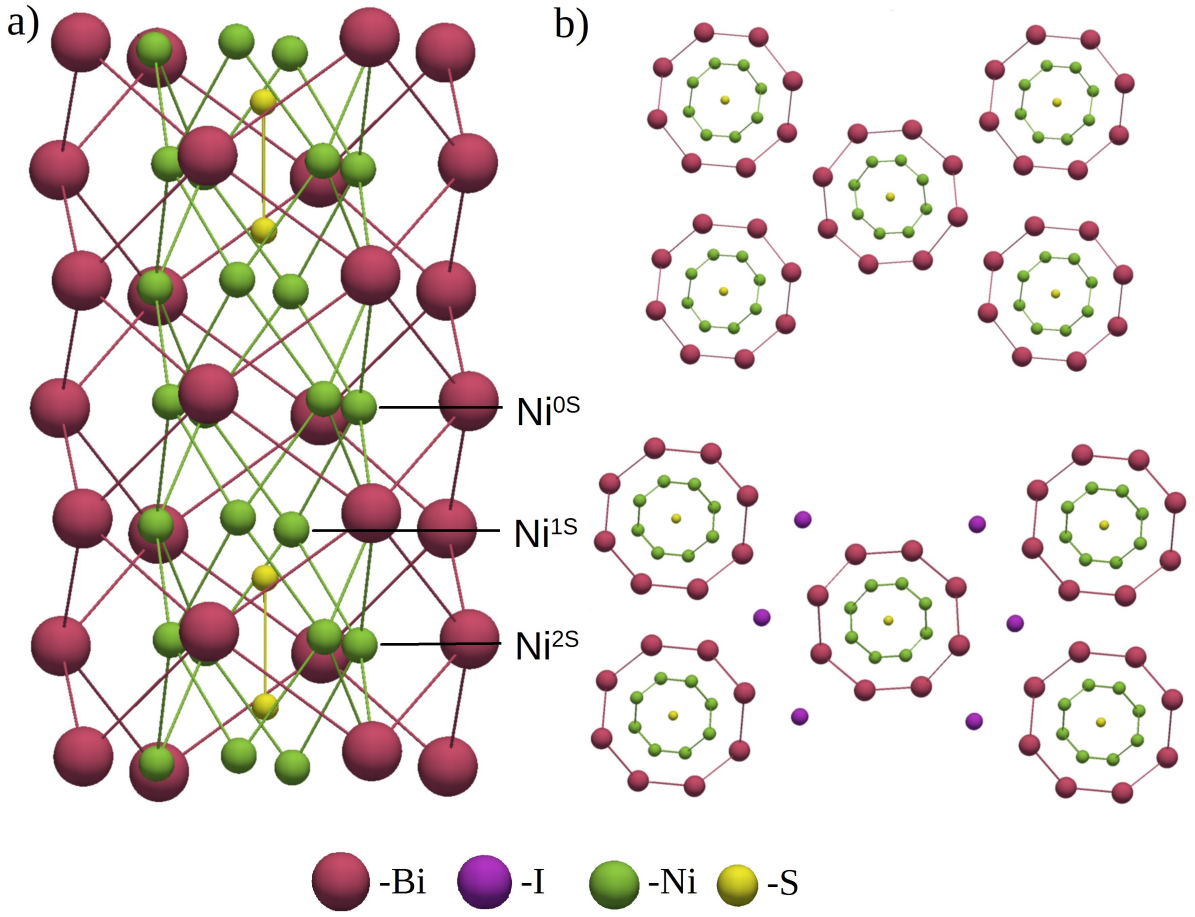

Figure 6.6: a) Structure of Bi_8Ni_8S rod; b) arrangement of present rods in Bi_8Ni_8S (up) and $Bi_8Ni_8SI_2$ (down) structures.

corresponding delocalization and localization indices (table 6.7), indicates an essential metallic character in interaction of bismuth atoms with surroundings. For each bismuth atoms almost 2 electrons can be regarded as delocalized over surrounding atoms and 81 can be regarded as localized within native basin. The value of delocalization indices for interaction of two neighboring bismuth atoms from the same rod is a bit larger than 0.2 and is typical for metallic bonding. The great degree of delocalization is revealed not only among bismuth atoms within one rod, but also among bismuth atoms from different rods. Indeed, for one bismuth atom two another bismuth atoms at the distance lesser than 7 a.u. can be found on the neighboring rod; the corresponding delocalization index has the average value of 0.18. Thus a non-negligible metallic-like interaction – which should be stronger than the weak dispersive interaction proposed in original paper[193] – between different rods can be postulated.

Passing to the revealing of interrod chemical bonding patterns it is necessarily to distinguish three sorts of nickel atoms – the one which is between two bonded sulfur atoms (further referred as Ni^{2S} atom), the one which has only one sulfur atom as direct neighbor (Ni^{1S} atom), and the one which does not adjoin to any sulfur basin (Ni^{0S} atom). The close presence of a sulfur atom and the consecutive establishing of nickel-sulfur interaction results in a significant weakening of nickel-nickel interaction – thus, the value of the delocalization index between two Ni^{2S} (0.104) almost twice less than the value of the delocalization index between two Ni^{0S} atoms (0.200), assuming equal distances between considering atom pairs. In the same time the weakening of the nickel-bismuth interaction is not so drastic – thus, the value of the delocalization index for the Bi-Ni^{2S} interaction (0.409) only by 0.036 less, than the one for the Bi-Ni^{0S} interaction (0.445). The same effect manifests in the difference of QTAIM charges of Ni^{0S}, Ni^{1S} and Ni^{2S} basins. The last one is the lowest (28.08 electrons in the case Bi_8Ni_8S and 28.13 electrons in the case of $Bi_8Ni_8SI_2$) while the first one is the highest (28.18 electrons in the case Bi_8Ni_8S and 28.26 electrons in the case of $Bi_8Ni_8SI_2$) and contains nearly a two times higher amount of the additional charge than the QTAIM basin of the Ni^{2S} atom. All together shows that the Bi-Ni^{0S} interaction is stronger than the Bi-Ni^{2S} and Bi-Ni^{1S} interactions.

The presence of iodide atoms in $Bi_8Ni_8SI_2$, as expected, results in decrease of the amount of charge within bismuth basins, since iodide atoms tend to become anions by taking electrons from the environment in order to fill their electronic shells. It the same time it appears that the charge transfer not only from bismuth atoms to iodide atoms, but also from bismuth atoms to the inner shell of Bi-Ni rods – to nickel and sulfur atoms, – is presented. As a result the QTAIM charges of the nickel and sulfur atoms $Bi_8Ni_8SI_2$ are slightly higher than the QTAIM charges of the nickel and sulfur atoms in Bi_8Ni_8S. Moreover, it appears, that sulfur atoms use the additional charge to strengthen

Table 6.7: Localization and delocalization indices for QTAIM basins in the bimetallic sulfide Bi_8Ni_8S and its iodide precursor $Bi_8Ni_8SI_2$. Superscripts $0S$, $1S$ or $2S$ indicate how many sulfur basins adjoin to a given nickel basin, the absence of a superscript indicates that given basin does not adjoin to any sulfur basin.

Compound	Atom	$N(A)$	$\sigma^2(A)$	$\lambda(A)$	$A-B$	$\delta(A,B)$
Bi_8Ni_8S	Bi	82.79	1.86	80.93	Bi-Bi(6.52 a.u.)[1]	0.244
					Bi-Bi(6.67 a.u.)[1]	0.207
					Bi-Bi(7.93 a.u.)[1]	0.044
					Bi-Bi(6.91 a.u.)[2]	0.177
					Bi-Ni^{2S}	0.409
					Bi-Ni^{1S}	0.433
					Bi-Ni^{0S}	0.445
					Bi-S	0.022
	Ni	28.18	2.05	26.13	Ni^{0S}-Ni^{0S}(5.40 a.u.)	0.200
					Ni^{0S}-Ni^{1S}(4.91 a.u.)	0.315
	Ni^{1S}	28.15	2.14	26.01	Ni^{1S}-Ni^{1S}(5.25 a.u.)	0.163
	Ni^{2S}	28.08	2.15	25.93	Ni^{2S}-Ni^{1S}(4.93 a.u.)	0.235
					Ni^{2S}-Ni^{2S}(5.40 a.u.)	0.104
	S	16.45	2.53	13.92	S-S	0.512
					S-Ni^{1S} (4.19 a.u.)	0.581
					S-Ni^{2S} (4.24 a.u.)	0.475
					S-Ni^{2S} (4.48 a.u.)	0.362
$Bi_8Ni_8SI_2$	Bi	82.60	1.84	80.76	Bi-Bi(6.67 a.u.)[1]	0.209
					Bi-Bi(6.77 a.u.)[1]	0.181
					Bi-Bi(7.86 a.u.)[1]	0.049
					Bi-Bi(9.10 a.u.)[2]	0.013
					Bi-Ni^{2S}	0.396
					Bi-Ni^{1S}	0.423
					Bi-Ni^{0S}	0.448
	Ni	28.26	2.06	26.20	Ni^{0S}-Ni^{0S}(5.40 a.u.)	0.236
					Ni^{0S}-Ni^{1S}(4.87 a.u.)	0.327
	Ni^{1S}	28.17	2.15	26.02	Ni^{1S}-Ni^{1S}(5.25 a.u.)	0.137
	Ni^{2S}	28.13	2.18	25.95	Ni^{2S}-Ni^{1S}(4.93 a.u.)	0.242
					Ni^{2S}-Ni^{2S}(5.25 a.u.)	0.125
	S	16.60	2.65	13.95	S-S	0.743
					S-Ni^{1S} (4.19 a.u.)	0.566
					S-Ni^{2S} (4.18 a.u.)	0.484
					S-Ni^{2S} (4.25 a.u.)	0.456
	I	53.49	1.12	52.36	I-I	0.099
					I-Bi	0.138

[1] Atoms belong to the same rod.
[2] Atoms belong to neighboring rods.

the S-S bond, since the corresponding delocalization index significantly increases by 0.221. Consequently the number of shared electron pairs for Ni^{0S}-Ni^{0S}, Ni^{2S}-Ni^{1S} and Ni^{2S}-Ni^{2S} interactions is also sightly increased. Contrary, the lose of charge by bismuth atoms does not result in changing of the values of the delocalization indices – only the corresponding localization indices are decreased. As for interaction of iodide and bismuth ions, except the electrostatic contribution, it is worth to admit the presence of a covalent contribution, since the corresponding delocalization index is equal to 0.138, that is bigger than a typical value of delocalization indices for cation-anion interaction (see, for example, Na-Cl and Mg-B interactions in natrium-chloride and magnesium diboride consequently (table 5.3)).

DAFH orbital analysis points towards an essential delocalized bonding pattern within Bi-Ni rods. Even the set of DAFH orbital for the sulfur basin shows a significant degree of delocalization, typical for elemental metals. There are four orbitals – one s-type and three p-type – which can be attributed to upper occupied atomic orbitals – 3s and 3p (fig. 6.7b-d), – and five highly delocalized orbitals with lower occupancy and low orbital norm preserved within the native basin, which shapes are rather complicated and can not be attributed to any specific atomic orbitals (thus further they will be referred as mixed types DAFH orbitals)(fig. 6.7e). All orbitals significantly contribute to the sulfur-nickel interaction, thus confirming its multicenter character. Most of those orbitals also make contribution to sulfur-sulfur interaction, however one orbital can be distinguished, which contributes much more than others. It is a p-type orbital with occupancy of 1.15 electrons (fig. 6.7d). Since this orbital is by 12% localized within the neighboring sulfur basin, it contributes $2 * 0.12 * 1.15 = 0.276$ (53.9%) to the S-S delocalization index (see table 6.7). The second largest contribution comes from one of the mixed types orbital with an occupancy of 0.14 electrons and in three times smaller. Thus sulfur-sulfur bond can be regarded as a mainly covalent bond. In contrary, the S-Ni^{2S} interaction can not be described just with one DAFH orbital. All three p-like DAFH orbitals make comparable contributions to the S-Ni^{2S} delocalization index – 21.0%, 20.8% and 14.5% (the lowest contribution comes from the DAFH orbital which is in charge for the S-S interaction). The remaining part is covered by the five low occupied DAFH orbitals of mixed types.

The set of DAFH orbitals for the nickel basin (here will be considered only Ni^{2S} type of atom) includes four perfectly localized orbitals – one of s-type, attributed to 3s atomic orbital, and three of p-type, attributed to 3p atomic orbitals, – five not so perfect but still substantially localized d-type orbitals – associated with 3d atomic orbitals, – and four with low occupancy and low orbital norm preserved within the native basin. However, unlike to the case of the sulfur atom, the latter DAFH orbitals have well defined shapes – one of them is of s-type and can be associated with 4s state, and three of them are of p-type and can be associated with 4p states. The Ni^{2S}-S interaction can be described

Table 6.8: DAFH orbital analysis for Bi_8Ni_8S and $Bi_8Ni_8SI_2$.

Atom	DAFHo type	Bi_8Ni_8S			$Bi_8Ni_8SI_2$		
		n_i^A[a]	p_i^A[b]	$p_i^A(B)$[c]	n_i^A[a]	p_i^A[b]	$p_i^A(B)$[c]
Bi	s-type(6s)	1.89	0.94	-	1.87	0.94	-
	p-type(6p)	0.83	0.42	0.27(Ni), 0.15(Bi[1]), 0.05(Bi[2])	0.80	0.45	0.30(Ni), 0.16(Bi[1])
		0.82	0.41	0.29(Ni), 0.15(Bi[1]), 0.03(Bi[2])	0.77	0.42	0.30(Ni), 0.12(Bi[1])
		0.82	0.41	0.28(Ni), 0.14(Bi[1]), 0.05(Bi[2])	0.68	0.36	0.27(Ni), 0.13(Bi[1]), 0.17(I)
S	s-type(3s)	1.74	0.87	0.07(Ni)			
	p-type(3p)	2×1.24	0.62	0.32(Ni)			
		1×1.15	0.57	0.12(S'), 0.22(Ni)			
	mixed types	2×0.15	0.08	0.03(S'), 0.78(Ni), 0.04(Bi)			
		2×0.14	0.07	0.05(S'), 0.83(Ni), 0.03(Bi)			
		1×0.14	0.08	0.32(S'), 0.55(Ni)			
Ni^{2S}	s-type(4s)	2.00	1.00	-			
	p-type(3p)	3×2.00	1.00	-			
	d-type(3d)	2×1.79	0.92	-			
		1×1.74	0.91	-			
		1×1.67	0.87	-			
		1×1.60	0.85	0.06(S)			
	s-type(5s)	0.56	0.29	0.06(S), 0.12(Ni), 0.48(Bi)			
	p-type(4p)	1×0.25	0.13	0.06(S), 0.30(Ni), 0.44(Bi)			
		2×0.22	0.13	0.42(S), 0.26(Ni), 0.15(Bi)			

[a] DAFH orbital occupation.
[b] DAFH orbital norm in corresponding QTAIM basin.
[c] DAFH orbital norm in QTAIM basins of the coordination shell.
[1] Atoms belong to the same rod.
[2] Atoms belong to neighboring rods.

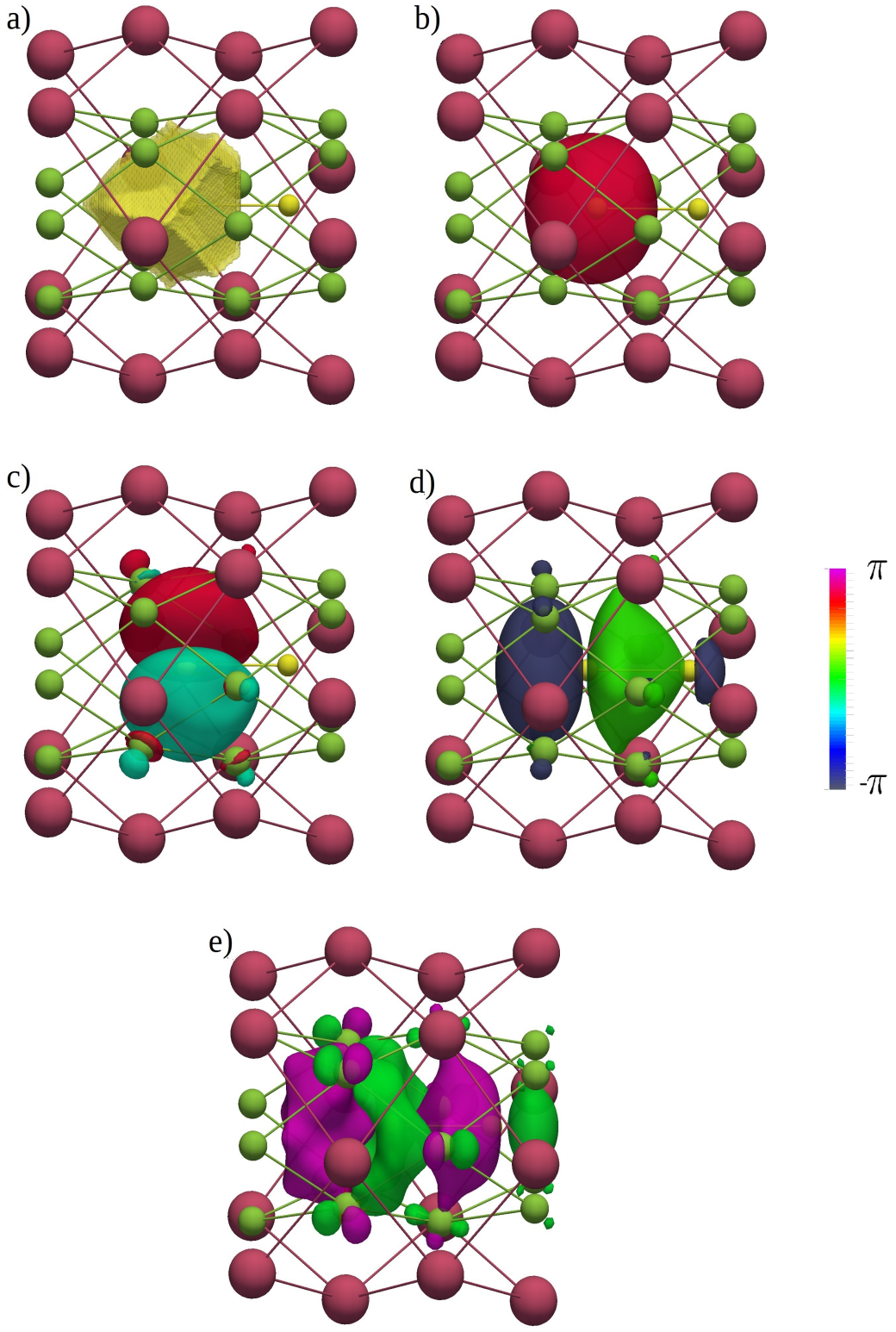

Figure 6.7: a) QTAIM basin for the sulfur atom inside [Bi_8Ni_8S] rod; b) s-like DAFH orbital, occupancy 1.74 electrons; c) p-like DAFH orbital, occupancy 1.24 electrons, represents S-Ni interaction; d) p-like DAFH orbital, occupancy 1.15 electrons, makes the most contribution to S-S bond; e) DAFH orbital with occupancy 0.14 electrons, makes the second largest contribution to S-S bond. The amplitude of the orbital isosurface is equal to 0.03.

Table 6.9: DAFH orbital analysis for iodide atom in $Bi_8Ni_8SI_2$ crystal structure.

Atom	n_i^A[a]	$p_i^A(A)$[b]	DAFHo type	$\sum_i n_i^A$[c]
I	1×1.97	0.99	s-type(5s)	7.05
	1×1.79	0.91	p-type(5p)	
	1×1.73	0.89	p-type(5p)	
	1×1.56	0.81	p-type(5p)	

[a] DAFH orbital occupation.
[b] DAFH orbital norm in corresponding QTAIM basin.
[c] Sum of DAFH orbital occupations.

with two DAFH orbitals – one p-like with occupancy of 0.22 electrons (fig. 6.8d), which due to it high localization degree within sulfur basin contributes $2 * 0.38 * 0.22 = 0.167$ (35.2%) to the corresponding Ni^{2S}-S delocalization index (here the distance between nickel and sulfur atoms is equal to 4.25 a.u.), and one d-like with occupancy 1.60 electrons (fig. 6.8b), which localizes within sulfur basin only by 3%, but due to it high occupancy contributes $2 * 0.03 * 1.60 = 0.192$ (40.4%) to the same delocalization index. The rest is mainly evenly covered by one s-like and two remaining p-like DAFH orbitals with low occupancies, and three d-like DAFH orbitals. Thus the nature of the Ni^{2S}-S bond is once again proved to be similar to that in simple metals. The analogous conclusions can be made regarding the Ni^{2S}-Bi bond. All above mentioned DAFH orbitals with low occupancies and two d-like DAFH orbitals make contributions to it. The highest one, however, comes from s-like orbital with occupancy 0.56 electrons (fig. 6.8c). This DAFH orbital ensures the interactions with all four nearest bismuth atoms and, since it localizes within single bismuth basin by 10-14%, its contribution can be evaluated as equal to 0.112-0.157 (27.4%-38.3%) electron pairs.

The decrease of the electron population of the bismuth basin in the $Bi_8Ni_8SI_2$ structure in comparison to the electron population of the bismuth basin in the Bi_8Ni_8S structure is manifested via the decrease of the occupation numbers of the three p-like DAFH orbitals, attributed to 6p atomic orbitals. The lowest occupation is characteristic for DAFH orbital that is mostly in a charge for Bi-I interaction. All other DAFH orbitals contribute no more than 2% from their norm. Contrary to the case of nickel atom and simple metals, the s-like bismuth DAFH orbital (which may be attributed to 6s atomic orbital) in both compounds is well localized within the native basin and almost does not take part in bonding with the surroundings. Since bismuth belongs to the class of post-transition elements, it is reasonable to assume, that such strong localization is the manifestation of the inert pair effect [201].

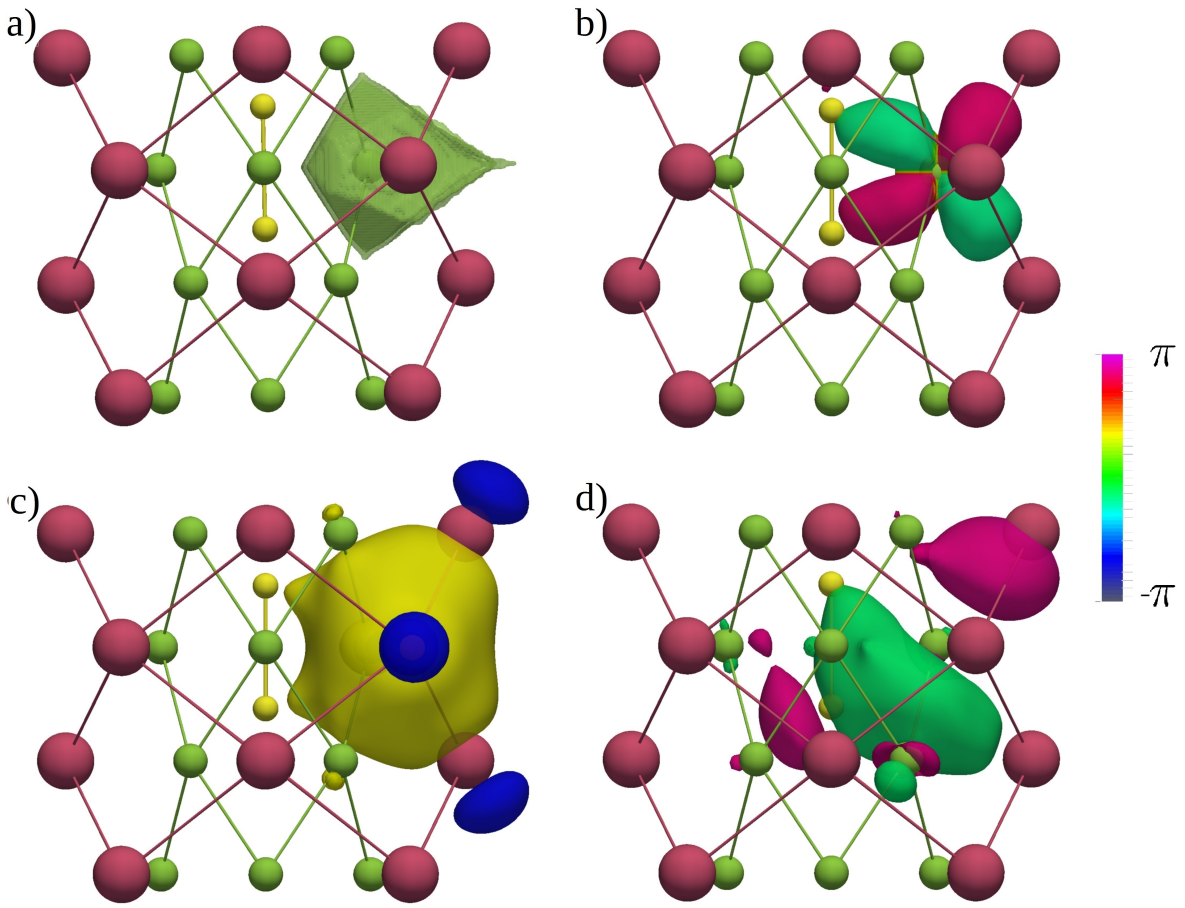

Figure 6.8: a) QTAIM basin for the nickel atom inside a [Bi_8Ni_8S] rod; b) d-like DAFH orbital associated with 3d atomic orbital, occupancy 1.60 electrons; c) s-like DAFH orbital associated with 4s atomic orbital, occupancy 0.56 electrons; d) p-like DAFH orbital associated with one of 4p atomic orbital, occupancy 0.22 electrons. The amplitude of the orbital isosurface is equal to 0.03.

The set of DAFH orbitals for the iodide atom is typical for atoms involved in mainly electrostatic interactions. All DAFH orbitals with high occupancy are rather well localized within the native iodide basin and the sum of their occupancies cover all valence electrons (here only 5s and 5p states are considered as valence, table 6.1). The maximum localization degree within the basins from the first coordination shell is equal only to 9% (within bismuth basin) and covers the covalent part of the Bi-I interaction (fig. 6.9b). It is worth to admit that almost all QTAIM charges of the iodide basin gained from bismuth basins is concentrated within eleven DAFH orbitals with occupancies in the range of 0.02-0.05 electrons.

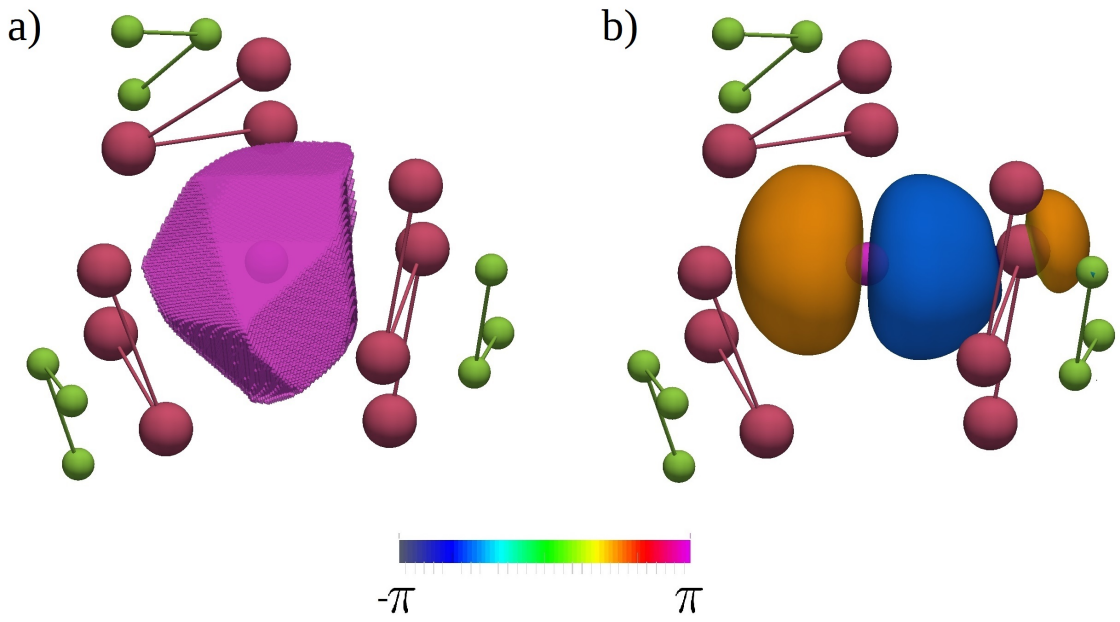

Figure 6.9: a) QTAIM basin for the iodide atom in the $Bi_8Ni_8SI_2$ structure; b) p-like DAFH orbital associated with 5p atomic orbital, occupancy 1.56 electrons. The amplitude of the orbital isosurface is equal to 0.03.

General Conclusions

In quantum chemistry a state of a system is described with the corresponding wave function. The last can be used for revealing any related properties that is crucial for theoretical investigations of a matter in modern material science.

The electronic-structure calculations of periodic systems are often performed in the framework of the density functional theory in combination with a plane wave basis set. The last possesses a number of advantages such as simplicity, unbiasedness and convenience for Fourier transformations. The main disadvantage of this basis set lies in the difficulty to reproduce the highly oscillating behavior of a wave function in the vicinity of nuclei. To overcome this problem, the general solutions are either to ignore core states, like in the case of the pseudopotential approach, or to account for them with different molecular-like basis set, like in the case of the family of APW methods. A tempting alternative to them is the PAW method, which allows to reconstruct the true wave function for core states from plane wave solution and precomputed for an isolated atoms set of partial wave functions. Since the process of reconstruction of core states is linear, the computational complexity of the PAW method is on the same level with pseudopotential approaches, while it accuracy is comparable with the (L)APW method.

After the recovering of a wave function, the post-processing electron distribution analysis, aiming to reveal chemical bonding peculiarities of the system under investigation, is reachable. For that purpose a variety of approaches for chemical-bonding investigations were developed, which are based generally either on the current basis set representation, or on the some order reduced density matrix. Methods, based on second order reduced density matrix, like localization/delocalization indices and DAFH orbitals, are especially prominent, since they are capable to discover true two center delocalization behavior of interatomic interaction and do not suffer from basis set dependence. One of the possible reasons why these approaches did not become regular tools for chemical-bonding analysis is their relative complexity. Indeed, they require an evaluation of so-called domain overlap matrix elements, that is not a trivial task even for modern computers.

In this work, the implementation of localization/delocalization indices, DAFH orbitals and ELI approaches for the PAW method is described. The implementation is based on a novel algorithm for the evaluation of domain overlap matrix elements from

plane wave basis sets. This algorithm is based on Fourier transformations and due to FFT algorithm scales as $O(N \log N)$ process. Within the framework of the PAW method, the formal derivation of the expressions for the plane wave part and the partial waves parts together with implementation peculiarities, which make the process of evaluation even more efficient, were presented.

ELI-D analysis shows the interchangeability of implementations for the PAW and the (L)APW methods – both reveal identical pictures. However the use of good PAW data sets eliminates the appearance of artifacts on muffin-tin boundaries, which often accompany the analogous analysis from the (L)APW method.

The values of the localization/delocalization indices calculated with the PAW method for simple compounds show nice agreement with the values obtained with the (L)APW method, that proves the correctness of the described implementation and the adequacy of using the PAW method for such type of chemical bonding analysis. A significant speed-up of the implementation for the PAW method comparing to the implementation for the (L)APW method was detected. A set of complex solid structures – the niobium (IV) complex $Nb_2(Se_2)_2(AlCl_4)_4$ with dominant covalent bonding pattern, two rhodium chalcogenides $Rh_{17}S_{15}$ and $Cu_2Rh_{34}S_{30}$ with different conducting properties, and two bimetallic sulfides Bi_8Ni_8S and $Bi_8Ni_8SI_2$ with mixed metallic, ionic and covalent bonding patterns – were analyzed with the current implementation.

Governing by the obtained results several tendencies can be outlined. It was shown, that generally a 2e-2c covalent bond is represented with a delocalization index with a value higher then 0.5, through it can be a bit lower in the case of a polar bond. For a such type of bond generally one could find one DAFH orbital that makes the most contribution (in several times greater than the individual contributions from other orbitals) to the corresponding delocalization index. Its occupancy is greater than 1 in the case of a non-polar covalent bond, but is lower than 1 in the case of a donor atom involved in polar covalent bonding. It demonstrates a significant degree of localization (>10%) not only within the native basin but also within the basin of the neighboring atom, with which a bond is formed. For a metallic type of bonding, delocalization indices in the range of 0.1-0.4 are characteristic. A set of DAFH orbitals for an atom, involved in metallic bonding, is characterized by the presence of a number of delocalized orbitals, which norms are spread among the first coordination shell. There can be distinguished DAFH orbitals, which have a comparatively high localization degree within the native basin (>70%) and can be associated with the upper occupied atomic orbitals. However, there are also a number of DAFH orbitals with lower occupancy (<1.0 electrons), which localization degree within the native basin is low (<50%) and which can be related either to the lower unoccupied atomic orbitals or to their mixture.

Further work might be concerned with the adaptation of the current implementation

of real space bonding indicators to the cases of non-collinear spin magnetism and spin coupling.

Appendix A

Input files for generated partial, pseudo partial and projector functions with ATOMPAW program

Al
Al 13
GGA-PBE loggrid 2001
3 3 0 0 0 0
3 1 1
0 0 0
c
c
v
c
v
2
2.2 2.0 2.2 2.2
y
6.4
n
y
7.1
n
y
0.5
y

7
n
custom rrkj vanderbiltortho besselshape
3 0 troulliermartins
2.2
2.2
2.2
2.2
2.2
2.2
2
prtcorewfn
0

S
S 16
GGA-PBE scalarrelativistic loggrid 1400
3 3 0 0 0 0
3 1 4
0 0 0
c
c
v
c
v
1
1.7 1.6 1.7 1.4
y
6.0
n
y
1.5
n
custom rrkj
2 0.0
1.7
1.7

1.7
1.7
2
prtcorewfn
0

Rh
Rh 45 GGA-PBE scalarrelativistic loggrid 600 80 2.20
5 4 4 0 0 0
5 0 1
4 2 8
0 0 0
c
c
c
v
v
c
c
v
c
v
2
2.25 2.2 1.75 2.2
n
y
4.0
n
y
4.5
n
custom polynom2 7 10 vanderbiltortho
3 0.0 ultrasoft
2.25
2.25
2.20
2.20

2.0
2.0
2
prtcorewfn
0

Bibliography

[1] Hohenberg ,P.; Kohn, W., *Phys. Rev. B* 136, 864 (1964).

[2] Jensen, F., *Introduction to Computational Chemistry 2nd ed.*, John Wiley and Sons, Ltd.: Chichester, pp. 570-571 (2007).

[3] Parr, R. G.; Yang, W., *Density-Functional Theory of Atoms and Molecules*, Oxford University Press: USA, p. 53 (1989).

[4] Levy, M., *Phys. Rev. A* 26, 1200 (1982).

[5] Lieb, E., *Int. Jour. Quant. Chem.* 24, 243 (1983).

[6] Gilbert, T. L., *Phys. Rew. B* 12, 2111 (1975).

[7] Wang, Y. A.; Carter, E. A., *Orbital-Free Kinetic-Energy Density Functional Theory* in *Theoretical Methods in Condensed Phase Chemistry*, edit. by Schwartz, S. D., Kluwer: Dordrecht, pp. 117-184 (2000).

[8] Kohn, W.; Sham, L. J., *Phys. Rev.* 140, A1133 (1965).

[9] Slater, J. C., *Phys. Rev.* 34, 1293 (1929).

[10] Kübler, J.; Höck, H. H.; Sticht, J., *J. Appl. Phys.* 63, 3482 (1988).

[11] Kübler, J.; Höck, H. H.; Sticht, J.; Williams, A. R., *J. Phys. F.: Met. Phys.* 18, 469 (1988).

[12] Ceperley, D. M.; Alder, D. J., *Phys. Rev. Lett.* 45, 566 (1980).

[13] Perdew, J. P.; Wang, Y., *Phys. Rev. B* 45, 13244 (1992).

[14] Perdew, J. P.; Burke, K.; Ernzerhof, M., *Phys. Rev. Lett.* 77, 3865 (1996).

[15] Perdew, J. P.; Tao J.; Staroverov, V. N.; Scuseria G. E., *J. Chem. Phys.* 120, 6898 (2004).

[16] Cohen, A. J.; Mori-Sanchez, P.; Yang, W., *Science* 321, 792 (2008).

[17] Perdew, J. P.; Zugner, A., *Phys. Rev. B* 23, 5048 (1981).

[18] Vydrov, O. A.; Scuseria, G. E.; Perdew, J. P.; Ruzsinszky, A.; Csonka, G. I., *J. Chem. Phys.* 124, 094108 (2006).

[19] Mori-Sanchez, P.; Cohen, A. J.; Yang, W., *J. Chem. Phys.* 125, 201102 (2006).

[20] Haunschild, R.; Henderson, T. M.; Jimenez-Hoyos, C. A.; Scuseria, G. E., *J. Chem. Phys.* 133, 134116 (2010).

[21] Becke, A. D., *J. Chem. Phys.* 140, 18A301 (2014).

[22] Zhao, Y.; Schultz, N. E.; Truhlar, D. G, *J. Chem. Phys.* 123, 161103 (2005); *J. Chem. Theory Comput.* 2, 364 (2006).

[23] Zhao, Y.; Truhlar, D. G., *J. Chem. Phys.* 125, 194101 (2006); *Theor. Chem. Acc.* 120, 215 (2006); *J. Phys. Chem. A* 110, 13126 (2006); *J. Chem. Theory Comput.* 4, 1849 (2008).

[24] Peverati, R.; Truhlar, D. G., *J. Phys. Chem. Lett.* 2, 2810 (2011); *J. Phys. Chem. Lett.* 3, 117 (2012); *J. Chem. Theory Comput.* 8, 2310 (2012); *Phys. Chem. Chem. Phys.* 14, 13171 (2012); *Phys. Chem. Chem. Phys.* 14, 16187 (2012).

[25] Zhao, Y.; Truhlar, D. G. *Chem. Phys. Lett.* 502, 1 (2011).

[26] Shil, S.; Bhattacharya, D.; Sarkar, S.; Misra, A., *J. Phys. Chem. A* 117, 4945 (2013).

[27] Zhang, Y.; Yang, W., *Phys, Rev, Lett.* 80, 890 (1998).

[28] Hammer, B.; Hansen, L. B.; Noerskov, J. K., *Phys. Rev. B* 59, 7413 (1999).

[29] Perdew, J. P.; Ruzsinszky, A.; Csonka, G. I.; Vydrov, O. A.; Scuseria, G. E.; Constantin, L. A.; Zhou, X.; Burke, K., *Phys. Rev. Lett.* 100, 136406 (2008).

[30] Anisimov, V. I.; Gunnarsson, O., *Phys. Rev. B* 43, 7570 (1991).

[31] Anisimov, V. I.; Zaanen, J.; Andersen, O. K., *Phys. Rev. B* 44, 943 (1991).

[32] Anisimov, V. I.; Aryasetiawan, F.; Lichtenstein, A. I., *J. Phys.: Condens. Matter* 9, 767 (1997).

[33] Cremer, D., *Mol. Phys.* 99, 1899 (2001).

[34] Grimme, S.; Waletzke, M., *J. Chem. Phys.* 111, 5645 (1999).

[35] Lyskov, I.; Kleinschmidt, M.; Marian, C. M., *J. Chem. Phys.* 144, 034104 (2016).

[36] *Electron Correlations and Materials Properties 2*, edit. by Gonis, A.; Kioussis, N.; Ciftan, M., Springer-Verlag US: New York, p. 389 (2003).

[37] Vuckovic, S.; Wagner, L. O.; Mirtschink, A.; Gori-Giorgi, P., *J. Chem. Theory Comput.* 11, 3153 (2015).

[38] Vuckovic, S.; Irons, T. J. P.; Savin, A.; Teale, A. M.; Gora-Giorgi, P., *J. Chem. Theory Comput.* 12, 2598 (2016).

[39] Jensen, F., *Introduction to Computational Chemistry 2nd ed.*, John Wiley and Sons, Ltd.: Chichester, p. 259 (2007).

[40] Cybulski, S. M.; Seversen, C. E., *J. Chem. Phys.* 122, 014117 (2005).

[41] Guan, J.; Duffy, P.; Carter, J. T.; Chong, D. P.; Casida, K. C.; Casida, M. E.; Wrinn, M., *J. Chem. Phys.* 98, 4753 (1993).

[42] Jensen, F., *Introduction to Computational Chemistry 2nd ed.*, John Wiley and Sons, Ltd.: Chichester, pp. 255-256 (2007).

[43] Hartree, D. R., *Math. Proc. Camb. Philos. Soc.* 24, 89; 426 (1928).

[44] Fock, V., *Z. Phys.* 61, 126 (1930).

[45] Jensen, F., *Introduction to Computational Chemistry 2nd ed.*, John Wiley and Sons, Ltd.: Chichester, p. 133 (2007).

[46] Moeller, C.; Plesset, M. S., *Phys. Rev.* 46, 618 (1934).

[47] Jensen, F., *Introduction to Computational Chemistry - 2nd ed.*, John Wiley and Sons, Ltd.: Chichester, pp. 163-164 (2007).

[48] Sherrill, C. D.; Schaefer, H. F., *Adv. Quant. Chem.* 34, 143 (1999).

[49] Raghavachari, K.; Anderson, J. B., *J. Phys. Chem.* 100, 12960 (1996).

[50] Shepard, R., *Adv. Chem. Phys.* 69, 63 (1987).

[51] Jensen, F., *Introduction to Computational Chemistry 2nd ed.*, John Wiley and Sons, Ltd.: Chichester, p. 154 (2007).

[52] Werner, H.-J.; Knowles, P. J., *J. Chem. Phys.* 89, 5803 (1988).

[53] Bartlett, R. J., *J. Phys. Chem.* 93, 1697 (1989).

[54] Jensen, F., *Introduction to Computational Chemistry 2nd ed.*, John Wiley and Sons, Ltd.: Chichester, p. 172 (2007).

[55] Metropolis, N.; Rosenbluth, A. W.; Resenbluth, M. N.; Teller, A. H., *J. Chem. Phys.* 21, 1087 (1953).

[56] *Quantum Monte Carlo Methods in Physics and Chemistry*, edit. by Nightingale, M. P.; Umrigar, C. J., Kluwer Academic Publishers: Dordrecth (1998).

[57] Jensen, F., *Introduction to Computational Chemistry 2nd ed.*, John Wiley and Sons, Ltd.: Chichester, pp. 187-189 (2007).

[58] McMillan, W. L., *Phys. Rev.* 138, A442 (1965).

[59] Ceperley, D.; Chester, G. V.; Kalos, M. H., *Phys. Rev. B* 16, 3081 (1977).

[60] Reynolds, P. J.; Ceperley, D. M.; Adler, b. J.; Lester Jr., W. A., *J. Chem. Phys.* 77, 5593 (1982)

[61] Foulkes, W. M. C.; Mitas, L.; Needs, R. J.; Rajagopal, G., *Rev. Mod. Phys.* 73, 33 (2001).

[62] Zhang, S.; Krakauer, H., *Phys. Rev. Lett.* 90, 136401 (2003).

[63] Barker, J. A., *J. Chem. Phys.* 70, 2914 (1979)

[64] Ceperley, D. M., *Rev. Mod. Phys.* 67, 279 (1995).

[65] Dewing, M.; Ceperley, D. M., *Methods in Coupled Electron-Ion Monte Carlo*, in *Recent Advances in Quantum Monte Carlo Methods II*, edit. by Lester Jr., W. A.; Rothstein, S.; Tanaka, S., Wold Science Publishing Co. Pte. Ltd.: Singapore (2002).

[66] Pierleoni, C.; Ceperley, D. M., *The Coupled Electron-Ion Monte Carlo Method*, in *Computer Simulation in Condensed Matter Physics: From Materials to Chemical Biology Volume 1*, edit. by Ferrario, M.; Ciccotti, G.; Binder, K., Springer-Verlag Berlin: Heildelberg (2006).

[67] Baroni, S.; Moroni, S., *Phys. Rev. Lett.* 82, 4745 (1999).

[68] Corney, J. F., Drummond, P. D., *Phys. Rev. Lett.* 93, 260401 (2004).

[69] Rousseau, V. G., *Phys. Rev. E* 77, 056705 (2008).

[70] Booth, G. H.; Thom, A. J. W.; Alavi, A., *J. Chem. Phys.* 131, 054106 (2009).

[71] Spencer, J. S.; Blunt, N. S.; Foulkes, W. M. C., *J. Chem. Phys.* 054110 (2012).

[72] Blunt, N. S.; Alavi, A.; Booth, G. H., *Phys. Rev. Lett.* 115, 050603 (2015).

[73] Eschrig, H., *Optimized LCAO Method and the Electronic Structure of Extended Systems*, Akademie-Verlag: Berlin, p. 29 (1988).

[74] Junquera, J.; Paz, O.; Sanchez-Portal, D.; Artacho, E., *Phys. Rev. B* 64, 235111 (2001).

[75] Hamann, D. R.; Schlueter, M.; Chiang, C., *Phys. Rev. Lett.* 43, 1494 (1979).

[76] Hamann, D. R., *Phys. Rev. B* 40, 2980 (1989).

[77] Martin, R. M., *Electronic Structure Basic Theory and Practical Methods*, Cambridge University Press: Cambridge, pp. 212-213 (2004).

[78] Vanderbilt, D., *Phys. Rev. B* 32, 8412 (1985).

[79] Kerker, G. P., J. *Phys. C: Solid. St. Phys.* 13, L189 (1980).

[80] Martin, R. M., *Electronic Structure Basic Theory and Practical Methods*, Cambridge University Press: Cambridge, pp. 219 (2004).

[81] Srivastava, G. P., *Theoretical Modelling of Semiconductors Surfaces: Microscopic Studies of Electrons and Phonons*, World Scientific Publishing Co. Pte. Ltd.: Singapore, p. 39 (1999).

[82] Troullier, M.; Martins, J. L., *Phys. Rev. B* 43, 1993 (1991).

[83] Troullier, M.; Martins, J. L., *Phys. Rev. B* 43, 8861 (1991).

[84] Vanderbilt, D., *Phys. Rev. B* 41, 7892 (1990).

[85] Laasonen, K.; Car, R.; Lee, C.; Vanderbilt, D., *Phys. Rev. B* 43, 6796 (1991).

[86] Laasonen, K.; Pasquarello, R.; Car, R.; Lee, C.; Vanderbilt, D., *Phys. Rev. B* 47, 10142 (1993).

[87] Slater, J. C., *Phys. Rev.* 51, 846 (1937).

[88] Slater, J. C., *Phys. Rev.* 81, 385 (1951).

[89] Singh, D. J.; Nordstroem, L., *Planewaves, Pseudopotentials and the LAPW Method 2nd ed.*, Kluwer Academic: Boston, p. 43 (2006).

[90] Singh, D. J., *Phys. Rev. B* 43, 6388 (1991).

[91] Sjoestedt, E.; Nordstroem, L.; Singh, D. J., *Solid State Commun.* 114, 15 (2000).

[92] Cottenier, S., *Density Functional Theory and the Family of (L)APW-Methods: a Step-by-Step Introduction*, Instituut voor Kern-en Stralingsfysica: K. U. Leuven (2002) (www.wien2k.at/reg_user/textbooks).

[93] Bloechl, P. E., *Phys. Rev. B* 50, 17953 (1994).

[94] Kresse, G.; Joubert, D., *Phys. Rev. B* 59, 1758 (1999).

[95] Holzwarth, N. A. W.; Tackett, A. R.; Matthews, G. E., *Comput. Phys. Commun.* 135, 329 (2001).

[96] Lewis, G. N., . *Am. Chem. Soc.* 38, 762 (1916).

[97] Gillespie, R. J.; Nyholm, R. S., *Quart. Rev. Chem. Soc.* 11, 339 (1957).

[98] Gillespie, R. J., *J. Chem. Educ.* 47, 18 (1970).

[99] Mayer, I., *Chem. Phys. Lett.* 97, 270 (1983).

[100] Bader, R. F. W., *J. Phys. Chem.* 113, 10391 (2009).

[101] Lowdin, P.-O., *Phys. Rev.* 97, 1474 (1955).

[102] Foster, J. P.; Weinhold, F., *J. Am. Chem. Soc.* 102, 7211 (1980).

[103] Reed, A. E.; Weinhold, F., *J. Chem. Phys.* 78, 4066 (1983).

[104] Reed, A. E.; Weinstock, R. B.; Weinhold, F., *J. Chem. Phys* 83, 735 (1985).

[105] Weinhold, F., *Natural Bond Orbital Methods*, in *Encyclopedia of Computational Chemistry*, edit. by Schleyer, P. v. R.; Allinger, N. L.; Clark, T.; Gasteiger, J.; Kollman, P. A., Wiley UK: Chichester, vol. 3, pp. 1792 - 1811 (1998).

[106] Jensen, F., *Introduction to Computational Chemistry 2nd ed.*, John Wiley and Sons, Ltd.: Chichester, p. 311 (2007).

[107] Reed, A. E.; Weinhold, F., *J. Chem. Phys.* 83, 1736 (1985).

[108] Zubarev, D. Yu.; Boldyrev, A. I., *Phys. Chem. Chem. Phys.* 10, 5207 (2008).

[109] Hughbanks, T.; Hoffmann, R., *J. Am. Chem. Soc.* 105, 3528 (1983).

[110] Hoffmann, R., *Angew. Chem. Int. Ed. Engl.* 26, 846 (1987).

[111] Dronskowski, R., *Computational Chemistry of Solid State Materials*, Wiley-VCH Verlag GmbH and Co. KGaA: Weinheim, pp. 87-89 (2005).

[112] Dronskowski, R.; Bloechl, P. E., *J. Phys. Chem.* 97, 8617 (1993).

[113] Boernsen, N.; Meyer, B.; Grotheer, O.; Fauhnle, M., *J. Phys.: Condens. Matter* 11, L287 (1999).

[114] Grechnev, A.; Ahuja, R.; Eriksson, O., *J. Phys.: Condens. Matter* 15, 7751 (2003).

[115] Deringer, V. L.; Tchougreeff, A. L.; Dronskowski, R., *J. Phys. Chem. A* 115, 5461 (2011).

[116] Wannier, G. H., *Phys. Rev.* 52, 191 (1937).

[117] Marzari, N.; Mostofi, A. A.; Yates, J. R.; Souza, I.; Vanderbilt, D., *Rev. Mod. Phys.* 84, 1419 (2012).

[118] Marzari, N.; Vanderbilt, D., *Phys. Rev. B* 56, 12847 (1997).

[119] Foster, J. M.; Boys, S. F., *Rev. Mod. Phys.* 32, 300 (1960).

[120] Souza, I.; Marzari, N.; Vanderbilt, D., *Phys. Rev. B* 65, 035109 (2001).

[121] Jensen, F., *Introduction to Computational Chemistry 2nd ed.*, John Wiley and Sons, Ltd.: Chichester, p. 242 (2007).

[122] Bader, R. F. W., *Chem. Rev.* 91, 893 (1991).

[123] Pendas, A. M.; Blanco, M. A.; Costales, A.; Sanchez, P. M.; Luana, V., *Phys. Rev. Lett.* 83, 1930 (1999).

[124] Bader, R. F. W., *J. Phys. Chem. A* 102, 7314 (1998).

[125] Bader, R. F. W., *J. Chem. Phys. A*, 114, 7431 (2010).

[126] Pendas, A. M.; Francisco, E.; Blanco, M. A.; Gatti, C., *Chem–Eur. J.* 12, 9362 (2007).

[127] Ponec, R.; Gatti, C., *Inorg. Chem.* 48, 11024 (2009).

[128] Becke, A. D., *Int. J. Quantum Chem.* 23, 1915 (1983).

[129] Becke, A. D.; Edgecombe, K. E., *J. Chem. Phys.* 92, 5397 (1990).

[130] Savin, A.; Jepsen, O.; Flad, J.; Andersen, O. K.; Preuss, H.; von Schnering, H. G., *Angew. Chem. Int. Ed. Engl.* 31, 187 (1992).

[131] Tal, Y.; Bader, R. F. W., *Int. J. Quantum Chem. Quantum Chem. Symp.* 12, 153 (1978).

[132] Kohout, M.; Savin, A., *Int. J. Quantum Chem.* 60, 875 (1996).

[133] Savin, A.; Nesper, R.; Wengert, S.; Faussler, T, F., *Angew. Chem. Int. Ed. Engl.* 36, 1808 (1997).

[134] Kohout, M., *Int. J. Quantum Chem.* 97, 651 (2004).

[135] Kohout, M.; Pernal, K.; Wagner, F. R.; Crin, Yu., *Theor. Chem. Acc.* 112, 453 (2004).

[136] Kohout, M.; Pernal, K.; Wagner, F. R.; Crin, Yu., *Theor. Chem. Acc.* 113, 287 (2005).

[137] Kohout, M., *Faraday Discuss.* 135, 43 (2007).

[138] Wagner, F. R.; Bezugly, V.; Kohout, M.; Grin, Yu., *Chem. Eur. J* 13, 5724 (2007).

[139] Kohout, M.; Wagner, F. R.; Grin, Yu., *Theor. Chem. Acc.* 119, 413 (2008).

[140] Dobson, J. F., *J. Chem. Phys.* 94, 4328 (1991).

[141] Bader, R. F: W.; Stephens, M. E., *J. Am. Chem. Soc.* 97, 7391 (1975).

[142] Fradera, X.; Austen, M. A.; Bader, R. F. W., *J. Chem. Phys. A* 103, 304 (1999).

[143] Angyan, J.; Loos, M.; Mayer, I., *J. Phys. Chem.* 98, 5244 (1994).

[144] Fulton, R. L.; Mixon, S. T., *J. Phys. Chem.* 97, 7530 (1993).

[145] Macchi, P.; Sironi, A., *Coord. Chem. Rev.* 238-239, 383 (2003).

[146] Matito, E.; Sola, M., *Coord. Chem. Rev.* 253, 647 (2009).

[147] Baranov, A. I.; Kohout, M., J. Comput. Chem. 32, 2064 (2011).

[148] Poater, J.; Sola, M.; Duran, M.; Fradera, X., *Theor. Chem. Acc.* 107, 362 (2002).

[149] Wang, Y.-G.; Matta, C.; Werstiuk, N. H., *J. Comput. Chem.* 24, 1720 (2003).

[150] Ponec, R., *J. Math. Chem.* 21, 323 (1997).

[151] Ponec, R., *J. Math. Chem.* 23, 85 (1998).

[152] Baranov, A. I.; Ponec, R.; Kohout, M., *J. Chem. Phys.* 137, 214109 (2012).

[153] Francisco, E.; Pendas, A. M.; Costales, A., *Phys. Chem. Chem. Phys.* 16, 4586 (2014).

[154] Bader, R. F. W.; MacDougall, P. J.; Lau, C. D. H., *J. Am. Chem. Soc.* 106, 1594 (1984).

[155] Schmider, H.; Sagar, R. P.; Smith, V. H. Jr., *J. Chem. Phys.* 94, 3627 (1991).

[156] Bader, R. F. W.; Johnson, S.; Tang, T.-H.; Popelier, P. L. A., *J. Chem. Phys.* 100, 15398 (1996).

[157] Menendez, M.; Boto, R. A.; Francisco, E.; Pendas, A. M., *J. Comput. Chem.* 36, 833 (2015).

[158] Bickelhaupt, F. M.; van Eikema Hommes, N. J. R.; Fonseca Guerra, C.; Baerends, E. J., *Organometallics* 15, 2923 (1996).

[159] Fonseca Guerra, C.; Handgraaf, J.-W.; Baerends, E. J.; Bickelhaupt, F. M., *J. Comput. Chem.* 25, 189 (2004).

[160] Voronoi, G. F.; Reine, Z., *Z. Angew. Math.* 134, 198 (1908).

[161] Holzwarth, N. A. W.; Matthews, G. E.; Dunning, R. B.; Tackett, A. R.; Zeng, Y., *Phys. Rev. B* 55, 2005 (1997).

[162] Valiev, M.; Weare, J. H., *J. Phys. Chem. A* 103, 10588 (1999).

[163] Torrent, M.; Jollet, F.; Bottin, F.; Zerah, G.; Gonze, X., *Comput. Mater. Sci.* 42, 337 (2008).

[164] Arfken, G., *Mathematical Methods for Physicists 3rd ed.*, Academic Press: Orlando, p. 681 (1985).

[165] Shannon, C. E., *Proc. Institute of Radio Engineers* 37, 10 (1949).

[166] Press, W. H.; Teukolsky, S. A.; Vetterling, W. T.; Flannery, B. P., *Numerical Recipes in C: The Art of Scientific Computing 2nd ed.*, Cambridge University Press: Cambridge, p. 501 (1992).

[167] Landau, L. D.; Lifshitz, E. M., *Quantum Mechanics Non-Relativistic Theory 2nd ed.*, Pergamon Press Ltd.: Bristol, pp. 411-412 (1965).

[168] Meyer, B., *The Pseudopotential Plane Wave Approach* in *Computational Nanoscience: Do It Yourself!*, edit. by Grotendorst, J.; Blügel, S.; Marx, D., John von Neuman Institute for Computing: Jülich, p. 78 (2006).

[169] Moore, E. A., *Chem. Modell.* 5, 119 (2008).

[170] Messiah, A., *Quantum Mechanics. Volume 2*, North-Holland Publishing Company: Amsterdam, p. 1056 (1965).

[171] Dewhurst, J. K.; Sharma, S.; Nordström, L.; Cricchio, F.; Bultmark, F.; Granäs, O.; Gross, E. K. U., *The Elk Code Manual: Version 4.3.6*, `http://elk.sourceforge.net/elk.pdf` (accessed 06.04.2017), pp. 92-93.

[172] Press, W. H.; Teukolsky, S. A.; Vetterling, W. T.; Flannery, B. P., *Numerical Recipes in C: The Art of Scientific Computing 2nd ed.*, Cambridge University Press: Cambridge, pp. 113-116 (1992).

[173] Feagin, J. M., *Methoden der Quantenmechanik mit Mathematica*, Springer-Verlag: New-York, p. 304 (1995).

[174] Kohout, M., *Program DGrid-4.7*, Radebeul (2012).

[175] Gonze, X.; Beuken, J.-M.; Caracas, R.; Detraux, F.; Fuchs, M.; Rignanese, G.-M.; Sindic, L.; Verstraete, M.; Zerah, G.; Jollet, F.; Torrent, M.; Roy, A.; Mikami, M.; Ghosez, Ph.; Raty, J.-Y.; Allan, D. C., *Comput. Mater. Sci.* 25, 478 (2002).

[176] Gonze, X.; Amadon, B.; Anglade, P.-M.; Beuken, J.-M.; Bottin, F.; Boulanger, P.; Bruneval, F.; Caliste, D.; Caracas, R.; Cote, M.; Deutsch, T.; Genovese, L.; Ghosez, Ph.; Giantomassi, M.; Goedecker, S.; Hamann, D. R.; Hermet, P.; Jollet, F.; Jomard, G.; Leroux, S.; Mancini, M.; Mazevet, S.; Oliveira, M. J. T.; Onida, G.; Pouillon, Y.; Rangel, T.; Rignanese, G.-M.; Sangalli, D.; Shaltaf, R.; Torrent, M.; Verstraete, M. J.; Zerah, G.; Zwanziger, J. W., *Computer Phys. Comm.* 180, 2582 (2009).

[177] Kohout, M., *DGrid-4.6 User's Guide*, `http://www2.cpfs.mpg.de/~kohout/Documents/DGrid-4.6.pdf` (accessed 06.04.2017).

[178] Baranov, A, I.; Kohout, M., *J. Phys. Chem. Solids* 71, 1350 (2010)

[179] `https://software.intel.com/en-us/node/521956` (accessed 06.04.2017).

[180] `http://www.netlib.org/lapack/explore-html/d6/dee/zheev_8f.html` (accessed 06.04.2017).

[181] `https://software.intel.com/en-us/intel-mkl` (accessed 06.04.2017).

[182] Cioslowski, J., *Int. J. Quant. Chem.* 38, 15 (1990).

[183] `http://www.openmp.org/` (accessed 06.04.2017).

[184] `http://www.abinit.org/downloads/PAW2` (accessed 06.04.2017).

[185] Hachmann, J.; Cardoen, W.; Chan, G. K.-L., *J. Chem. Phys.* 125, 144101(2006).

[186] Tsuchimochi, T.; Scuseria, G. E., *J. Chem. Phys.* 131, 121102 (2009).

[187] Stella, L.; Attaccalite, C.; Sorella, S.; Rubio, A., *Phys. Rev. B* 84, 245117 (2011).

[188] Sinitskiy, A. V.; Greenman, L.; Mazziotti, D. A., *J. Chem. Phys.* 133, 014104 (2010).

[189] Nagamatsu, J.; Nakagawa, N.; Muranaka, T.; Zenitani, Y.; Akimitsu, J., *Nature* 410, 63 (2001).

[190] Chol, H. J.; Roundy, D.; Sun, H.; Cohen, M. L.; Loule, S. G., *Nature* 418, 758 (2002).

[191] Ormeci, A.; Rosner, H.; Wagner, F. R.; Kohout, M.; Grin, Y., *J. Phys. Chem. A* 110, 1100 (2006).

[192] Müller, U.; Isaeva, A.; Ruck, M., *Z. Anorg. Allg. Chem.* 640 (8-9), 1564 (2014).

[193] Kaiser, M.; Isaeva, A.; Skrotzki, R.; Schwarz, U.; Ruck, M., *Z. Anorg. Allg. Chem.* 637, 2026 (2011).

[194] Pitzer, K. S., *J. Am. Chem. Soc.* 70, 2140 (1948).

[195] Back, T. G.; Barton, D. H. R.; Britten-Kelly, M. R.; Guziec, F. S., *J. Chem. Soc. Perkin Trans.* 1, 2079 (1976).

[196] Ishii, A.; Okazaki, R.; Inamoto, N., *Bull. Chem. Soc. Jpn.* 61, 861 (1988).

[197] Dovell, F. S., *J. Am. Chem. Soc.* 87, 2767 (1965).

[198] Naren, H. R.; Thamizhavel, A.; Nigam, A. K.; Ramakrishnan, S., *Phys. Rev. Lett.* 100, 26404 (2008).

[199] Uhlarz, M.; Ignatchik, O.; Wosnitza, J.; Naren, H. R.; Thamizhavel, A.; Ramakrishnan, S., *J. Low Temp. Phys.* 159, 176 (2010).

[200] Roslova, M.; Golub, P.; Opherden, L.; Ovchinnikov, A.; Uhlarz, M.; Baranov, A. I.; Prots, Y.; Herrmannsdoerfer, T.; Wosnitza, J.; Doert, T.; Ruck, M., *in press.*

[201] Sidgwick, N. V., *The Electronic Theory of Valency*, Oxford: Clarendon, pp. 178-181 (1927).

Acknowledgement

First at all I would like to thank my supervisor Prof. Michael Ruck for giving me a great opportunity to work in his group and to get in touch with real science. His constant indifferent attention to his students together with the valuable advices make the creation of the present thesis is possible.

The special thank I would like to give to Dr. Alexey Baranov, who was in charge of the corresponding project and mentored the research. It is really hard to overestimate his help in every aspect of the investigation starting from the very beginning, when the necessary software only was installed, and ending with the revision of the final version of the thesis.

A nice atmosphere in the room is of especial importance for a theoretician, because he is tied to his working place and has no possibility to hide in a laboratory. Therefore, I would like to thank my long-term roommates and colleagues Dr. Anna Isaeva, Dr. Maria Roslova and, again, Dr. Alexey Baranov for a great working atmosphere. They also constantly provided structures for the computation thus stimulating me and promoting the development of the algorithm and its improvement.

For the provided computational facilities I would like to thank the ZIH TU Dresden, where a bulk of the calculations was performed.

Last but bot least I would like to thank for the personal support my family, relatives, friends and all other people who in that or other way implicated to the way that led me to this.

List of Publications

Results presented within this work have already been published within the following article.

1. Golub, P.; Baranov, A. I., "Domain overlap matrices from plane-wave-based methods of electronic structure calculation", *J. Chem. Phys.* 145, 154107 (2016).

The following articles have also been published but are not connected to the results presented within this work.

1. Golub, P.; Borzda, T.; Doroshenko, I.; Pogorelov, V., "Cluster Structure of Liquid Alcohols from Vibrational Spectroscopy and Quantum Chemical Calculations", *J. Spectrosc. Dyn.*, 2:20 (2012).

2. Golub, P.; Pogorelov, V.; Doroshenko, I., "The Structural Peculiarities of Liquid n-Heptanol and n-Octanol", *J. Mol. Liq.* 169, 80 (2012).

3. Golub, P.; Doroshenko, I.; Pogorelov, V., "Quantum Chemical Modeling of Energy Parameters and Vibrational Spectra of Chain and Cyclic Clusters of Monohydric Alcohols", *Phys. Lett. A* 378, 1937 (2014).

Versicherung und Erklärung

Hiermit versichere ich, dass ich die vorliegende Arbeit ohne unzulässige Hilfe Dritter und ohne Benutzung anderer als der angegebenen Hilfsmittel angefertigt habe; die aus Quellen direkt order indirekt übernommenen Gedanken sind als solche kenntlich gemacht. Die Arbeit wurde bisher im Inland noch im Ausland in gleicher oder ähnlicher Form einer anderen Prüfungsbehörde vorgelegt.

Die vorliegende Arbeit wurde an der Professur für Anorganische Chemie II der Technischen Universität Dresden unter wissenschaftlicher Betreuung von Herrn Prof. Dr. rer. nat. habil. Michael Ruck im Zeitrum Februar 2014 bis März 2017 angefertigt.

Es haben keine früheren erfolglosen Promotionsverfahren stattgefunden.

Hiermit erkenne ich die Promotionsordnung der Fakultät Mathematik und Naturwissenschaften der Technischen Universität Dresden in der Fassung vom 23 Februar 2011, zuletz geändert am 15 Juni 2011 und 18 Juni 2014, an.

Dresden, April 2017 Pavlo Golub